

Microchannel Thermal Management Analysis and Simulation Tool for Integration into Electronic Component Design

by

Kelli M. Waterman

B.S. Mechanical Engineering
United States Naval Academy, 2015

Submitted to the Department of Mechanical Engineering in partial fulfillment of the requirements for the degrees of

Naval Engineer

and

Master of Science in Mechanical Engineering

at the

Massachusetts Institute of Technology

May 2022

©2022 Massachusetts Institute of Technology. All rights reserved.

Author

Naval Construction and Engineering
Department of Mechanical Engineering
April 29, 2022

Certified by

Julie Chalfant
Research Scientist, Design Laboratory, MIT Sea Grant College Program
Thesis Supervisor

Certified by

Chathan Cooke
Principal Research Engineer, Research Laboratory of Electronics
Thesis Supervisor

Certified by

Chryssostomos Chryssostomidis
Professor of Mechanical and Ocean Engineering
Thesis Supervisor

Accepted by

Nicolas G. Hadjiconstantinou
Professor of Mechanical Engineering
Chair, ME Committee on Graduate Studies

Microchannel Thermal Management Analysis and Simulation Tool for Integration into Electronic Component Design

by

Kelli M. Waterman

Submitted to the Department of Mechanical Engineering on April 29, 2022 in Partial Fulfillment of the Requirements for the degrees of Naval Engineer and Master of Science in Mechanical Engineering

ABSTRACT

This study focuses on the use of microchannel cold plates as a thermal management solution. The goal of the study was to build the Microchannel Simulation Library Tool (MSLT), which allows cold plate designers to analyze possible solutions to electronic component cooling. The MSLT relies on a library of geometries built in the Star-CCM+ software suite, but pulls the user interaction level to a Matlab interface for ease of access to said library and implementation by designers.

Four basic geometries are included that have been shown to provide cooling enhancement to cold plates: straight microchannels, zig-zagged microchannels, straight microchannels with cavities, and oblique pin fins. Geometric parameters including channel width, length and depth as well as cold plate and working fluid material properties are variable from the Matlab user interface level. Pre-processing to ensure viable geometries and the generation of a Java script to dictate run parameters of the simulation sweeps are completed within Matlab prior to Star-CCM+ running simulations through its Design Manager tool. The data is then retrieved and post-processed from Matlab to generate performance metrics for use.

The straight microchannel simulation set-up was validated against published experimental data with temperature trends and pressure drop analyzed.

Trend analysis was conducted for the geometric features showing the relationship between performance in terms of maximum cold plate temperature and channel width, as well as the impact that it has on pressure drop across the cold plate. Generally, results show that smaller channels provide better performance in the form of lower maximum cold plate temperatures but at the cost of a higher pressure drop. Additionally, features that enhance flow redirection and mixing also cause lower maximum cold plate temperatures at the cost of higher pressure drops.

The MSLT can be used by cold plate designers to simply and cheaply generate modeling of a wide range of microchannel cold plate solutions. This ease of solution analysis allows for integration of thermal management into component design rather than a problem to be solved later. This is especially useful in the case of heat generating components in the developmental stages of the design process with potentially changing conditions.

Thesis Supervisor: Chryssostomos Chryssostomidis

Title: Professor of Mechanical and Ocean Engineering

Acknowledgements

This thesis, and my completion of the Naval Construction and Engineering (2N) program, would not have been possible without the support, instruction and encouragement I have received along the way.

The Naval Construction and Engineering Program at MIT is truly one of the Navy's hidden gems and I am beyond grateful to have been afforded the opportunity to study alongside some of the brightest engineers in the world. I would like to thank the US Navy, Engineering Duty Officer community, and 2N leadership for providing this opportunity. I would also like to thank my parents, Bob and Dori Freer, for consistently inspiring me to excellence through their love, encouragement and phenomenal example, despite my father's insistence that we only 'strive for mediocrity.'

I cannot put into words the totality of my gratitude for my advisory team. Their incredible intellect, guidance, expertise and patience made the experience of working on a thesis challenging and invigorating in the best way possible.

- Professor Chrysostomos Chrysostomidis - Thank you for your candid feedback, directed vision, and continued support and encouragement. I appreciate your patience and candor at every interaction and thank you for your guidance and shaping of this project.
- Dr. Chathan Cooke - Thank you for your insight and critical intellect throughout the entire process. The driving questions, thoughtful analysis and considerate encouragement you offered the past two years have challenged me to understand and learn more than I thought possible.
- Dr. Julie Chalfant - Thank you for your careful review, technical expertise, and drive for excellence. I am inspired by your attention to detail in not only the technical rigor of your work but in its presentation as well. I have learned so much from your thoughtful feedback throughout this process.

Additional gratitude is owed to Dr. Zhicheng Wang and Jose del Aguila Ferrandis for their CFD expertise, patience and guidance allowing me to understand and use Star-CCM+ to complete this.

This material is based upon research supported by, or in part by, the U.S. Office of Naval Research (ONR) under award number ONR N00014-16-1-2945 Incorporating Distributed Systems in Early-Stage Set-Based Design of Navy Ships and ONR N00014-16-1-2956 Electric Ship Research and Development Consortium. Thank you to Kelly Cooper and L.J. Petersen from ONR for sponsoring this work.

To my work family, the 2N cohort class of 2022, I will forever owe much of my success to your camaraderie, support, and brilliance. I have learned so much working along side this professional and intelligent group of individuals. The long days were made shorter by the laughter and geniality you provided. I cannot envision success in this program without each of you.

Finally, none of this would have been remotely feasible without the love and encouragement of my husband Tim. Your endless support, both emotionally and in the very tangible form of dinners cooked, laptop specs researched and countless other small and big things along the way have been truly instrumental in allowing me the space, resources and time to complete the coursework and research needed to get to this point. The patience you showed while listening to me ramble on about topics you thought you left behind in your own Masters Degree studies was second to none, and your unending encouragement drives me to be the best version of myself.

Contents

Abstract	2
Acknowledgements	3
List of Figures	8
List of Tables	9
List of Abbreviations	10
1 Introduction and Motivation	11
2 Background	14
2.1 Thermal Engineering As Part of the Design Process	14
2.2 Microchannel Cold Plates	14
2.2.1 What is a Microchannel?	14
2.2.2 Studies of Microchannels	15
2.2.2.1 Straight Channel Variations	15
2.2.2.2 Varied Channel Cross-Sections	17
2.2.2.3 Fins and Flow Disruption Along Channel Length	19
2.2.3 Common Concerns About Usage of Microchannels	21
2.2.4 Ways to Analyze Cold Plate Systems	21
2.3 Programs for MSLT Development	23
2.3.1 CFD Analysis Tools	23
2.3.2 User Interface Options	24
2.4 Definitions, Correlations and Background Theory	24
2.4.1 Variable Definitions	24
2.4.2 Fluid and Thermal Correlations	25
2.4.2.1 Standard Hydrodynamic and Thermal Fluids Correlations and Def- initions	25
2.4.2.2 Thermodynamic and Hydrodynamic Entry Length	27
3 Problem Description	28
3.1 Exploration of Microchannel Geometries	28
3.1.1 Base Model Correlations	29
3.2 MSLT Software Package	29
3.2.0.1 Files Included	29
3.2.0.2 Work Flow	30
3.2.1 Accessibility and Useability of the MSLT	32
3.3 Performance Metrics	33
3.3.1 Maximum Cold Plate Temperature	33
3.3.2 Temperature Rise Factor	33
3.3.3 Standard deviation of the bottom wall temperature σ	34
3.3.4 Pressure Drop	36

4	Microchannel Simulation Library Tool (MSLT)	37
4.1	Variable Features for All Models	37
4.2	Assumptions and Boundary Conditions	38
4.2.1	Thermal Boundary Conditions	39
4.2.2	Flow Boundary Conditions	39
4.3	Features	40
4.3.1	Straight Microchannels	40
4.3.2	Zig-Zag Microchannels	42
4.3.3	Micropins	44
4.3.4	Channels with Cavities	46
4.4	Library Features Applicabilities and Limitations	48
4.4.1	Parameters	48
4.4.2	Relationship Between Channel Width, Fin Width, Number of Channels and Plenum Width	49
4.4.3	Data Processing	50
4.4.3.1	Pre-Processing	50
4.4.3.2	Post-Processing	50
4.4.3.3	Prism Layer Determination	51
4.4.4	MSLT Limitations	51
4.4.4.1	Model Size	52
4.4.4.2	Geometric Definitions	52
4.4.4.3	Uniform Heat Flux and Channel Arrangements	52
4.4.4.4	Boundary and Flow Conditions	53
4.4.4.5	Stopping Criteria and Convergence	53
4.4.4.6	Turbulence Settings	54
4.4.4.7	Solution Integration to Real World System	55
5	Model Validation	56
5.1	Base Model Description	56
5.1.1	Lan Model Parameters	56
5.2	Simulation Setup	57
5.2.1	Geometry and Boundary Conditions	57
5.2.1.1	Symmetric Model Setup Validation	58
5.2.2	Meshing Parameters	59
5.2.2.1	Prism Layer	59
5.2.3	Physics Modeling	61
5.2.3.1	Turbulence Models	62
5.3	Validation	64
5.3.1	Channel Wall Temperature Validation	64
5.3.2	Average Wall Temperature Validation	65
5.3.3	Pressure Validation	66
5.3.3.1	Pressure Drop Due to Contraction	66
5.3.3.2	Pressure Drop Due to Expansion	67
5.3.3.3	Pressure Drop Due to Friction Losses	68
5.3.3.4	Pressure Drop Due to Flow Direction Change at Inlet and Outlet	69

5.3.3.5	Combined Formula for Pressure Drop in Straight Channels	69
5.3.4	Nusselt Number Validation	71
5.4	Validation Lessons Learned	72
6	Comparative Analysis of Features	73
6.1	Baseline Sweep Variations	73
6.1.1	Straight Channel Baseline Sweep	73
6.1.2	Inline Pin Fin Sweep	74
6.1.3	Zig-Zag Sweeps	76
6.1.4	Channels With Cavities Sweep	78
6.2	Comparative Results	78
6.3	Physical Phenomena Influencing Results	81
6.3.1	Effect of Surface Area on Heat Transfer	81
6.3.2	Effect of Flow Speed on Heat Transfer	82
6.3.3	Effect of Flow Disruption on Heat Transfer	84
6.3.4	Effect of Flow Disruption on Pressure Drop	88
6.3.4.1	Pressure Drop in Mitered Regions	88
7	Example Usage of MSLT	96
8	Conclusions and Future Work	105
A	Microchannel Simulation Library Tool User's Guide	113
A.1	Getting Started	113
A.2	Tool Overview	113
A.2.1	Work Flow	115
A.3	Step by Step Guide to Using the MSLT	115
A.4	Case Setup Problem Definition	117
A.4.1	Computer Setup and Run Time Inputs	117
A.4.2	Baseline Model Inputs	117
A.4.3	Problem Definition Inputs	118
A.5	Relationship Between Channel Width, Fin Width, Number of Channels and Plenum Width	125
A.6	Over-Definition Preventions	126
A.7	Post Processing Functionality	127
A.7.1	Scene Outputs	129
A.7.2	Report and Scene Output Variations	129
A.8	Considerations for Alternate Setups	129
A.9	Program Accessibility From Various Levels	130
A.10	Stopping Criteria	130
A.11	Solver Effect	131
A.12	Troubleshooting Tips	131

List of Figures

1	Pan et al. (2019) Fan Shaped Cavity Geometric Setup	17
2	Xia et al. (2011) Triangular Re-Entrant Cavities Geometric Setup	17
3	Straight-Wavy Hybrid Channel (Abdulqadur et al., 2019)	18
4	Gaikwad Channel Augmentation (Gaikwad et al., 2020)	19
5	Oblique fin Plan View by Lee et al. (2012)	20
6	Micro-pin Fin Heat Sink Structure studied by Singh et al. (2021)	20
7	Flow Chart of MSLT	28
8	Star-CCM+ Design Set User Interface	30
9	Matlab User Interface	31
10	Post Process Options Example	32
11	Distribution of Temperature points for Σ Calculation	35
12	Straight Base Geometry, Labeled	38
13	Straight Microchannels Base Geometry	40
14	Bottom View of Base Geometry	41
15	Isometric view of Cold Plate	42
16	Zig-Zag Microchannels Base Geometry	43
17	Zig Features Close Up	44
18	Gaikwad Channel Augmentation (Gaikwad et al., 2020)	44
19	Oblique fin Plan View (Lee et al., 2012)	44
20	Oblique Pin Fins model with 45 Degree Angled Fins and 90 Degree Angled Fins	45
21	Fin Parameters	46
22	Fan Cavity Microchannels Base Geometry	47
23	Pan et al. (2019) Fan Shaped Cavity Geometric Setup	48
24	Lan et al. (2021) Graph of Wall Temperature Averages	56
25	Model Geometry for Microchannel Model	57
26	Symmetric Half Model	58
27	Half Model Temp Distribution vs Full Model Temperature Distribution	59
28	View of Mesh Showing Prism Layer and Tetrahedral Cells	61
29	Model Turbulence Dependence	63
30	Point Temperatures Along Channel Wall	64
31	Average Wall Temperature vs Re	65
32	Numerical and Theoretical Pressure Drop	70
33	Average Nu vs Re	72
34	30, 60 and 90 degree angled fins with 0.8 mm channel widths	75
35	Surface Average Pressure Drop from Inlet to Outlet compared to Channel Width	76
36	Temperature Rise Factor Compared to Number of Channels for Baseline Geometries	79
37	Maximum Cold Plate Temperature Vs Number of Channels	79
38	Total Cold Plate Pressure Drop (Pa) compared to the Number of Channels	80
39	TRF vs Pressure Drop for baseline geometries	81
40	Relationship Between TRF and Surface Area	82
41	Maximum Cold Plate Temperatures vs inlet velocity for straight channels of different widths	83
42	Pressure Drop vs Inlet Velocity for Straight Channels of Different Widths	83

43	45 Degree Angled Fins at 0.8 mm fin width and channel width in Inline Geometry (L) and Offset Geometry (R)	85
44	Velocity for the Inline Fins (L) and Offset Fins (R) at 45 Degrees (inlet velocity is 0.4 m/s)	86
45	Offset Fins and Straight channels with 0.8 mm channels, 0.8 mm fin width and 0.4 m/s inlet velocity	88
46	Zig-Zag geometry with 0.4 mm channel width and 0.16 mm horizontal channel offset (L) and 0.8 mm channel width and 0.32 mm horizontal channel offset (R)	90
47	Pressure Drop varying horizontal flow path offset for 1 mm channel width	92
48	Theoretical Pressure Drop due to One Bend for Varying Channel Widths with Same Bend Offset	93
49	Pressure Drop from inlet to outlet across cold plate with varying channel widths and constant horizontal offset	94
50	Temperature Rise Factor vs Pressure Drop for Constant Offset and Varying Channel Widths	94
51	Computer Setup Parameters Example	96
52	Model Setup Parameters Example	97
53	Geometry and Boundary Condition Setup Parameters Example	98
54	Command Generation Example	98
55	Command Entered into Remote Server Command Shell	99
56	Checking on Project Completion Example	99
57	Second Project Computer Parameters Setup Example	99
58	Pin Fin Model Parameters Example Setup	100
59	Pin Fin Parameter Selection Example	100
60	Checking for Project Completion Example	100
61	Straight Channel Example Graph Generation	101
62	Overlay of Pin Fin Data with Straight Channel Data for Example Data Comparison	102
63	Pressure Drop Comparison Example Graph	103
64	Example of Generated Velocity Image	104
A.1	Straight Microchannels Base Geometry	121
A.2	Bottom View of Base Geometry	122
A.3	Isometric view of Cold Plate	123
A.4	Zig Features Close Up	123
A.5	Fin Parameters	124
A.6	Pan et al. (2019) Fan Shaped Cavity Geometric Setup	125

List of Tables

1	Giurgiu et al. (2016) Definitions of Channel Size	15
2	y^+ and Wall Treatment Recommendations	60
3	Temperature Along Channel Wall Validation Data	65
4	Straight Channel Sweep Cases	74
5	Pin Fin Sweep Cases	75
6	Zig-Zag Channel Width Sweep	76
7	Zig-Zag Offset Sweep	77
8	Zig-Zag Channel Width with Constant Offset	78
9	Channels With Cavities Width Sweep	78
10	Pressure Drop for Constant Total Channel Cross-Sectional Area	84
11	Inline Pins vs Offset Pins Results for 0.4 m/s Inlet Velocity	86

Acronyms

CCA Computer Card Assemblies.

CFD Computational Fluid Dynamics.

CSV Comma Separated Values.

ESRDC Electric Ship Research and Development Consortium.

MSLT Microchannel Simulation Library Tool.

PEBB Power Electronic Building Block.

TRF Temperature Rise Factor.

1 Introduction and Motivation

As technology advances to allow for better computation, electricity generation and transformation and work efficiency at smaller scales, one of the most pressing issues is thermal management at the component, sub-system and system levels. The increase in technological capability on-board military vessels is not immune to this issue. With the increased power needs that come with more advanced weaponry and computer network infrastructure comes the need for power generation and distribution innovation.

One example of this is the Power Electronic Building Block (PEBB). The Electric Ship Research and Development Consortium (ESRDC) is conducting research on the development of a power corridor which can be a self-contained electrical distribution system on board a ship. This would allow the the space allocation, boundaries, and connectivity throughout the ship to be well defined early in the design stages, as well as allow for the upgrading of a ship's electrical capability as the systems and electric draw increase over the lifetime of the ship (McCandless et al., 2019; Yang et al., 2019). A cornerstone of this module would be the PEBBs which would be programmable to the specific usage and designed to be 'plug and play' components with minimal connections. These PEBBs are being designed with sailor usability and maintainability in mind. The overall power corridor and PEBB designs are intended to improve sustainability and increase redundancy and flexibility in ship systems (Yang et al., 2019). Due to the high power density demands of the PEBB and the desire to have no liquid cooling interface to the PEBB itself, the issue of heat dissipation is a significant barrier to design (Yang et al., 2019). The PEBB, while still in development, is expected to output approximately 6 kW of thermal waste and it is likely to output waste unevenly. At approximately 0.3 m², this requires a thermal cooling density of at least 2 W/cm² with a goal of reaching 4 W/cm² on average with higher localized cooling due to the uneven output of waste heat (DiMarino, 2020). It is desired to have more targeted cooling of hot spots, if possible, in order to minimize the requirement for heat spreading and therefore size and weight requirements of the PEBBs themselves as well as the required containment structures. While one of the constraints placed on the design of the PEBB is that there are no direct liquid interfaces with the PEBB itself, there are still a number of advantages to integrating the thermal solution into the design process (whether or not it is a physical part of the designed component itself) rather than solving the thermal dissipation problem after the fact. The changing and developing nature of designs like the PEBB present a challenge to thermal engineers when there will be a requirement for an innovative thermal solution, but the design boundaries are not finalized.

There has been an extensive amount of work done in the field of micro-electronics to account for the increasing thermal waste of computer components at decreasing sizes. Conventional cold plate technology, which is typically used to cool larger scale electronic components, offers heat transfer capability much less than that of microchannel cold plates (T'Jollyn et al., 2017). Largely credited as the first to study microchannel heat sinks are Tuckerman and Pease (Kim and Kim, 2006). Using silicon wafers, Tuckerman and Pease showed a heat flux of 790 W/cm² and a thermal resistance of 0.1C/W for a 1 cm² area (Tuckerman and Pease, 1981). At a small scale, micro and mini channels have been shown to allow significant heat transfer, however understanding and optimization of microchannel heat exchangers and cold plates in a variety of applications is an ongoing field of study (Khan and Fartaj, 2020). One of the reasons why microchannels are so effective at heat transfer is that as a result of decreasing the volume to surface area density, more of the working fluid is in contact with the channel walls and inefficient axial heat conduction lessened (Khan and Fartaj, 2020).

This thesis studies the usage of micro/mini channels in a modular and adaptable way and seeks to create a design and analysis tool for future optimization of cold plate designs. The initial tool or Microchannel Simulation Library Tool (MSLT), is sized similarly to current micro/mini channel applications seen in applicable research, however the flexibility within the MSLT is designed to allow for it to be applied on a larger scale for customizable heat transfer solutions. There are a number of geometric design features that have been studied in micro/mini channels to help enhance heat transfer and diminish pressure losses. Some potential options to take advantage of and enhance the benefit of microchannels are interrupting fluid flow by using secondary channels, adjusting channel geometry, and using localized regions of microchannels. The usage of micro channels at a larger scale may require pumping power that is undesirable in a shipboard environment and around power electronics and this is a potential problem that may require study. The advantage in cooling that comes with micro/mini channel cold plates comes with greater resistance and pressure drop across the cold plate, which makes it a solution that requires study and optimization, rather than just new technology implementation. This variety of geometric features and their applicability to a specific thermal management solution can be highly variable. By using Computational Fluid Dynamics (CFD), the capability to analyze the design space opens up significantly. However, wide variability and a large design space can become problematic if the exploration of that design space is too time consuming or expensive to pursue in the midst of component design. This is often why thermal management is left as a problem to solve after the fact rather than an integrated part of the process. Using CFD to study the variations in thermal management based on channel width, geometry and other physical metrics can save time and money over experimental variations, however the models need to be experimentally validated to ensure accuracy. Some concerns and pitfalls with modeling include modeling at fine enough scale for microchannels and at a large enough scale for the PEBBs with some modicum of computational efficiency.

The two-fold goal of the study is to: 1) analyze various geometric heat transfer augmentations utilized in microchannel studies to understand the physical phenomena driving performance metrics and provide a reliable and intuitive trend analysis; and 2) create a tool that can be used by component and cold plate designers alike to optimize a thermal management design using the benefits of microchannel enhancement with temperature and pumping rates in a reasonable range for shipboard chill water systems. This is accomplished by generating models within Star-CCM+ that have a variety of geometric features built in and using the exposed parameter feature within Star-CCM+ to allow for the user to easily change dimensions, heat transfer rates, working fluid properties and cold plate material properties with little interaction with the model. The Design Manager functionality available within the Star-CCM+ software suite is a powerful tool to study a wide variety of design options and easily compare their output. The MSLT seeks to streamline the input and post-processing of design decisions into a single user interface generated by Matlab. The extraction of design variable input to a widely known and used user interface such as Matlab coupled with a robust analysis of a library of geometries aim to allow users to easily dictate inputs and ideally find an optimal solution for a given specific thermal management problem. With this capability, the simulation modeling tool can allow for analysis of a broad range of thermal management solutions for given electronic cooling problems, allowing cooling to become an integrated part of the design process.

The remainder of this thesis is laid out as follows. Chapter two discusses the background on microchannels, and augmentations found in the literature, as well as definitions and correlations used throughout the rest of the study. Chapter three defines the problem and gives an overview of the

MSLT. Chapter four discusses the details of the MSLT. Chapter five lays out validation of the models included in the MSLT. Chapter six includes a comparative analysis of the performance of the different geometries included in the model simulation library and teases out the physical phenomena affecting that performance. Chapter seven lays out a step by step example usage of the MSLT Finally, chapter eight discusses conclusions and future work opportunity from this study.

2 Background

2.1 Thermal Engineering As Part of the Design Process

Often times, design limits include component temperature limits, heat dissipation requirements and spatial limits such as volume and weight limits. Solving an energy generation problem, computing power problem, or other complex electronic component problem without the ability to carry the heat away represents a useful technological innovation with limited practical application and implementation. For this reason, thermal engineering must be a part of the design process. However, including the thermal management of a system into the design feedback loop can be time consuming and expensive if it requires modeling, testing and data analysis. Furthermore, often times the skillset involved in designing the electronic component itself is not the same skillset necessary to model and test a thermal management design, experimentally or through numerical and computational methods. While CFD relies on computing power rather than manufacturing capability and lab equipment, using any given CFD software requires a significant learning curve even if the fundamentals of fluid and thermal dynamics, as well as numerical modeling, are well understood. Those are big and often unrealistic assumptions to impose on a electrical or computer engineering scholar whose focus is on the technical innovation within the electronic component itself. Thus, a multi-disciplinary approach is required to develop a functional system, one that includes fluid dynamicists and thermal engineers alongside the work of electronic component designers. However, if that work is linear rather than parallel, that feedback loop can be slow, inefficient and stifle innovation on the side of the electronics engineers. Parallel innovation, much like the work currently being undertaken by the ESRDC allows the mechanical, electrical, thermal and system engineering problems to be solved simultaneously and in concert. Many engineering teams in the academic research world, as well as in the commercial innovation field function well in this regard with consistent and clear communication across disciplines, however, organizations can be crippled by the increasing linearization of a process intended to be parallel. Therefore, continued integration of the thermal management solution into the overall design process is of critical importance. While a tool such as the MSLT with simple modeling and optimization options cannot replace the capabilities and functionality of an engineer with a strong background in fluid and thermal dynamics, it can be one option to offer to component designers to quickly test the capabilities of a certain thermal solution for feasibility with their heat dissipation requirements. Conversely, the ability for thermal engineers to apply a tool that can give quick, comparative results to assess the options available to them for further study can streamline the process and allow innovation to start at a more informed place. In this way, the software bundle that streamlines the main features of cold plate analysis for effective study such as the one developed in this study can add to the thermal engineer's toolbox and augment the feedback loop efficiency.

2.2 Microchannel Cold Plates

2.2.1 What is a Microchannel?

The definition of microchannels and minichannels is largely based on convention. Giurgiu et al. (2016) proposes the following delineations for channel size.

Microchannels	channel width < 0.2 mm
Minichannels	0.2 mm < channel width < 3 mm
Conventional channels	channel width > 3 mm

Table 1: Giurgiu et al. (2016) Definitions of Channel Size

Many studies loosely refer to microchannels as anything around or smaller than 1 mm in width. For the purposes of this paper, microchannels will adopt this convention and broadly refer to channels of about 1 mm or smaller as microchannels, with the understanding that minichannels are wider than microchannels. Specific channel widths will be included where relevant.

2.2.2 Studies of Microchannels

There have been many technological advances to enhance the heat transfer of microchannel cold plates, as well as address some of the known problems such as high pressure drop and high friction losses. Additionally, due to the scale of microchannel cooling, physics correlations regarding fluid flow and thermal properties have been studied extensively to validate consistency or departure from classic fluid dynamics.

Starting with the work of Tuckerman and Pease in 1981, the study into the use of microchannels to augment heat transfer for electronics has been extensive, with a lot of focus on identifying departures and consistencies with classic fluid and thermal mechanics. There has been debate over the last 40 years on how closely flow characteristics at the micro level can be described in terms of well established empirical relationships. This has been studied with air and fluid flow. Much of what is not known about microchannel usage is how well known correlations and fluid flow properties are maintained at the scale of passages less than 1 mm. An example of this is the significant debate in the literature as to friction factor for microchannels and where turbulence transition occurs (Favre-Marinet et al., 2004).

2.2.2.1 Straight Channel Variations

Many researchers have studied correlations with straight channel microchannel cold plates, varying the channel width, height, and aspect ratio. Dang and Teng (2011) compared microchannels and minichannels ranging in width from 0.5 mm to 2 mm while varying channel depth and number of channels to maintain a constant total channel cross-section. They determined that the smallest width channel studied (500 micrometers) had the best heat transfer performance but at the cost of the greatest pressure drop (Dang and Teng, 2011).

Gunnasegaran et al. (2010) numerically studied the contrast of various microchannel shapes (rectangular, triangular and trapezoidal) and analyzed correlations with a cold plate that had 25 channels across. They found that across all three channel shapes, the heat transfer coefficient decreased with increased hydraulic diameter. Hydraulic diameter is a measure based on size and shape of a duct. Hydraulic diameter for rectangular ducts can be found in Equation 4. When comparing each channel across the width of the cold plate, they found that the channels in the center had a higher heat transfer rates and lower overall substrate temperatures (Gunnasegaran et al., 2010). When comparing their work to trends found by Steinke and Kandlikar (2006), they concurred with the conclusions that lower

Re flow and higher heat flux boundary conditions, which both caused increased working fluid output temperature, led to lower pressure drops. Both research groups attributed this to the viscosity decrease at higher temperatures.

Moharana and Khandekar (2012) varied channel height and width to analyze the effect of aspect ratio on overall heat transfer. They analyzed a single channel numerically and ran a variety of tests maintaining constant cross sectional area, constant heating perimeter, constant width and constant height, to tease out the relationships between heat transfer and channel geometry for a rectangular channel. They found a minimum Nusselt value at an aspect ratio of approximately 2, finding better heat transfer in the channels at smaller and larger aspect ratios (Moharana and Khandekar, 2012). The Nusselt number, or Nu , is a non-dimensional number used to express convective heat transfer. The definition of Nu can be found in Equation 37.

Kowsary et al. (2008) varied aspect ratios and cross-sections and identified optimized points given consistent aspect ratio or given consistent cross-section for a sweep of Re from 150-500. While finding different optimum aspect ratios for each Reynolds number for varying cross sectional areas, they found results consistent with most other works that increased Re for the same geometry results in increased Nu (Kowsary et al., 2008).

Raghuraman et al. (2017) also numerically studied the effect of aspect ratio in rectangular micro channels with significantly deeper channels than many other studies (3-7 mm) leading to higher aspect ratios analyzed (20, 30, 46.66). For the geometries studied, Raghuraman et al. (2017) found an optimum heat transfer at aspect ratio equal to 30, taking other flow and friction factors into account.

Qu et al. (2000) experimentally studied varying hydraulic diameter in trapezoidal microchannels specifically, with 5 microchannels per plate across. Rather than studying optimization, Qu et al. (2000) were trying to identify the appropriateness of heat transfer correlations between numerical and experimental models for this specific set up. As such, they recognize the increased impact that roughness has on microchannels compared to larger, conventional channels, and propose a changed relationship with Nu to explain the difference between their numerical and experimental results (Qu et al., 2000). Gao et al. (2002) modified channel height from 1 mm to 0.1 mm experimentally for a single width (25 mm) channel and saw a departure from classic Nu correlations at channel heights less than 0.4 mm.

Along with studying the physics governing the flow through microchannels, many have set out to find optimizations and augmentations to enhance the convective heat transfer of the forced flow. Bejan and Sciubba (1992) studied laminar forced air convection between parallel plates to find optimal distance between them in a stacked plate heat exchanger. The original concept was to look at how Computer Card Assemblies (CCA) that generated heat could be cooled with forced air flow between them. This was done analytically, and the conclusion was that the optimal spacing is that which imposes a thermal entry length equivalent to the length of the plate (Bejan and Sciubba, 1992). They found that this agreed with earlier analytical results found by Bar-Cohen and Rohsenow (1984) and Bejan's previous work. This makes good sense, as the developing boundary layer is tied to increased heat transfer in convection (Ramakrishnan et al., 2018). Additionally, they found that spacing increases with the length of the channel and decreases with the pressure drop across the channel (Bejan and Sciubba, 1992). As Favre-Marinet et al. (2004) points out, Bejan and Sciubba show that a trade-off exists between the boundary layer given by large spacing and the extra surface area exposed in small spacing

between plates.

The studies referenced in this section generally concluded that smaller channels provided increased heat transfer to the working fluid and lower cold plate temperatures. However, the wide variety of findings given various specific applications of straight micro and mini channels points to a need for further study, to include the specific sizing, spacing and application for any given thermal model solution. The optimization studies that highlight trade-offs point to the value of a tool to easily generate an accurate CFD model for a given solution to prevent the need for broad range experimental testing.

2.2.2.2 Varied Channel Cross-Sections

The ultimate goal of many researchers is to decrease the thermal resistance of any thermal management solution. Bau (1997) discusses the benefit of changing microchannel cross-section along the length of the channel with a goal of decreasing thermal resistance and therefore increasing convective heat transfer and shows analytically and theoretically that this is possible. It is also discussed in this study the existence of an optimization in channel width by balancing the calometric resistance of the fluid energy flow and the cross-section thermal resistance as they have inverse relationships for a given pressure drop across a given channel length (Bau, 1997). This is because thermal resistance decreases as the cross-sectional area of the channel decreases, however that allows for less fluid flow at a given pump pressure or maximum fluid velocity, and therefore less potential for heat to be carried away via the working fluid. However, due to the neglect of axial conduction in the analytical method of this study, it is useful for qualitative trend analysis rather than quantitative solutions (Bau, 1997).

In many instances where better heat transfer is achieved, it comes at a cost of higher pressure drop, as in studying the departure from straight channels with cavities, wavy channels, flow disruptions and other non-uniformities. Huang et al. (2020) discusses the necessity for creative designs to reduce pressure drop with increased heat transfer rates and studied the impact of adding cavities to microchannels to increase heat transfer rates in straight channels. Pan et al. (2019) used fan shaped cavities along the length of the microchannels (seen in Figure 1), and Xia et al. (2011) added triangular re-entrant cavities (seen in Figure 2). The addition of cavities decreased pressure losses and increased heat transfer due to causing a re-development of thermal entry regions (Huang et al., 2020; Pan et al., 2019; Xia et al., 2011).

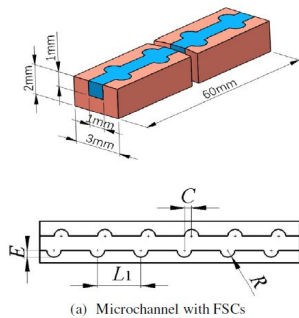


Figure 1: Pan et al. (2019) Fan Shaped Cavity Geometric Setup

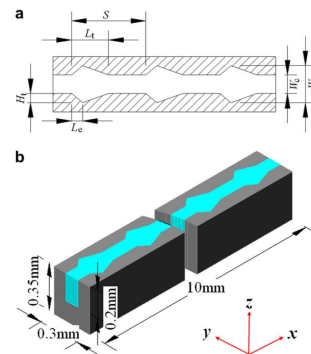


Figure 2: Xia et al. (2011) Triangular Re-Entrant Cavities Geometric Setup

There are many ways to target hot spots including concentrating microchannels in areas of interest on the electronic component as seen in the work done by Ramakrishnan et al. (2018). Significant improvement was found by Ramakrishnan et al. (2018) by localizing microchannels to specific hot spots based on die placement and therefore localized heat flux compared to the cold plate surface. Additionally, by targeting hot spots, microchannels can also help reduce temperature gradients which helps to prevent positional discrepancies in heat stress, fatigue and other adverse temperature based material properties (Bau, 1997). The reduction of hot spots is not only important for absolute temperature operating limits but also in reducing varied thermal stresses which may cause adverse effects in electronic components.

In a cylindrical heat exchanger set up, Abdulqadur et al. (2019) studied numerically and experimentally combinations of straight and wavy hybrid mini channels. An example of the flow setup studied is shown in Figure 3. In their study, the inside core of the cylinder (denoted by red) is a heat flux boundary surface, while the working fluid flows between the straight and wavy channel sections shown and an adiabatic wall (Abdulqadur et al., 2019). They found that introducing waves along the channel after the entry region allowed for augmented heat transfer and that the straight-wavy channel heat sink performed better than the straight channel heat sinks studied. Gong et al. (2011) also studied wavy channel performance compared to straight channels and optimized the channels based on amplitude, wavelength and aspect ratio of the channels. They found heat transfer performance increase of up to 55% using optimum wavy channels compared to straight channels (Gong et al., 2011).

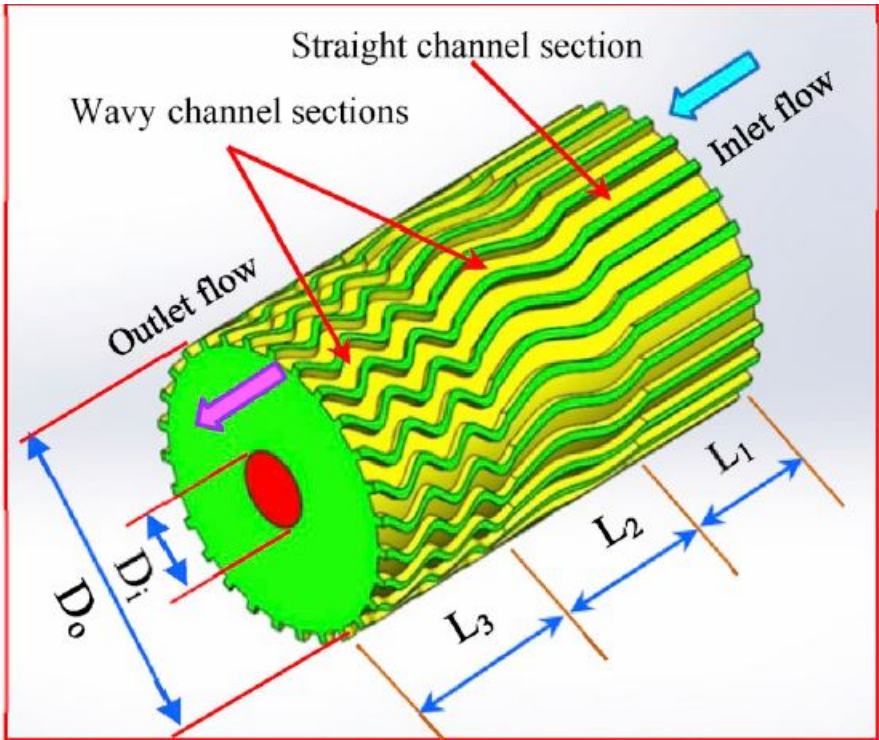


Figure 3: Straight-Wavy Hybrid Channel (Abdulqadur et al., 2019)

The studies referenced in this section generally showed that hot spot targeting and augmented heat

transfer could be achieved by varying the cross-section along the length of the channel, but that often times this came with an increase in pressure drop.

2.2.2.3 Fins and Flow Disruption Along Channel Length

Many researchers have looked into the benefits of increasing heat transfer in micro and mini channel cold plates by introducing fin structures rather than straight uninterrupted channels. This can not only increase the surface area in contact with the working fluid even greater, but break up the fluid flow which can increase heat transfer due to a redeveloping boundary layer. Gaikwad et al. (2020) created angled secondary flow paths between primary channels and numerically studied this geometric enhancement. An image representing the offset oblique fins studied by Gaikwad et al. (2020) is shown in Figure 18. They found that this increased heat transfer performance, but like many other set ups, came with a pressure drop consequence.

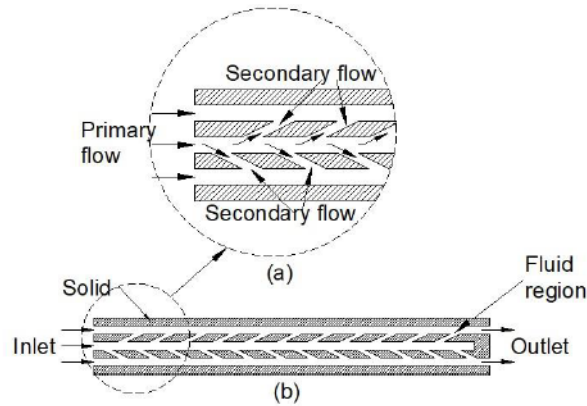


Figure 1. Enhanced MCHS (a) flow definition and (b) computational domain

680

Figure 4: Gaikwad Channel Augmentation (Gaikwad et al., 2020)

Lee et al. (2012) looked at using oblique fins in a similar setup, experimentally and numerically. They saw increased performance gains with increased Reynolds numbers, and for this setup found little excess pressure drop when the fin is 500 micrometers for low Re (up to 400).

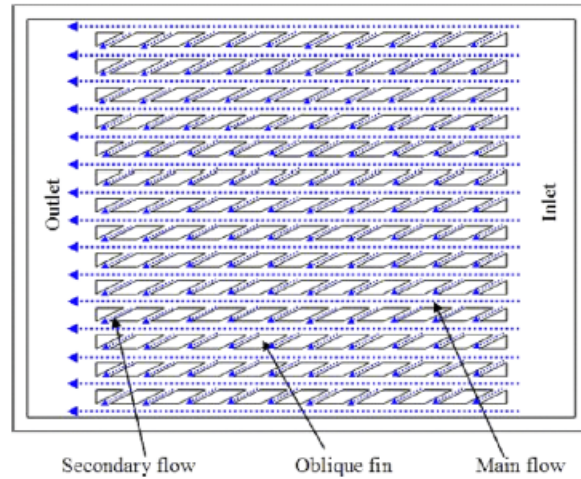


Fig. 1 Plan view of microchannel heat sink with oblique fins

Figure 5: Oblique fin Plan View by Lee et al. (2012)

Singh et al. (2021) studied more general micro-pin-fin heat sinks as compared to straight uninterrupted channels numerically. They found increased thermal performance for all variations of the pin fin heat sink structures as compared to straight wall fins.

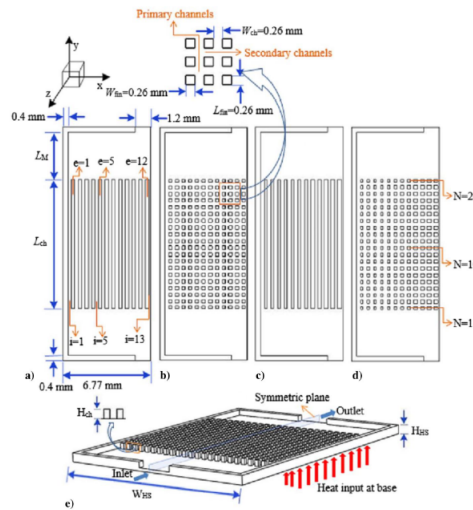


Figure 6: Micro-pin Fin Heat Sink Structure studied by Singh et al. (2021)

Wang et al. (2014) numerically studied the phenomenon of flow disruption in mini-channels by interrupting fluid flow at low Reynolds numbers with ribs in the middle of the channels. They also drew correlations between entropy generation and heat transfer performance, suggesting that an increase in entropy in the system is tied to physical phenomena that also increase heat transfer (like increased turbulence and flow disruption) (Wang et al., 2014). They found that the flow disruption and secondary

flow caused by the ribs in the middle of the channels caused increased heat transfer efficiency as well as increased fluid resistance.

A number of studies have shown that flow disruption, often in the form of fins along the length of channels, leads to better cold plate performance in terms of lower temperature rise, but typically at the cost of increased fluid resistance. However, some researchers have found optimizations with flow disruption that limit the fluid resistance increase while still providing augmented heat transfer.

2.2.3 Common Concerns About Usage of Microchannels

While there are significant benefits to using microchannels in cold plates and heat exchangers, there are a number of areas that require careful study.

Cold plates utilizing microchannels versus conventional cold plates frequently see an increase in pressure drop (Chen and Wang, 2020). Dang and Teng (2011) compared microchannel and minichannel heat exchangers and found that microchannels had higher heat transfer at the expense of a higher pressure drop. Luo and Fan (2008) found that microchannels are also more likely to experience channel surface issues such as corrosion and noted the difficulties of researchers to find effective implementation of the high heat transfer rates of microchannels at larger scales. Additionally, due to the decreased wall thickness, there are structural concerns of the channels if dealing with high pressure fluid flow. Due to the small size of the channels, fouling and roughness at the microscale have much greater implications than conventional channels in cold plates and heat exchangers (Luo and Fan, 2008). As Xia et al. (2011) discusses, Rosa et al. (2009) found that while traditional fluid flow and heat transfer laws can cover the thermal effects in microchannels versus macrochannels, aspects of fluid flow that are often considered negligible have much greater effect in microchannels, like roughness, temperature dependent properties, and entrance effects. As Perry (2018) notes, fouling is one of the issues, along with blocking and decay that has been keeping large scale microchannel cooling from progressing in the larger commercial market. This presents an opportunity to solve an operational use deficiency in cold plates by recognizing the maintenance needs. Gunnasegaran et al. (2010) describes how Qu and Weilin et al. ((Weilin et al., 2000; Qu et al., 2000)) found that there is a higher susceptibility to surface roughness in microchannels leading to a higher pressure drop and flow friction. Kumaraguru-paran et al. (2011) studied how flow mal-distribution occurs in microchannels when there are multiple parallel channels where undesirable recirculation is caused by pressure gradients against the direction of intended flow. These pressure differences can become relevant when utilizing changing channel widths as done by Ramakrishnan et al. (2018). Increased pressure drop can be an issue for a number of reasons. Cold plates in use with electronics could have fluid pressure limits in order to prevent degradation mishaps which could damage electronic components if leakage occurs. Additionally, there may be physical system limitations on pumping power which can limit the pressure drop acceptable across the cold plate.

Concerns such as fouling, pressure drop increases, and non-conventional empirical relationships demand further exploration in the study and implementation of microchannel cooling solutions.

2.2.4 Ways to Analyze Cold Plate Systems

In any heat transfer problem, the gold standard is experimental analysis of the system, because only experimentally can real practical working conditions be maintained and simulations and analytical

solutions are fraught with the errors imposed on model setup. However, analytical methods offer an excellent framework to simply evaluate the generic trends and expected outcomes in any system. Conversely, numerical simulation methods are becoming more and more advanced and while computationally expensive, can offer very thorough results with a plethora of data available for analyzing. There have been many unique approaches that researchers have taken since Tuckerman and Pease's work in the early 1980s to analyze and optimize heat transfer with cold plates.

While analytical methods to analyze microchannel cold plates are the simplest and least expensive, they often lead to very good approximate results. Knight et al. (1991) used a fin model to analytically determine the ideal number and sizing of channels for a microchannel heat sink. Bejan and Sciubba (1992) used an analytical method to determine the ideal spacing between stacked parallel plates for forced air laminar convection. Liu and Garimella (2005) used a numerical simulation model and compared it to five different analytical models to develop an optimization model as applied to a single channel. Kim and Kim (1999) derived analytical results using a porous media approach and compared that to numerical simulation results also using a porous media model. These results were compared to the experimental and analytical results derived by Tuckerman and Pease (1981) and Knight et al. (1991) with generally good agreement. This work was continued when Kim (2004) compared the analytical fin model, the porous media model and numerical simulations and identified some simplifications that application of the fin model inherits which decreases its applicability with larger aspect ratios. They find that using the numerical simulation and porous media models are both more accurate for determining optimized channel parameters (Kim, 2004).

Experimental methods have been employed since Tuckerman and Pease (1981) started the investigation into usage of microchannels for enhanced heat transfer. Favre-Marinet et al. (2004) compared the work done by Gao et al. (2002) and Bejan and Sciubba (1992) to experimentally investigate an optimum channel depth. Weilin et al. (2000) studied the pressure drop across trapezoidal microchannels to identify departures from laminar flow theory specifically relating to friction losses. They present that surface roughness likely has a larger relative effect on microchannel flow (Weilin et al., 2000). Chen et al. (2021) conducted a mathematical optimization for the microchannel geometric parameters, including height, length, depth and number of channels. They experimentally validated this optimized construction and found that it performed best for what it was optimized for: maximum heat transfer for minimum pumping power. However, this study highlights that other geometries had better overall heat transfer performance, and therefore the optimization metric is of critical importance (Chen et al., 2021). Steinke and Kandlikar (2006) ran experiments to analyze friction factors that help characterize fluid flow in microchannels, and subsequently ran destructive analysis on the experimental rigs to look at any discrepancies from intended geometry that may have had an impact on results.

With increasing capability of numerical simulation models and software, the exploration and design space for microchannel research has opened up. While modeling can save time and money over experimentation in many arenas, the manufacturing difficulties make numerical simulations particularly beneficial for microchannels. Kim and Kim (2006) used an averaging approach to one-dimensionally solve heat transfer equations in microchannels and compared across aspect ratios. Xu et al. (2008) similarly looked at taking advantage of the benefits of the thermal and hydraulic entry layer and proposed transverse zones across the cold plate between microchannel sections. This numerical simulation in Ansys required using denser grids at the entrance of each separated zone for appropriate analysis of thermal and fluid effects (Xu et al., 2008).

There are also some concerns about the modeling and performance estimates for microchannels. Qu and Mudawar (2003) found that while fin models are fairly accurate analytical models to analyze microchannel heat sinks, entrance effects can not be neglected, so the more successful fin models include thermal entrance effects in their analyses. Steinke and Kandlikar (2006) performed a thorough literature review and analysis of available data sets for single phase microchannel studies and noted this very clearly. Their C^* metric shows the ratio of experimental fRe to theoretical fRe reported for each of the studies included and is therefore a metric of how close the experimental data matched the author's theoretical values (Steinke and Kandlikar, 2006). The authors noticed that the studies with greater discrepancies, and therefore C^* values deviating significantly from 1, were studies that ignored entrance and exit effects and developing flow. This is in good agreement with the conclusions that Qu et al. came to and supports not ignoring developing flow in entrance regions for microchannel analyses. Further complicating the theoretical analysis of microchannels, Wang and Peng (1994) point out that the transition to turbulence may be earlier than in conventional fluid flow based on their experimental results using forced-convection of water through microchannels.

A number of studies have been done solely through analytical equations, simulation, or experimentation, or have shown some comparison between the two. All studies found in my literature survey showed good agreement between the simulation and analytical based methods and the experimentation.

2.3 Programs for MSLT Development

2.3.1 CFD Analysis Tools

Researchers have used many different CFD programs to analyze cold plates and microchannel structures in Cold Plates. Labade et al. (2019) and Della Torre et al. (2019) used OpenFoam in their research to model cold plates for computing servers and plate heat exchangers, respectively. OpenFoam is an open source modeling tool that is publicly available. However, its user interface and use of multiple files for each simulation make it necessary to have strong computer literacy and a strong CFD background in order to appropriately use and implement. For this study in which a large portion of the work done was to validate the use of CFD on a model with small scales and then make that tool accessible to designers - not CFD experts - OpenFoam was deemed too unapproachable. Too many inputs in a non-intuitive user interface lends itself to too many opportunities for error. Giuliani et al. (2012) and Cova et al. (2020) used COMSOL in modeling cold plates. COMSOL is an extremely powerful user suite that can model many facets of the physical world from fluid and thermal dynamics, structural mechanics and electronics. Sabin and Piva (2014) and Panchal et al. (2017) used ANSYS for cold plate modeling, with Panchal et al. (2017) using ANSYS for mini channel modeling in cold plates. Similar to COMSOL, ANSYS is widely used for fluid and thermal modeling and is a design suite with a well developed and integrated user interface at a commercial quality. Star-CCM+ is another modeling software suite that has a well-designed user interface, commercial quality support and tutorial guidance. In this realm, the commercial software packages were more attractive for use due to the need to learn the program, develop and validate models, and mature the project into a usable tool for future cold plate designers to use. Of the major options available, Star-CCM+ was available with students working in a similar field using it at MIT for ship and wave modeling. After confirming its applicability and capabilities to handle internal flow, Star-CCM+ was chosen as the modeling software of choice for this study due to its robust user interface, commercial support availability and in house

guidance and support available.

2.3.2 User Interface Options

There is a plethora of data acquisition, analysis and presentation options available, including many that can interface easily with the use of Star-CCM+ through standard file formats such as text and Comma Separated Values (CSV) files. Programming languages with well known development environments and user interface generation capabilities like Python, C++ and Java would offer robust data analysis capabilities with near limitless future growth functionality. However, while many engineers work in and use one or more of these languages, the IDE of choice often differs, and while the programming at its core for major languages shares a lot of commonality, use of one of these languages introduces another layer of learning curve that defeats the purpose of creating a tool that opens up access to CFD modeling to a designer. Therefore, Matlab was chosen as the user interface environment. The Matlab live editor environment allows for an immediately usable user interface for anyone, including those that don't have any prior Matlab experience. Also, due to the commonality of Matlab use in even the most basic levels of engineering and mathematics education it is all but guaranteed that the user will have prior exposure to the software. Therefore, that opens up the 'under the hood' experience for future designers and developers to customize the analysis or data presentation or expand the functionality of the simulation tool architecture, with minimal program specific study required.

2.4 Definitions, Correlations and Background Theory

The library of fluid and thermal theoretical correlations is vast. This section lays out basic fluid flow correlations, definitions and their relative importance in the field of micro and mini channels that are used in calculations throughout the rest of this study.

2.4.1 Variable Definitions

The following are definitions used in equations throughout the study:

- μ_{wf} : dynamic viscosity of the working fluid, defined at average fluid temperature [$Pa - s$]
- ν_{wf} : kinematic viscosity of the working fluid, defined at average fluid temperature [$\frac{m^2}{s}$]
- ρ : density [$\frac{kg}{m^3}$]
 - ρ_{wf} : working fluid density, defined at average fluid temperature [$\frac{kg}{m^3}$]
 - ρ_{solid} : solid density, defined as constant and non-temperature dependent [$\frac{kg}{m^3}$]
- u : velocity [m/s]
 - u_{inlet} : surface average velocity at inlet of cold plate [m/s]
 - u_{chan} : channel average velocity [m/s]
- A_c : Cross-sectional area [m]
- P : perimeter [m]
- c_p : specific heat (constant pressure) [$\frac{J}{kg-K}$]

- $c_{p,wf}$: specific heat (constant pressure) of the working fluid, defined at average fluid temperature $[\frac{J}{kg-K}]$
- $c_{p,solid}$: specific heat (constant pressure) of the solid, defined as constant and non-temperature dependent $[\frac{J}{kg-K}]$
- k : thermal conductivity $[\frac{W}{m-K}]$
 - k_{solid} : Thermal conductivity of the solid, defined as constant and non-temperature dependent $[\frac{W}{m-K}]$
 - k_{wf} : Thermal conductivity of the working fluid, defined at average fluid temperature $[\frac{W}{m-K}]$
- D_h : Hydraulic Diameter [m]
- α : thermal diffusivity of a liquid $[m^2/s]$
- Re : Reynolds number
 - Re_{chan} : channel average Reynolds number
 - Re_{inlet} : inlet average Reynolds number
- Pr : Prandtl Number
- $x_{e,h}$: Hydrodynamic entry length [m]
- $x_{e,t}$: Thermal entry length [m]
- $width_{chan}$: Channel Width [m]
- $height_{chan}$: Channel Height [m]
- α_c : Channel aspect ratio
- Pe : Peclet Number
- $T_{solid,max}$: Maximum cold plate temperature in the solid domain [K]
- $T_{inlet,wf}$: Inlet temperature of the working fluid [K]
- A_{HS} : Heater Surface area $[m^2]$
- \dot{q} : Heat Flux into heater surface $[W/m^2]$
- r_{inlet} : Inlet radius into cold plate plenum [m]
- n_{chans} : Number of channels across the cold plate

2.4.2 Fluid and Thermal Correlations

2.4.2.1 Standard Hydrodynamic and Thermal Fluids Correlations and Definitions

Reynolds Number is calculated using

$$Re = \frac{\rho u D_h}{\mu} \quad (1)$$

Channel Reynolds number is calculated by

$$Re_{chan} = \frac{u_{chan} * D_h * \rho_{wf}}{\mu} \quad (2)$$

Channel velocity is calculated by

$$u_{chan} = u_{inlet} \pi r_{inlet}^2 / (n_{chans} width_{chan} height_{chan}) \quad (3)$$

Hydraulic Diameter is calculated using

$$D_h = \frac{4A_c}{P} \quad (4)$$

Many correlations and definitions rely on the aspect ratio of the rectangular shape of channels, which is found using

$$\alpha_c = \frac{width_{chan}}{height_{chan}} \quad (5)$$

Since the equations that use α_c rely on it being less than 1, if the result of equation 5 is greater than one then

$$\alpha_c = \frac{height_{chan}}{width_{chan}} \quad (6)$$

is used.

Thermal diffusivity of a liquid or solid is described by

$$\alpha = \frac{k}{\rho c_p} \quad (7)$$

Prandtl number, which describes the relationship between kinematic viscosity and thermal diffusivity in liquids is defined by

$$Pr = \frac{\nu_{wf}}{\alpha_{wf}} = \frac{\mu_{wf} c_{p, wf}}{k_{wf}} \quad (8)$$

and is dimensionless.

Boundary layers can be defined by the dimensionless Peclet number, or Pe . Pe defines the ratio as between the physical capability of the boundary layer of fluid to carry energy to the heat conductance perpendicular to channel wall (or axially) of the fluid boundary layer (Lienhard IV and Lienhard V, 2019). Pe is defined as

$$Pe = \frac{\rho_{wf} c_{p, wf} u \Delta T}{k_{wf} \Delta T} \quad (9)$$

where ΔT is the difference between the wall and the bulk fluid flow.

2.4.2.2 Thermodynamic and Hydrodynamic Entry Length

As Gunnasegaran et al. (2010) notes in their work examining laminar microchannel flow, the heat transfer coefficient decreases along the length of the microchannel. This is due to the effect of the thermal boundary layer that develops. As Steinke and Kandlikar (2006) points out in their literature review of existing microchannels studies, the entrance effects of fluid are important to take into account in order to properly predict pressure drop and heat transfer characteristics in microchannels. White (1974) presents an approximation for the hydrodynamic entry length for laminar flow in a channel:

$$x_{e,h} = (0.04Re + 0.5)D_h \quad (10)$$

The definition of the hydrodynamic entry length is the length at which the flow boundary layers on each side of the duct merge together to create a uniform flow profile (White, 1974). Up until this point the flow is considered hydrodynamically developing.

Shah and London (1978) presents more specific tabulations for a dimensionless hydrodynamic entry length specifically for rectangular shaped channels based on experimental data by a number of researchers. Those equations are presented in Section 5.3.3.3.

Thermal entry length for a constant heat flux into a pipe for laminar flow that is hydrodynamically fully developed given by Lienhard IV and Lienhard V (2019) is given as (Shah and London, 1978; Shah and Bhatti, 1987)

$$x_{e,t} = 0.043RePrD_h \quad (11)$$

for a pipe with constant heat flux boundary conditions around the pipe walls. More specific data based tabulations are provided for thermal entry length by Shah and London (1978) for rectangular ducts. For the H1 boundary condition (constant heat flux on all duct walls), the tabulated data for L_{th}^+ , or non-dimensional thermal entry length, can be approximated by

$$L_{th}^+ = -0.979\alpha_c^2 + 0.1325\alpha_c + 0.0122 \quad (12)$$

Thermal entry length can then be calculated using equation 13 (Shah and London, 1978)

$$x_{e,t} = L_{th}^+ D_h Pe \quad (13)$$

Lienhard IV and Lienhard V (2019) notes that the coefficient 0.043 is actually higher if the flow is developing both thermally and hydrodynamically at the same time, which is the case for most real world applications of internal fluid flow, therefore equation 11 is a conservatively low estimate for thermal entry length and equation 12 can also be considered a conservatively low estimate for thermal entry length. With the geometric setup employed in most real world cold plate applications, as well as in this simulation library, the flow can be considered to be developing simultaneously. The conservative estimate using equation 11 will be used to estimate the entry length for the channels used in this study.

3 Problem Description

The goal of this study is to produce a software package that can allow users to study and analyze estimated cold plate performance for a wide range of geometric parameters easily customizable to their specific heat transfer problem at hand. By including geometric variations already seen to improve heat transfer in microchannel cold plate designs, users can use a streamlined tool package to tap into the robust functionality that Star-CCM+ offers for design and analysis. The four basic geometries are further described in Section 4. The intent is to provide a library of geometric features with a simple user interface which allows users to access that library in a format tailored to solving a cooling problem which allows for pre-processing, simulation running and post-processing to be streamlined in a simple Matlab format. The MSLT takes the immense learning curve of using an CFD model and the background research surrounding microchannel cold plate augmentations and streamlines it to be a usable tool for thermal engineers looking to optimize a cooling solution without having to learn about, build, and validate a model from scratch. The major goals of the project are further expanded upon in the following sections.

The software package, bundled together as the MSLT, takes user inputs via a Matlab interface which tailors a Java script to customize simulation files that are built for various microchannel geometries. After running the simulations, results are output back via a CSV and post-processing is done within Matlab to generate graphs and output performance metrics based on the data gathered from the simulation models. Plots are available for pressure drop, Maximum Cold Plate Temperature, Cold Plate Temperature Deviation, Temperature Rise Factor (TRF) and Average Cold Plate Temperature and the user can use the CSV results to do more data processing as desired. In Figure 7, processes conducted within Matlab are in orange boxes while processes completed within Star-CCM+ are in blue boxes.

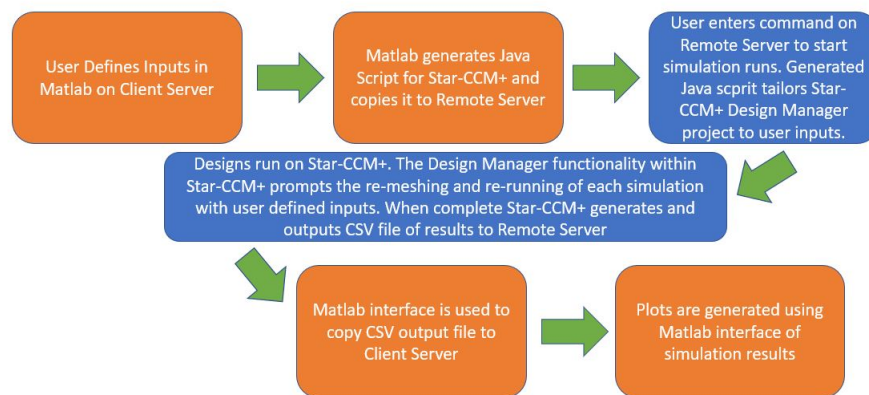


Figure 7: Flow Chart of MSLT

3.1 Exploration of Microchannel Geometries

In order to create a library of microchannel geometries useful for implementation, four specific geometric augmentations to standard microchannels were used as ‘base case’ geometries for the mi-

crochannel simulation library. These geometries were chosen based on their proven augmentation in previous studies. Each of these geometries and basic variations on the dimensions of them were explored in order to determine performance trends including average centerline wall temperature, maximum cold plate temperature and pressure drop across cold plates for varying geometric changes. The four basic geometries chosen were straight microchannels, zig zagged microchannels, straight channels with cavities along the length, and oblique fin microchannels. The four basic geometries are further described in Section 4.

3.1.1 Base Model Correlations

The following trends will be discussed for the four base models:

1. Effect of Surface Area on Heat transfer (i.e. Maximum temperature rise per total channel surface area)
2. Pressure Drop Trends based on channel width changes
3. Temperature Rise Factor analysis based on equation 14
4. Maximum Cold Plate Temperature

This tool package, with basic correlations for the individual geometries included in the simulation library, will be available to allow the user to further design customizations based on their specific size, heat transfer, working fluid and cold plate material constraints and to run analysis on these customizations with the ability to compare results across different geometries. The Matlab user interface was developed in order to streamline access to all four of these geometries and make the library of simulation models into a functional tool.

3.2 MSLT Software Package

The streamlined software package with a Matlab user interface is designed to have the base layer of user interaction in a familiar and simple format while still being able to access the Star-CCM+ CFD solver functionality. This streamlined package is intended to simplify access to the library of features modeled, collect user defined custom model parameters for intended study, pre-process necessary features that go into model development, pass relevant information to the Star-CCM+ design model, collect results, and post-process those results to give relevant performance metrics. The tool itself is outlined here.

3.2.0.1 Files Included

1. Matlab files for user input and post-processing
 - MSLT_INTERACTIVE.mlx
 - DatabaseParse3.m
 - DataSeries3.m
2. Sixteen Base Case Simulation Files including each combination of each of the following:

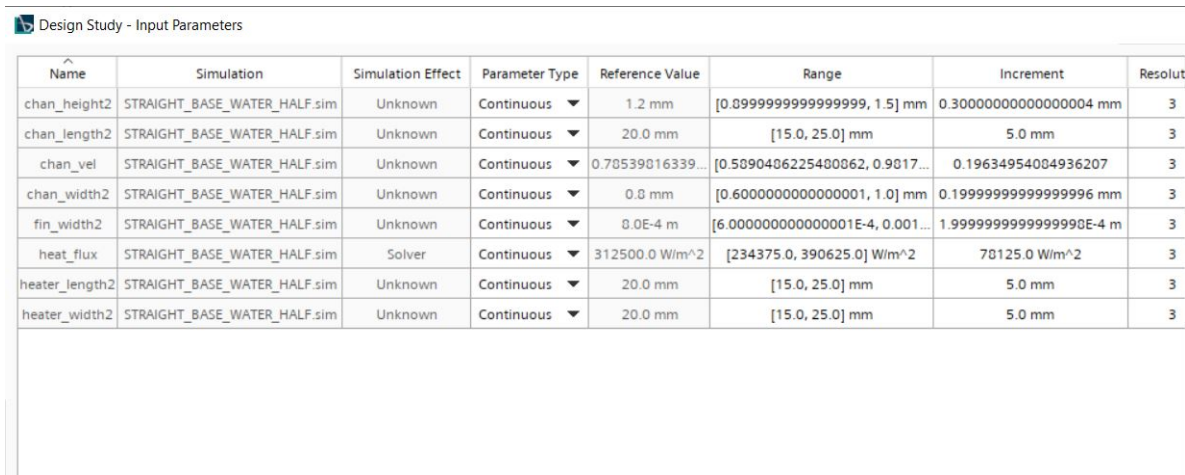
- 4 Geometries: Straight Channels, Channels with semi-circular cavities, Zig-Zagged Cavities, Parallelogram Pin Fins
- Model Size: Whole and Symmetric Half Models
- Working Fluid: Water, User Defined

3. DEFAULT.dmprj

4. MSLT User's Guide

3.2.0.2 Work Flow

The Design Manager functionality of Star-CCM+ is pulled up into Matlab by using the macro generator function within Star-CCM+. This allows the user to not interact with Star-CCM+ at all, if desired, rather interacting by pre-processing and analyzing simulation data using Matlab. Star-CCM+'s inherent macro generator function, tailored by the user inputs using MSLT_INTERACTIVE.mlx makes the hugely powerful in-house functionality of the Design Manager accessible by Matlab. Star-CCM+'s Design Manager allows for exposed parameters to be changed in sweeps of simulations and provides the backbone for running the Star-CCM+ simulations with changing parameters. It will re-mesh and run each simulation, as required, based on desired user inputs. An example of the Star-CCM+ Design Manager interface is shown in the screenshot in Figure 8.



Design Study - Input Parameters

Name	Simulation	Simulation Effect	Parameter Type	Reference Value	Range	Increment	Resolut
chan_height2	STRAIGHT_BASE_WATER_HALF.sim	Unknown	Continuous ▼	1.2 mm	[0.0999999999999999, 1.5] mm	0.3000000000000004 mm	3
chan_length2	STRAIGHT_BASE_WATER_HALF.sim	Unknown	Continuous ▼	20.0 mm	[15.0, 25.0] mm	5.0 mm	3
chan_vel	STRAIGHT_BASE_WATER_HALF.sim	Unknown	Continuous ▼	0.78539816339...	[0.5890406225480062, 0.9017...	0.19634954004936207	3
chan_width2	STRAIGHT_BASE_WATER_HALF.sim	Unknown	Continuous ▼	0.8 mm	[0.6000000000000001, 1.0] mm	0.1999999999999996 mm	3
fin_width2	STRAIGHT_BASE_WATER_HALF.sim	Unknown	Continuous ▼	8.0E-4 m	[6.000000000000001E-4, 0.001...	1.999999999999990E-4 m	3
heat_flux	STRAIGHT_BASE_WATER_HALF.sim	Solver	Continuous ▼	312500.0 W/m^2	[234375.0, 390625.0] W/m^2	78125.0 W/m^2	3
heater_length2	STRAIGHT_BASE_WATER_HALF.sim	Unknown	Continuous ▼	20.0 mm	[15.0, 25.0] mm	5.0 mm	3
heater_width2	STRAIGHT_BASE_WATER_HALF.sim	Unknown	Continuous ▼	20.0 mm	[15.0, 25.0] mm	5.0 mm	3

Figure 8: Star-CCM+ Design Set User Interface

Using the ability to change the Design Manager inputs with a java macro file, the Matlab user interface (MSLT_INTERACTIVE.mlx) generates this macro script based on MSLT user inputs removing the need to interact directly with the Design Manager, and putting pre and post processing in one location. This also reduces the number of steps required by the user to start a simulation sweep and introduces error checks to prevent impossible geometries.

The steps for the user are identified below with the processes that happen described. These are for a user running Matlab and visual processing on a local client and Star-CCM+ on a remote client.

1. Necessary Requirements/Pre-Steps

- Star-CCM+ installed with capability to run from command line (remote server side)
- File package downloaded (with .sim/.dmp/rj files installed in the same user directory on remote server side and Matlab files downloaded on client side)

2. Within Matlab, open MSLT_INTERACTIVE.mlx. Input and identify max/min, number of points for chosen variables as seen in Figure 9.

Check any parameters you would like to change from the default. To include as a range, enter different values for min and max and include how many resolution data points you would like to include. To keep constant (but different from simulation default), set min and max to same desired value and set resolution to 1.

<input checked="" type="checkbox"/> inlet velocity (m/s)	Minimum Value	<input type="text" value="0.1"/>	Maximum Value	<input type="text" value="0.7"/>	Resolution (how many data points - integers only)	<input type="text" value="5"/>
<input checked="" type="checkbox"/> channel width (mm)	Minimum Value	<input type="text" value="2.4"/>	Maximum Value	<input type="text" value="2.4"/>	Resolution (how many data points - integers only)	<input type="text" value="1"/>
<input checked="" type="checkbox"/> channel height (mm)	Minimum Value	<input type="text" value="1.2"/>	Maximum Value	<input type="text" value="1.2"/>	Resolution (how many data points - integers only)	<input type="text" value="1"/>
<input checked="" type="checkbox"/> channel length (mm)	Minimum Value	<input type="text" value="20"/>	Maximum Value	<input type="text" value="20"/>	Resolution (how many data points - integers only)	<input type="text" value="1"/>
<input checked="" type="checkbox"/> fin width (mm)	Minimum Value	<input type="text" value="2.4"/>	Maximum Value	<input type="text" value="2.4"/>	Resolution (how many data points - integers only)	<input type="text" value="1"/>
<input checked="" type="checkbox"/> number of channels (integers only)	Minimum Value	<input type="text" value="5"/>	Maximum Value	<input type="text" value="5"/>	Resolution (how many data points - integers only)	<input type="text" value="1"/>
<input checked="" type="checkbox"/> inlet radius (mm)	Minimum Value	<input type="text" value="3"/>	Maximum Value	<input type="text" value="3"/>	Resolution (how many data points - integers only)	<input type="text" value="1"/>
<input checked="" type="checkbox"/> inlet temperature (K)	Minimum Value	<input type="text" value="293"/>	Maximum Value	<input type="text" value="293"/>	Resolution (how many data points - integers only)	<input type="text" value="1"/>
<input checked="" type="checkbox"/> heat flux (W/m ²)	Minimum Value	<input type="text" value="312500"/>	Maximum Value	<input type="text" value="312500"/>	Resolution (how many data points - integers only)	<input type="text" value="1"/>
<input checked="" type="checkbox"/> Gauge pressure out (Pa)	Minimum Value	<input type="text" value="0"/>	Maximum Value	<input type="text" value="0"/>	Resolution (how many data points - integers only)	<input type="text" value="1"/>
<input checked="" type="checkbox"/> Plate Thickness (mm)	Minimum Value	<input type="text" value="3.6"/>	Maximum Value	<input type="text" value="3.6"/>	Resolution (how many data points - integers only)	<input type="text" value="1"/>
<input type="checkbox"/> Plate Width (mm)	Minimum Value	<input type="text" value="41"/>	Maximum Value	<input type="text" value="41"/>	Resolution (how many data points - integers only)	<input type="text" value="1"/>
<input checked="" type="checkbox"/> Heater Length (mm)	Minimum Value	<input type="text" value="20"/>	Maximum Value	<input type="text" value="20"/>	Resolution (how many data points - integers only)	<input type="text" value="1"/>

Figure 9: Matlab User Interface

3. User clicks Run Button

- (a) Matlab code runs, and generates macro file
- (b) Macro file is copied (automatically if passwordless setup enabled) from Matlab running on client

4. User runs batch simulation from command terminal of remote workstation being used to run Star-CCM+ (using command generated by Matlab for user).

- Command line launches Star-CCM+ in batch simulation mode. The .java file argument was the macro generated by Matlab, which inputs the user's changes from default into the Design Manager, builds the Design Set for Star-CCM+ to run a sweep of changes, and starts the run.
5. When simulation is done, Star-CCM+ will output CSV file of results back to the directory the user is working in on Remote client side. User clicks 'Check If Sim Is Done Running' Button in Matlab to verify if the simulation is done running and if so, copy the file back to working Matlab Directory on the client.
 6. User can click on variety of post-process buttons to generate graphs based on data, and the results CSV is available to them for any customized data processing they would like to do. Figure 10 shows an example of a graph generated based on results output from the Star-CCM+ simulation.

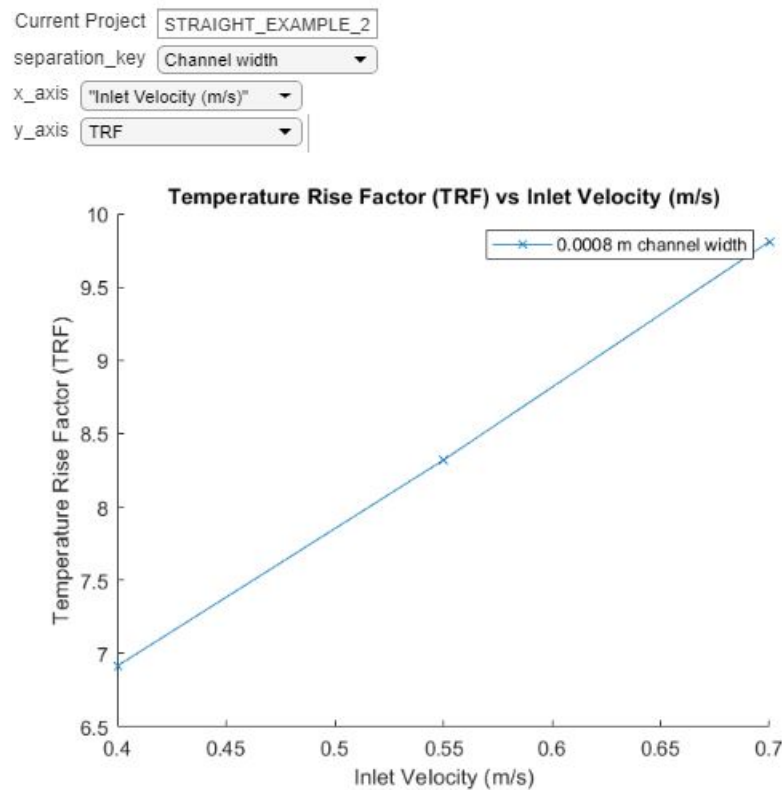


Figure 10: Post Process Options Example

3.2.1 Accessibility and Useability of the MSLT

The Microchannel Simulation Library Tool can be augmented at many levels to provide the support needed. For designers not looking to understand more than the inputs and outputs of the system, the only interaction required is with the Matlab interface which is designed to require minimal program specific knowledge to use. However, for designers looking to use this framework to expand to other

geometric enhancements, the source code and ability to integrate new base case simulations into the tool's framework is explained in the User's Guide to allow that interaction. Additionally, if more or less fidelity in the solution is desired, parameters dealing with the meshing and CFD simulations themselves are accessible. In this way, the tool can be expanded and validated at many levels or used at its most basic interface depending on the needs of the designer.

3.3 Performance Metrics

3.3.1 Maximum Cold Plate Temperature

The simplest and most direct performance metric to study is the maximum cold plate temperature. This will show the maximum temperature the solid substrate comes to in the steady state solution for a given cold plate, in degrees K. This is good for applying to temperature limits and can be a direct comparative measure but does not take into account other factors such as material property changes, inlet velocity changes, and boundary conditions changing. However, it is necessary to include maximum cold plate temperature in any comparison when the surrounding conditions are not the same to understand the applicability of a specific cold plate, not just its comparative performance.

3.3.2 Temperature Rise Factor

The Temperature Rise Factor (TRF) metric is a unitless indicator of how much the cold plate temperature rises compared to other factors influencing its performance. This metric provides a unitless way to compare cold plate performance in terms of meeting the goal of minimal temperature rise. Since the mission of liquid cooled cold plates is to keep the attached component from overheating, quantifying the cold plate's performance in terms of minimizing temperature rise is an effective way to compare various geometries. In order to define the performance metric, individual factors that impact the cold plate's performance other than geometry were identified and incorporated into the overall metric in order to compare cold plates across a variety of use scenarios. The other independent variables and their general relationship to maximum cold plate temperature at steady state are:

1. Heat applied \dot{q} [W/cm^2] - positively correlated (as heat applied to heater surface increases, maximum cold plate temperature increases)
2. Total Heater Surface Area [m^2] - positively correlated (larger heater surface is overall more heat into system)
3. Inlet flow temperature [K] - positively correlated (as inlet water temperature increases, maximum cold plate temperature increases)
4. Inlet volumetric flow rate [m^3/s] - negatively correlated (as inlet flow rate increases, maximum cold plate temperature decreases)
5. Specific Heat ($c_{p,wf}$) of the working fluid [$J/kg - K$] - negatively correlated (as specific heat increases, heat storage capacity increases)
6. Density (ρ_{wf}) of the working fluid [kg/m^3] - negatively correlated (as density increases, for the same specific heat, it takes more energy to raise the temperature of the same volume of working fluid)

In order to generate the TRF metric these variables were combined in a way reflective of their respective expected impact. The temperature rise, or the difference between the maximum cold plate temperature and the inlet flow temperature was adjusted based on the factors which affect it. Since the objective is to minimize the TRF, variables with a positive correlation were included in the denominator and variables with negative correlation were included in the numerator. This led to the metric described by

$$TRF = \frac{(T_{solid,max} - T_{inlet,wf})\dot{V}_{inlet}c_{p,wf}\rho_{wf}}{\dot{q}A_{HS}} \quad (14)$$

where $T_{solid,max}$ [K] is the cold plate maximum temperature, $T_{inlet,wf}$ is the inlet temperature of the working fluid [K], \dot{V}_{inlet} [m³/s] is the inlet volumetric flow rate of the working fluid, $c_{p,wf}$ [J/kg-K] is the specific heat of the working fluid at average fluid temperature, ρ_{wf} is the density of the working fluid at average fluid temperature, \dot{q} [W/m²] is the heat flux into the bottom of the cold plate and A_{HS} [m²] is the surface area of the heater surface. This metric can be used in isolation to show cold plate performance as it relates to temperature rise, or can be used in comparison to other measurements such as cold plate pressure drop to show a cost-performance analysis. Of note, Temperature Rise Factor alone is an appropriate metric to use only when considering similar inlet boundary conditions to compare the role the geometry plays on the performance of the cold plate. When considering the role that inlet working fluid velocity plays on the maximum temperatures seen at the cold plate, the TRF will provide a misleading conclusion if used alone because it will provide low TRF values for low inlet velocity flow rates, on an order unequal to the order at which the temperature rise will increase. Therefore, while a metric that shows the efficiency of the cold plate to transport heat out away from the system given the boundary conditions, it will not provide an apples to apples comparison for cold plate changes other than geometric. In this case other metrics such as Maximum Cold Plate Temperature must also be taken into account.

3.3.3 Standard deviation of the bottom wall temperature σ

The deviation of temperature throughout the cold plate is another performance metric that can show how well a cold plate is suited to a specific application. This metric is exceedingly important because localized hot spots can lead to significant thermal stress mismatches in a component which can lead to warping and failure. Lan et al. (2021) quantified this value and called it σ using

$$\sigma = \sqrt{\sum(T_{b,i} - T_{b,avg})^2 / (N - 1)} \quad (15)$$

where $T_{b,i}$ is a point temperature of the bottom wall of the microchannel heat exchanger, calculated using the 1-D heat conduction equation from thermocouples placed lower in the cold plate. $T_{b,avg}$ is the average temperature of the bottom wall using the five point values they collected using thermocouples. (More about the Lan et al. (2021) experimental setup is included in Section 5.3). This sigma value reported by Lan, however, only gives a picture of the deviation along the centerline channel and therefore the line of symmetry of the cold plate. This gives no look at the horizontal temperature gradation that is very evident in every simulation run. A more accurate way to capture the total plate temperature variation would be to collect data points from a grid of temperature data points across the plate in both the channel longitudinal direction and across the plate and to compute their sigma using the same formula but with many more points. The values for $T_{b,i}$ in the data collection are

gathered mid-depth between the channel bottom and the cold plate bottom in a grid comprising of 20 points. This grid is made up of 4 sets of 5 points each. The sets of 5 points are evenly spaced along the length of the channel with each set spaced horizontally such that the first line of points is under the center channel and the last line of points is at the edge of the cold plate. Due to the expected symmetrical or near symmetric heat spreading of whole plate models, only data from one half of the cold plate is collected for both half plate and whole plate models. An example of this distribution is shown in Figure 11. If a different distribution is desired, this can be manipulated by manipulating the data collection settings within the base files. More information on this manipulation is referenced in Appendix A.

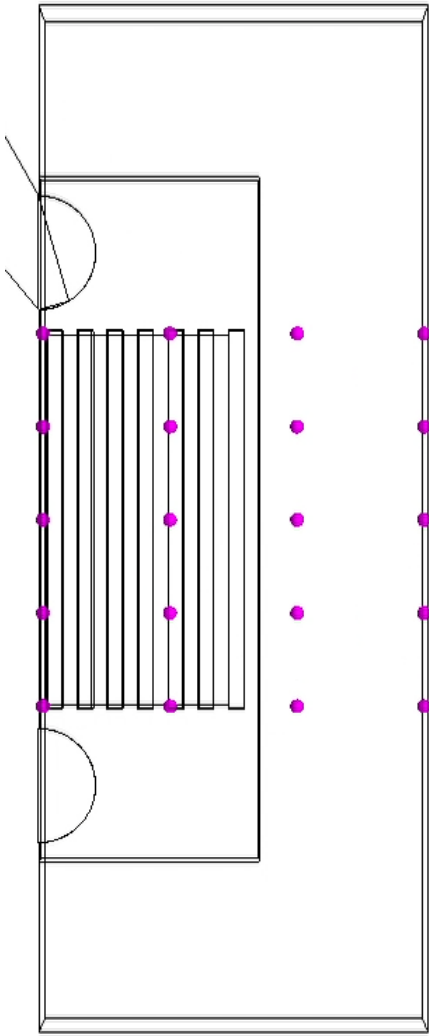


Figure 11: Distribution of Temperature points for Σ Calculation

3.3.4 Pressure Drop

The pressure drop across the entire cold plate is returned as a performance metric for plate analysis. An increased pressure drop is often seen as the ‘cost’ of using microchannels and geometric enhancements that augment microchannel performance. The pressure drop is determined by a surface average at the inlet of the cold plate and surface average at the outlet of the cold plate and therefore takes into account pressure drop due to inlet direction changes into the plenum, pressure drop across the inlet plenum, pressure drop due to the contraction of flow from the plenum to the channels, pressure drop within the channels, pressure drop due to the expansion of the fluid from the channels to the outlet plenum, and pressure drop from the change in direction from the outlet plenum to the outlet. Star-CCM+ assesses this surface average of pressure and reports it as an absolute pressure. Pressure drop is reported as the difference between the inlet and the outlets.

4 Microchannel Simulation Library Tool (MSLT)

The four main geometries built out and parametrized for study comprise the Model Simulation library and are described in the sections below. Each of these geometries has been studied in some form and is based off a study found in literature review that shows promising results for the enhancement of heat transfer over conventional cold plates. The four geometries are: straight microchannels, pin finned microchannels, zig-zag or mitered microchannels, and straight channels with semi-circular cavities off of them.

4.1 Variable Features for All Models

The following variables are exposed within the Star-CCM+ models and editable by the user via the Matlab interface for all geometry models.

- Channel Width
- Channel Depth
- Channel Length
- Inlet Velocity
- Working Fluid Inlet Temperature
- Fin Width (cold plate material width between channels)
- Heater Surface Length
- Heater Surface Width
- Number of Channels
- Plate Length
- Plate Width
- Plate Depth
- Inlet Radius
- Inlet Plenum Length
- Inlet Plenum Width
- Heat Flux Input
- Working Fluid Material Properties
- Cold Plate Material Properties

Each geometry has additional parametric values that can be edited based on the geometry. These are described in detail for each geometry in the following sections.

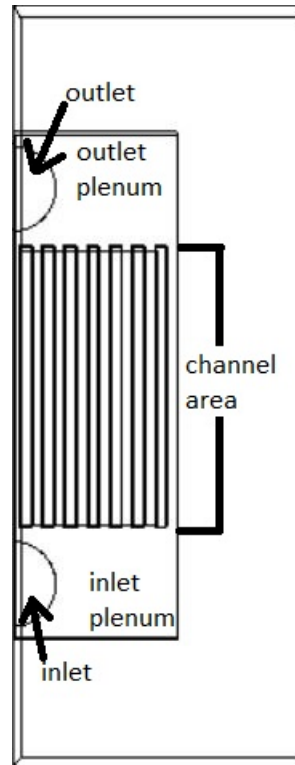


Figure 12: Straight Base Geometry, Labeled

Each of the parameters are set up to interact with each other such that the inlets, plenums, the channels, and the heater surface are centered on the cold plate. Additionally, the number of channels, channel width, fin width, and plenum widths can each be set independently, however, despite the fact that they are dependent parameters, changing one does not necessitate changing all of them, due to the way the parameters are set up within the base model simulations. For instance, if the channel width size is changed and the plenum width and number of channels are not changed, the number of channels will be adjusted to allow for the maximum number of channels in the default plenum width. However, if the channel width and channel number are both changed, the new plenum width will be calculated to be the correct width for the channel width and number of channels dictated. The formulas dictating the geometry are further laid out in Appendix A. Warnings are included in `MSLT_INTERFACE.mlx` to prevent the java file from being built in the event of conflicting geometric user inputs. An error message will display guiding the user as to what inputs are invalid. For example, due to the way the interfaces are defined, the channel depth must be less than the plate thickness. If this is not the case based on user inputs, the script will exit and an error message will display “PLATE THICKNESS MUST BE GREATER THAN CHANNEL DEPTH”.

4.2 Assumptions and Boundary Conditions

Models can be run with either the full model or symmetric half models. The validation of using symmetric half models is discussed in Section 5.2.1.1 however the model library is defined to allow for either half or full simulations to be run depending on post processing desires, geometric setup and

computational power available. The benefit of half model simulations is that they are half the total number of cells and therefore significantly less time per solver iteration, and less memory required for the meshing process. Memory can be also computational constraint because meshing completed by Star-CCM+ is done in a serial process so a larger mesh, for instance the whole model versus half symmetric model, can exceed memory requirements for a given system. Example limits are explored in Section 4.4.4. For the baseline models described in this section, symmetrical half models are used. Additionally, for this reason only geometric modifications that had only fluid on the symmetry plane in the channel region was used, to prevent any symmetry faux pas. However, this is another use of the full models - amplifying the geometric features in ways in which the channel geometry crosses over what would be the symmetry plane. An example of this would be a zig-zag pattern that has an amplitude greater than half the distance across the channel.

4.2.1 Thermal Boundary Conditions

The basic models available for each geometry are set to have a heating surface which is centered on the cold plate in both the length and width directions. The heat flux across this surface is even and is a changeable parameter. All interfaces between the liquid and solid regions are defined in the simulation to allow for conjugate heat transfer. The inlet is defined by a changeable radius parameter, inlet velocity, and inlet temperature. The outlet is defined by a pressure condition that is defaulted to atmospheric pressure but can be changed by an accessible parameter. All other external boundaries are set as adiabatic.

4.2.2 Flow Boundary Conditions

The inlet fluid boundary is defined by the circular inlet leading to the plenum as labeled in Figure 12. This circular inlet has a radius defined by the inlet radius parameter which defaults to 3 mm. The mass flow rate of the working fluid is controlled by setting the inlet velocity into this circular inlet. The default inlet velocity is set to 0.4 m/s. Inlet temperature is controlled by the Inlet Temperature parameter which has a default of 293 K. The outlet boundary condition is a pressure boundary defaulted to atmospheric absolute pressure or 0 Pa gauge pressure. The outlet section is extended vertically away from the plenum using the surface and volume extruder capabilities in Star-CCM+ to allow for the flow to cleanly flow out of the cold plate and parameters such as flow velocity, temperature and pressure to even out of the outlet. This allows the measurements at the outlet surface to be more realistic of flow conditions in a physical cold plate and is a commonly used technique in simulations to ensure that the outlet flow condition is not too ‘chaotic’ and causing backflow and pressure equalization errors. The working fluid is set to water governed by the IAPWS-IF97 equations which adjust water material properties based on the actual conditions (temperature, pressure, etc) seen at the locale rather than setting an estimate for material properties based on an approximate temperature and pressure (SIEMENS Digital Industries Software, 2021; International Association for the Properties of Water and Steam, 2007). Variability exists to change the working fluid to a generic fluid with set material properties. How to use this is explained in Appendix A. A version of each model exists with working fluid material properties that are variable other than water. However, for a working fluid other than water, constant material properties are used and the material properties set by the user will not be variable based on pressure or temperature changes in the same manner that the models using water as the working fluid are.

4.3 Features

4.3.1 Straight Microchannels

The straight microchannels serve as the basis for all the other geometry feature comparisons. There are no additional parameters other than those listed in Section 4.1. Straight microchannels have been studied exhaustively since the work done in 1981 by Tuckerman and Pease and often offer viable cold plate design solutions with no modification for many thermal management problems. The front face of the whole model for the straight channels is shown in Figure 13.

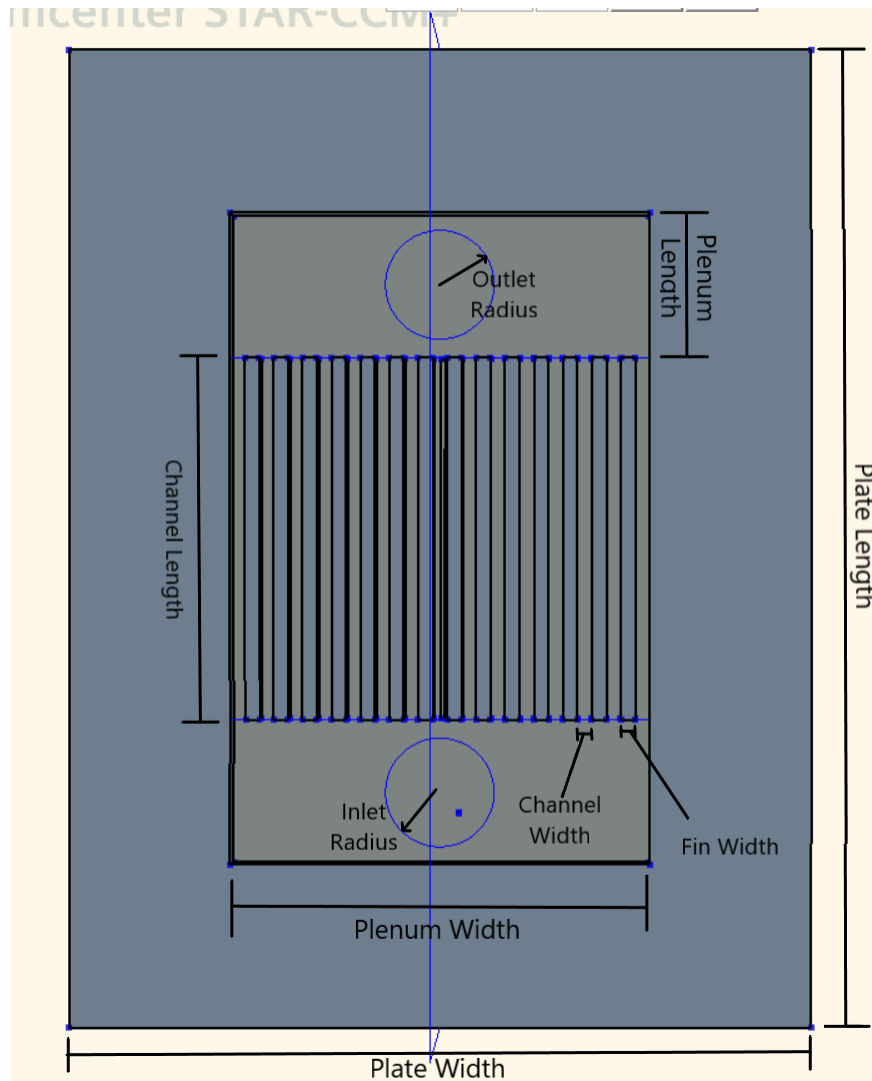


Figure 13: Straight Microchannels Base Geometry

The bottom surface of the cold plate is shown in Figure 14.

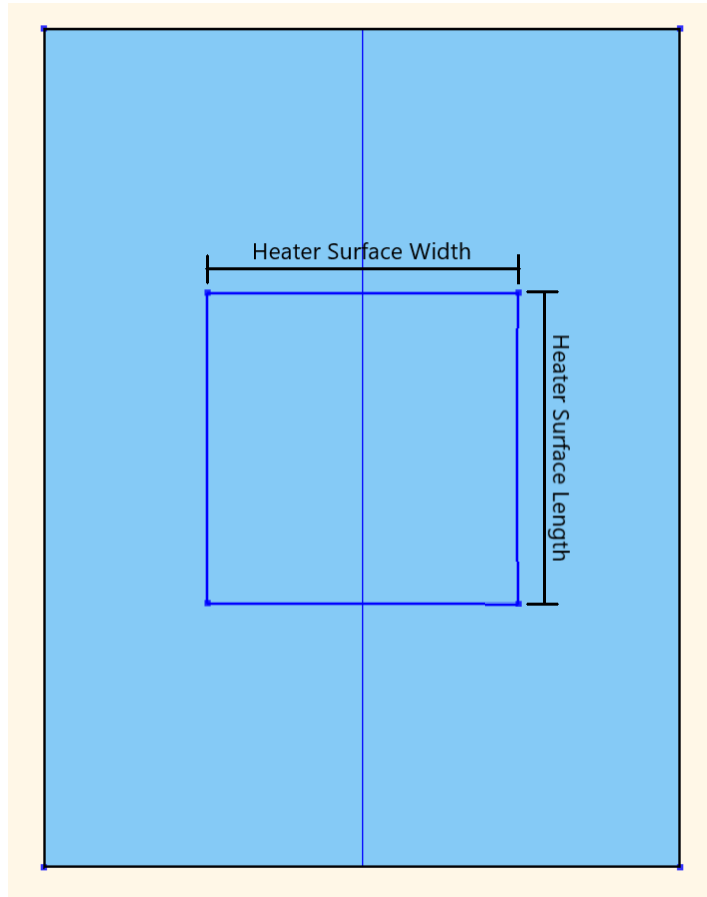


Figure 14: Bottom View of Base Geometry

An isometric view showing channel depth and plate depth are shown in Figure 15.

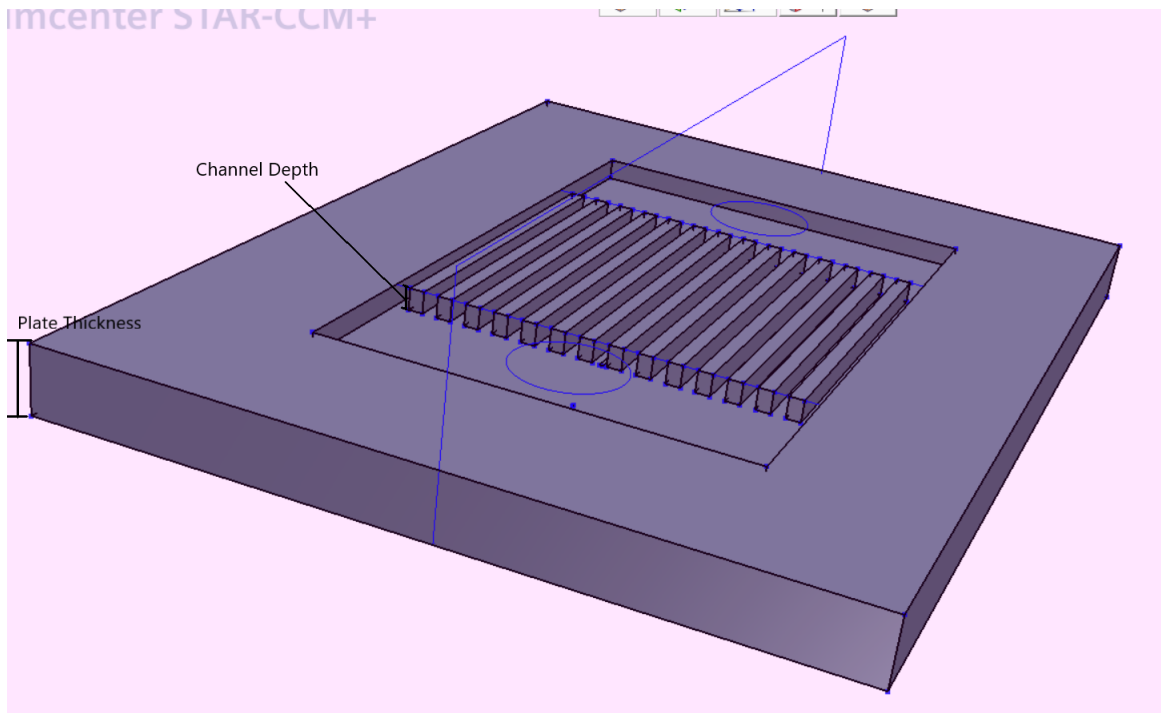


Figure 15: Isometric view of Cold Plate

4.3.2 Zig-Zag Microchannels

A number of researchers have identified benefits to re-directing the working fluid flowing through the cold plate. The zig-zag microchannels shown in Figure 16 allow for that redirection of flow along the length of the channel to take advantage of these benefits. Abdulqadur et al. (2019) studied hybrid straight-wavy channels in a cylindrical heat sink while Gong et al. (2011) studied wavy channels in a standard rectangular prism heat sink. Both saw reduced temperatures and improved performance compared to straight channels for their setup. This concept of flow re-direction was transformed from wavy channels to mitered channels in order to allow for the ease of parametrization within the simulation library. The repeatability of standard geometric shapes, including straight line representations, allow for the use of the Design Manager functionality which is highly capable. Therefore, the concepts of flow re-direction benefits seen with wavy channels were mimicked with zig-zags.

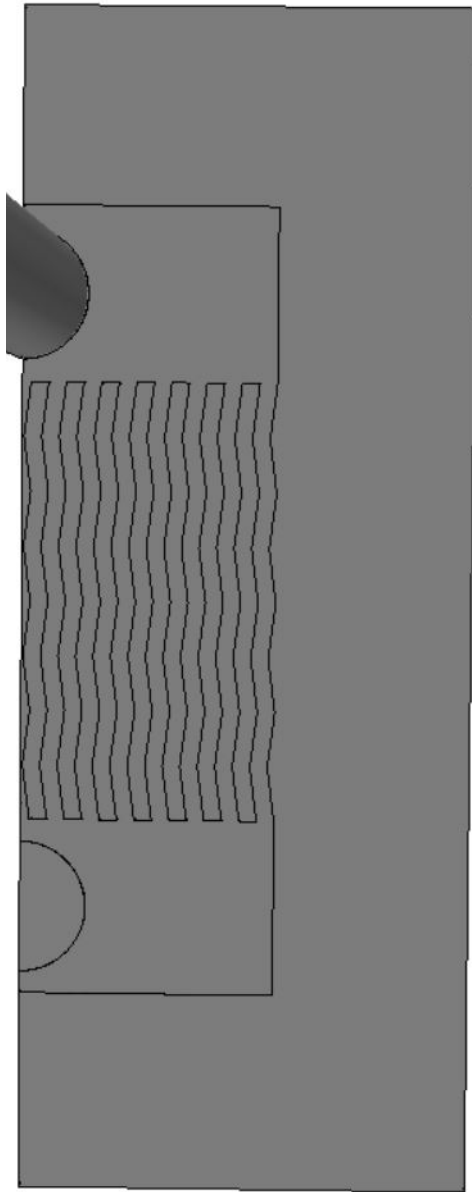


Figure 16: Zig-Zag Microchannels Base Geometry

The added features of customization for the zig-zag microchannels are:

- Zig Offset
- Zig Height

Zig Offset describes the horizontal distance the channel deviates, akin to the amplitude of a sine wave. Zig Height describes the distance vertically at which the offset pattern repeats. It can also be defined as the channel length divided by twice the number of bends in the channel. The half models can only

be used for zig offsets less than 50% of the channel width or else the simulation geometry will not build. This is due to the fact that the cold plate material will cross the boundary of the centerline symmetry plane and create a non-continuous channel domain. These are shown in Figure 17

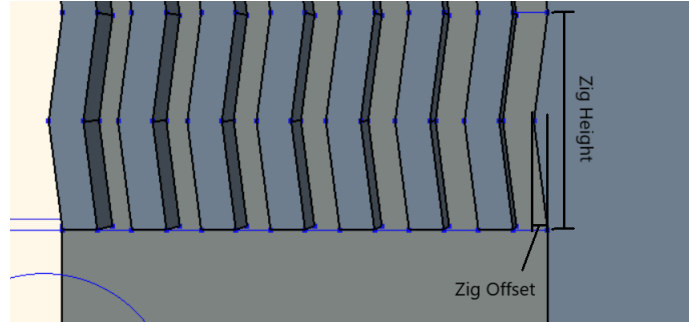


Figure 17: Zig Features Close Up

Of note, the half symmetric zig-zag models are not true representations of a cold plate geometry with parallel zig-zag channels all the way across, because the center channel is not symmetric about the centerline. If using the half-symmetric zig-zag model, and over prediction in the pressure drop is to be expected due to the centerline geometry that the simulation is actually modeling. It is included in the MSLT for use if desired, but it is recommended to use full model representations for any zig-zag geometry exploration.

4.3.3 Micropins

By departing from the concept of a fin that spans the entire length of the channel, cross channels of fluid flow can be developed. The benefit of cross flow has been studied by a number of researchers. Gaikwad et al. (2020) numerically studied angled secondary flow paths between primary channels. Lee et al. (2012) looked at using oblique fins in a similar setup, experimentally and numerically. Tikadar (2019) also numerically and experimentally studied secondary flows for parallel and counter flow mini-channel heat sinks. Some examples of their layouts are shown in Figures 18 and 19.

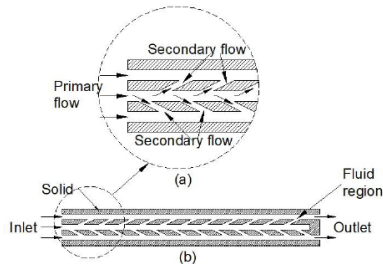


Figure 1. Enhanced MCHS (a) flow definition and (b) computational domain

680

Figure 18: Gaikwad Channel Augmentation (Gaikwad et al., 2020)

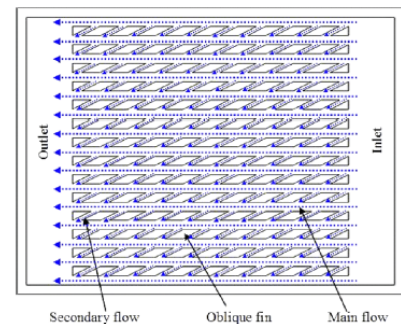


Fig. 1 Plan view of microchannel heat sink with oblique fins

Figure 19: Oblique fin Plan View (Lee et al., 2012)

The fins are intended to both disrupt the fluid flow to ensure a re-developing boundary layer, as well as encourage fluid mixing, which further disrupts the fluid flow (Lee et al., 2012). In this sense the fins and the secondary flow are almost separate phenomena intended to increase heat transfer. Half model examples of the oblique pin fins model generated for the model simulation library are depicted in Figure 20.

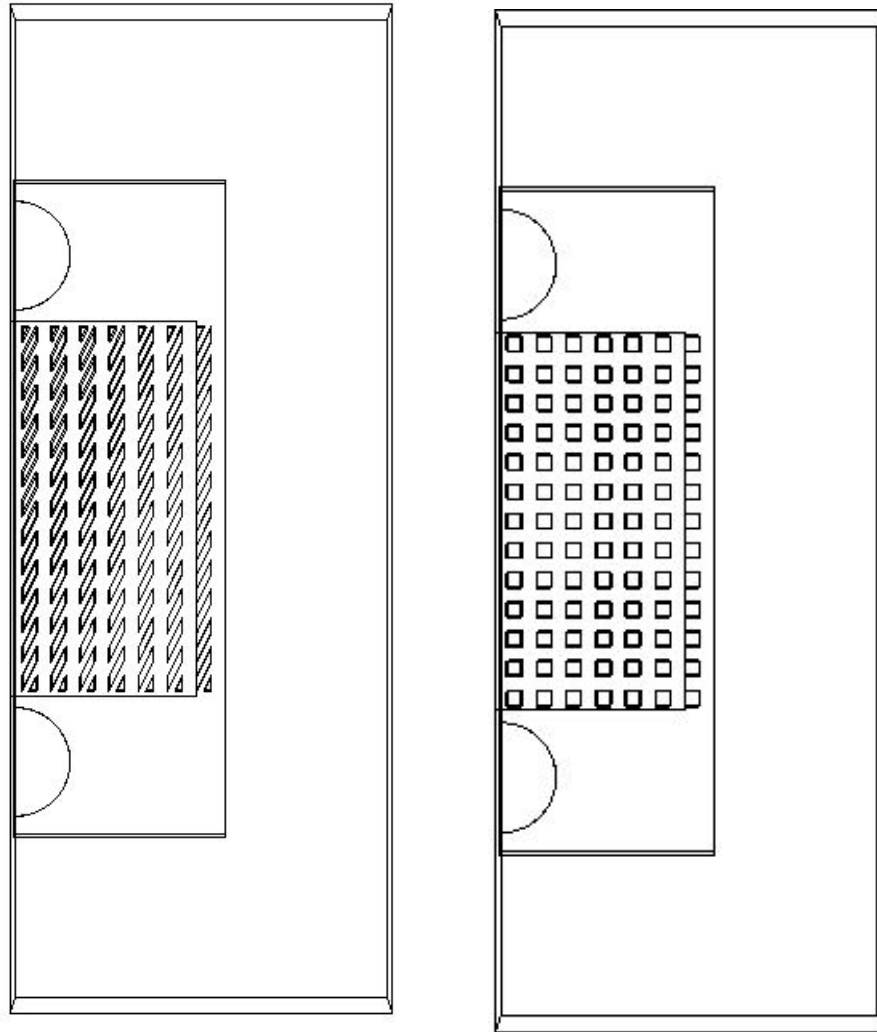


Figure 20: Oblique Pin Fins model with 45 Degree Angled Fins and 90 Degree Angled Fins

The additional parameters available for the finned models are:

- Fin angle of obliqueness
- Fin length
- Longitudinal fin spacing

Since the number of fins per channel is dependent on the fin length, fin spacing and channel length, the

number of fins per channel are set to auto calculate based on the other set parameters. Figure 20 shows an example where the fins are angled at 45 degrees (L) and an example where the fins are angled at 90 degrees (R). The additional fin parameters are shown in Figure 21.

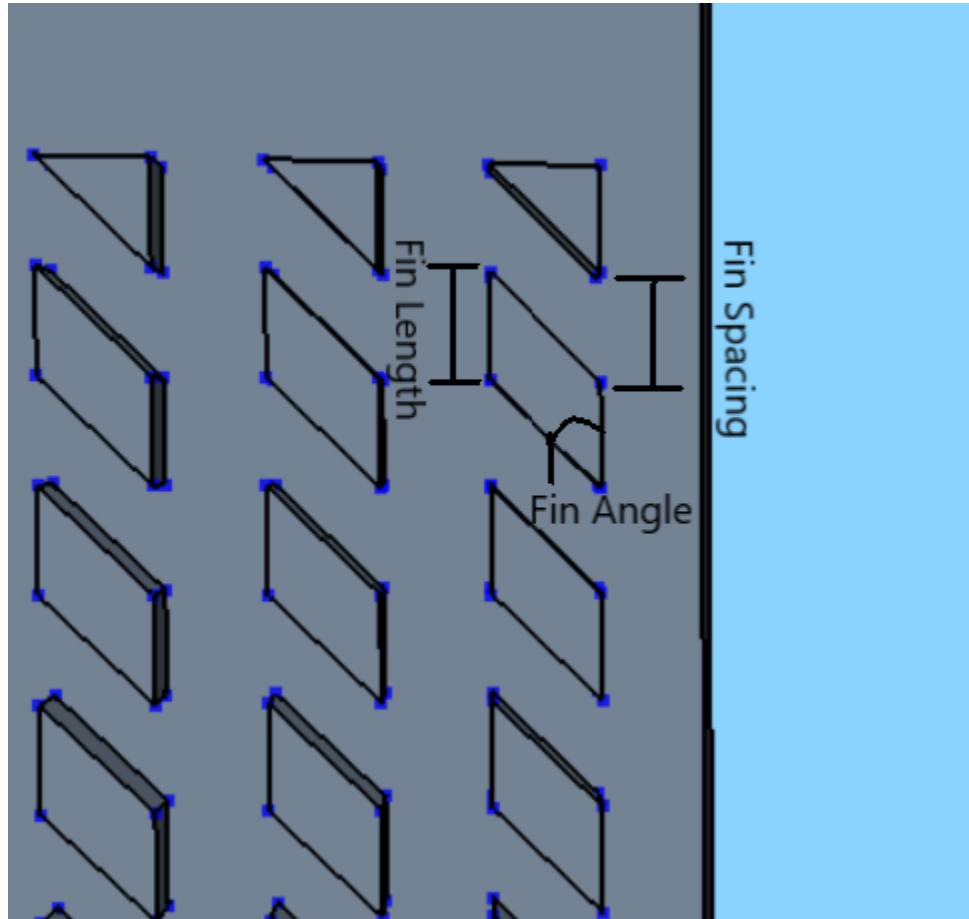


Figure 21: Fin Parameters

4.3.4 Channels with Cavities

The concept of channels with cavities has been studied by researchers to provide a different type of flow disruption within the path of the fluid flow. Xia et al. (2011) used triangular re-entrant cavities along the length of straight microchannels to augment heat transfer within microchannels in an attempt to increase fluid mixing, and disrupt boundary layers by disrupting the smooth flow path in comparison to straight, unaugmented microchannels. Pan et al. (2019) studied rectangular microchannels augmented with semi-circular cavities along the sides with a similar intent. The chosen microchannel library feature mimics that of Pan et al. (2019) in its construction and variation of semicircular cavities. A half model example of the base geometry is shown in Figure 22.

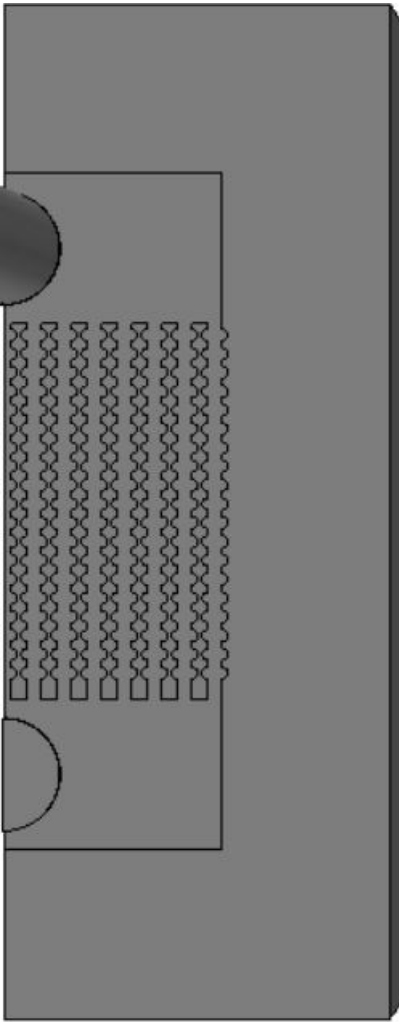


Figure 22: Fan Cavity Microchannels Base Geometry

The additional parameters available for the channels with cavities models are:

- Semi-Circle Depth off of straight channel (E)
- Semi-Circle Offset from opposing cavity in channel (C)
- Semi-Circle Radius (R)
- Semi-Circle longitudinal spacing

These, combined, allow the simulation to be manipulated to study how different depths of cavities, offsets creating asymmetric flow paths and opening widths compared to cavity depth can affect performance. These are defined the same way as in Figure 23 by Pan et al. (2019). Similarly to the finned channels, the number of cavities per channel is calculated based on the length of the channel, spacing of the cavities and size of the cavities.

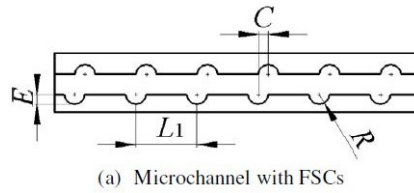


Figure 23: Pan et al. (2019) Fan Shaped Cavity Geometric Setup

4.4 Library Features Applicabilities and Limitations

4.4.1 Parameters

All parameters listed in above sections can be varied numerically. The combined list of changeable parameters, including their default values or formulas, is listed here to show the geometric interaction between dependent variables. All values listed as a default of an equation can be changed to a specific number or range of numbers via the Matlab interface. They are, however, set up to be calculated based on other independent variables, and therefore care must be taken to ensure that the geometry is as expected when changing parameters independently.

- Channel Height ($height_{chan}$): 1.2 mm
- Channel Length ($length_{chan}$): 20 mm
- Channel Width ($width_{chan}$): 0.8 mm
- Fin Width ($width_{fin}$): $width_{fin} = width_{chan}$
- Heat Flux (\dot{q}): 31.25 W/cm^2
- Heater Length ($length_{heater}$): 20 mm
- Heater Width ($width_{heater}$): 20 mm
- Inlet Temperature ($temp_{inlet}$): 293 K
- Inlet Velocity (u_{inlet}): 0.4 m/s
- Number of channels (n_{chans}): calculated using the equations in Section 4.4.2
- Plate Length ($length_{plate}$): $length_{plate} = length_{chan} + 2length_{plenum} + 2overhead$
- Plate Thickness ($thickness_{plate}$): $thickness_{plate} = height_{chan} + 2.4mm$
- Plate Width ($width_{plate}$): 0.041 mm
- Plenum Depth ($depth_{plenum}$): $depth_{plenum} = height_{chan}$
- Plenum Length ($length_{plenum}$): 8 mm
- Plenum Width ($width_{plenum}$): $width_{plenum} = width_{chan}n_{chans} + (n_{chans} - 1)width_{fin}$
- Outlet Pressure Boundary Condition (p_{outlet}): 0 Pa (gage pressure)
- Inlet Radius (r_{inlet}): 3 mm

- Solid k (k_{solid}): 108.86 W/m-K
- Solid specific heat ($c_{p,solid}$): 381 J/kg-K
- Solid Solid Density (ρ_{solid}): 8430 kg/m^3
- Working Fluid Density (ρ_{wf}): set to 999 kg/m^3
- Working Fluid Dynamic Viscosity (μ_{wf}): set to 0.0011373 Pa-s
- Working Fluid Specific Heat ($c_{p,wf}$): 4190 J/kg-K
- Working Fluid k (k_{wf}): 0.586 W/m-K
- Working Fluid Turbulent Prandtl Number: 0.9
- Additional Parameters for Finned Geometry:
 - Fin Length ($length_{fin}$): $length_{fin} = width_{chan}$
 - Fin Spacing ($spacing_{fin}$): $spacing_{fin} = length_{fin}$
 - Fin Width ($width_{fin}$): $width_{fin} = width_{chan}$
 - Pin Angle ($angle_{pin}$): 45 degrees
- Additional Parameters for Zig-Zag Geometry:
 - Height of Repeated Zig-Zag ($height_{zig}$): 5 mm
 - Horizontal Offset of Zig-Zag ($offset_{zig}$): $offset_{zig} = 0.4width_{chan}$
- Additional Parameters for Fan Cavity Geometry:
 - Fan offset (C_{fan}): 0 mm
 - Distance Between Fans ($dist_{fan}$): $dist_{fan} = 2R_{fan}$
 - Fan Depth (E_{fan}): $E_{fan} = R_{fan}$
 - Fan Radius (R_{fan}): $R_{fan} = 0.4width_{chan}$

4.4.2 Relationship Between Channel Width, Fin Width, Number of Channels and Plenum Width

If the channel width, fin width and number of channels is defined by the user, then the plenum width is sized accordingly to be flush with the outside walls of the outside channels. If the channel width and fin width are defined by the user, then the number of channels are sized based on the maximum odd number of channels that can fit in the original 23.2 mm plenum width using the following process.

The number of channels is determined using an approach to garner as close to the defined plenum width defined while keeping the number of channels at an odd number. This is important because the temperatures taken to compute wall temperatures at the channel walls are taken at the centerline of the overall cold plate (the edge of the symmetry plane for half model simulations) and need to be taken at a fluid boundary with the solid wall at the bottom of the channel in order to be an adequate

comparison. If some simulations are taking measurements in the middle of solid substrate fins and some at the liquid/solid interface at the bottom of the channel wall, the results would be incomparable due to the difference in how heat conducts and convects in those scenarios. Plenum width can be calculated using equation 16.

$$width_{plenum} = n_{chans} * width_{chan} + (n_{chans} - 1) * width_{fin} \quad (16)$$

Rearranging equation 16 to solve for number of channels, initial determination of the maximum number of channels was calculated using equation 17.

$$n_{chans,init} = floor(width_{plenum} + 0.1mm + width_{fin}) / (width_{chan} + width_{fin}) \quad (17)$$

The floor function rounds the answer down to the closest scalar to avoid making a larger plenum and to allow the maximum channels possible in the original 23.2 mm plenum width. $n_{chans,init}$ was then checked to for evenness by verifying the modulus of $n_{chans,init} / 2$. If the modulus was 0, the number of channels was reduced by one, otherwise the final number of channels was equal to $n_{chans,init}$.

Actual plenum width for the simulation geometry is then calculated using actual n_{chans} and equation 16.

4.4.3 Data Processing

4.4.3.1 Pre-Processing

There are a number of metrics based on geometry, and therefore can be calculated prior to any simulations run to be used in calculations which will aid in the display of results, or even the simulation set-up itself.

- Average Channel velocity [m/s]: $u_{chan,avg} = u_{inlet} \pi r_{inlet}^2 / (n_{chans} height_{chan} width_{chan})$
- Hydraulic Diameter [m]: $D_h = 4 width_{chan} height_{chan} / (2(width_{chan} + height_{chan}))$
- Channel Reynolds Number: $Re_{chan} = u_{chan,avg} D_h \rho_{wf} / \mu_{wf}$

4.4.3.2 Post-Processing

Values calculated after the simulation is run and results are reported are listed here.

- Average Centerline Channel Wall Temperature [K]: $temp_{wall,avg} = \Sigma(t_i) / n_{temp\ points}$
- Average Working Fluid Pressure [Pa]: $p_{wf,avg} = (p_{wf,inlet} + p_{wf,outlet}) / 2$
- Average Working Fluid Temperature [K]: $temp_{wf,avg} = (temp_{inlet} + temp_{outlet}) / 2$
- Average Working Fluid Specific Heat [$\frac{J}{kg-K}$]: $c_{p, wf, avg}$ Calculated using XSteam Matlab application based on $temp_{wf, avg}$
- Average Working Fluid Density [kg/m^3]: $\rho_{wf, avg}$ is calculated using XSteam Matlab application based on $temp_{wf, avg}$ and $p_{wf, avg}$

- Temperature Rise Factor as defined by equation 14
- Pressure Drop Across Cold Plate [Pa]: $p_{drop} = p_{wf,inlet} - p_{wf,outlet}$
- Plate Temperature Deviation [K]: $\sigma = \sqrt{\sum(t_i - temp_{plate,avg})^2 / (N - 1)}$

4.4.3.3 Prism Layer Determination

Prism layers are rectangular cells along the walls of the channels which are used to allow for more accurate depiction of what is occurring along the channel wall both hydrodynamically and thermally. The determination of how many prism layers to use and how thick they should be is discussed in detail in Section 5.2.2.1. There are different wall treatments available within Star-CCM+. The low y^+ wall treatment is used with the K-Omega turbulence model in the MSLT simulations which carries with it a recommendation for using 10-15 prism layers to achieve a Wall y^+ of 1 (Siemens Digital Industries Software, 2017). Due to the small nature of the microchannels, it may be impossible to get a full 10 layers in, and therefore the total prism layer thickness is determined in the following way as recommended by Siemens Digital Industries Software (2017).

$y_{n,L}$, which is the distance away from the wall the center of the first prism layer should be, is determined using Equations 19, 20 and 21. $y_{n,L}$ is based on fluid properties, geometric definitions, and flow velocity. If the simulation is set to water as the working fluid then the water material properties used are for water at 300 K (Engineering ToolBox, 2004, 2003). If the working fluid is set to other, the material properties input are used in the determination of $y_{n,L}$. While for both water and other working fluids these are a constant pressure and temperature fixed values, the determination of prism layer thickness is an iterative and approximate process and therefore this level of precision is deemed appropriate. Since the goal is to achieve 10 prism layers, the total prism layer thickness to achieve ten layers is calculated using

$$p_{ltot10layers} = 2y_{n,L}(1 + 1.2 + 1.2^2 + 1.2^3 + 1.2^4 + 1.2^5 + 1.2^6 + 1.2^7 + 1.2^8 + 1.2^9) \quad (18)$$

Since the maximum amount of the channel that can be filled by prism layers is set to 80%, the prism layer is also calculated for each integer number of prism layers from 5 to 10. In the event that 10 layers is greater than 40% of the channel width, the largest value of prism layers is chosen with its corresponding total prism layer thickness that is less than 40%. In the event that due to parameter definitions, 5 prism layers is still too large, the gap fill percentage will cap the total prism layer thickness to not allow prism layers greater than 40% of the channel width.

4.4.4 MSLT Limitations

The MSLT was designed at a scale mimicking experiments found in literature, with the base cases specifically modeled around a 0.8 mm channel width due to the availability of data given by Lan et al. (2021). The validations were conducted for straight channels at very specific conditions and those simulation settings used for other geometries and sizes. Significant trend analysis to validate expected performance was done for all four geometries analyzing the variation in pressure drop and temperature performance using Maximum Cold Plate Temperature and the TRF metric based on geometric changes such as channel width, and flow changes such as inlet mass flow rate. These results are included in Section 6. As such there are a number of limitations to consider with regards to the MSLT.

4.4.4.1 Model Size

The MSLT basecase models are generated for half models with symmetry planes defined down the longitudinal centerline along the channel flow paths and whole models which do not include symmetry planes. For designs that are not completely symmetric across the centerline, like zig-zag patterns or oblique fins at any other angle other than 90, using the half-symmetric model may not be as accurate as using the whole model. However, the benefit to using the half model is the saving of computational resources. The smaller the model is physically, the less cells the mesh is made up of. This leads to faster meshing, as well as faster run times. Using the same number of processing cores with the same performance metrics, a model with less cells will have shorter solver time for each iteration than a model with a larger number of cells.

Additionally, a half model can not be used if by virtue of the geometry defined the continuous fin will cross the longitudinal center line. This is because the way that the simulation file is built within the Star-CCM+ CAD modeler, it will fail if the center line is not continuous fluid domain for the length of the channels. This prevents the half symmetric base files from being used for zig zag geometries that include horizontal offsets at half the channel width or greater. However, the whole models can be used in this regard.

Model size is also a consideration for model scaling for validation and meshing. The model was validated at a channel width of 0.8 mm and 20 mm long. The validation results presented in Section 5.3 are for specific cases at this size. Changing the order of magnitude of the cold plate size would require further validation in order to trust accurate results. Based on trend analysis conducted on channel widths from 0.4 mm to 1.2 mm, it is estimated that channel widths on this order of magnitude will produce accurate results with the settings provided in the base simulation files. Additionally, the user is limited by their computational power on the size of the model in terms of number of cells. Since meshing is conducted on one single core, the limiting factor is often the computer's memory allocation. If there are too many cells, the meshing may fail due to a lack of memory.

4.4.4.2 Geometric Definitions

The program is set up to prevent geometries that will not build for all circumstances foreseen at the time of writing. However, there are always ways to 'break' the program. Troubleshooting tips to identify when a geometric definition was the cause of an error in the file build are included in Appendix A. Users of the MSLT must carefully define geometric parameters such that they are physically sensible.

The MSLT is limited to the four geometries discussed throughout this paper and Appendix A: straight channels, semi-circular channels with cavities, zig-zagged channels, and channels with oblique pin fins. However, the framework is open to allow for careful addition of template files which can allow for different geometries to be used within the MSLT.

4.4.4.3 Uniform Heat Flux and Channel Arrangements

The MSLT includes a single heater surface centered on the bottom of the cold plate for each simulation base file. While the heat flux through this surface and the length and width of this surface are definable by the user, it is still one surface vice multiple hotspots/heat generation surfaces. In practicality there

may be a number of heat flux surfaces. Based on the work of Ramakrishnan et al. (2018), it may be favorable to localize microchannels or augmented microchannel features based on heat generation locations. The MSLT uses uniformly distributed microchannels across a uniformly distributed heater surface, and therefore further augmentation would be required to the base simulation files to account for testing localization of heat flux and targeted cooling using localization of channels.

4.4.4.4 Boundary and Flow Conditions

The boundary conditions for all external boundaries of the cold plate and channel domains are set as adiabatic with the exception of the following:

- Inlet: Inlet Velocity and Temperature user defined
- Outlet: Outlet Pressure user defined
- Heater Surface: Constant Heat Flux and Heater Surface Size user defined

Star-CCM+ allows for the definition of external boundary conditions for a number of other conditions including constant temperature and atmospheric convection, however the ability to toggle those settings are not accessible from the Design Manager and therefore would require a different base simulation model. Inclusion of these boundary conditions can be done by augmenting the initial base files and more details are included in Appendix A. However, as the MSLT stands, the external boundary conditions are adiabatic.

The flow conditions are determined by inlet velocity, inlet temperature and inlet radius. Using these parameters any flow rate can be defined. Two base files for each geometry are included to allow for either water as the working fluid or a user defined working fluid. If water is selected, material properties will follow IAPWS-IF97 criteria based on temperature and pressure. If a different working fluid is selected, the working fluid will have constant material properties as set while setting other model parameters. This means that any working fluids that are highly temperature or pressure sensitive are ill suited to this simulation.

4.4.4.5 Stopping Criteria and Convergence

Stopping criteria for each simulation is based on getting to 15000 iterations, or meeting all three of the following criteria:

- Total Heat Transfer Asymptotic Limit: Over the most recent 100 samples, the total heat transfer can not have changed more than 10% of the current values (normalized change minimization of less than 0.1)
- Total Heat Transfer Maximum and Minimum: The absolute value of Total Heat Transfer must be less than the user defined percentage of the Heat Transfer introduced to the system via the heater surface. The default value is 2%. The Total Heat Transfer is defined as all heat leaving and entering the system and for a perfect steady state solution would be equal to 0 W. This is controlled using two different stopping criteria settings within Star-CCM+ - a maximum total heat transfer and a minimum total heat transfer. Both of these must be satisfied for the simulation to stop running prior to 15000 iterations.

The 15000 steps are included as a fail safe to keep the program from running indefinitely if settings are chosen that may not lead to steady state convergence within the parameters above. However, each base simulation file has a solution pre-loaded to lead to quicker convergence (base geometry settings and boundary conditions described in Section 6). The further away the settings are from those in the pre-set solution, the longer it may take to converge and 15000 iterations may not be sufficient. As the program is written, the stopping criteria maximum steps is embedded within the base files and cannot be accessed from the MSLT interface so if the simulation parameters are different enough from the base case such that greater than a total of 15000 iterations is desired, stopping criteria must be adjusted within the base files. This is addressed further in Appendix A.

The total heat transfer is included as an output accessible via the results CSV file generated and the Matlab interface for users to validate that metric of convergence. If the total heat transfer is high, particularly if it's outside of the maximum heat transfer percentage set by the user, the log files can be explored to check for good convergence. These log files are located within subfolders both on the client and remote side. For ease of user access, they are copied to the local client side within each Design's subfolder. Additionally, the number of iterations it took for the simulation to converge will be reported in the results CSV as well as a note output when graphs are generated annotating if each run converged or did not converge. If the iteration value is 15000 this means that the simulation was stopped by maximum number of steps, not by meeting convergence criteria. Exploration as to why this may be may be desired by the user, by looking past the data available by the MSLT.

Because the convergence metrics monitored are based on total heat transfer, this does leave ambiguity in the convergence of the simulations in other metrics such as pressure drop and maximum temperature. The data captured at the end of the simulation is based on the metrics from the last iterations and therefore variance between iterations may be significant depending on the level of fidelity required in analysis. For example, fluctuations of approximately +/-100 Pa were seen in the final 500 iterations of a zig-zag simulation run. This equates to less than .1% of absolute pressure measured or approximately +/-6% of the pressure drop measured within the simulation. This is only apparent in trend analysis identifying modest pressure drop changes, however it does represent a limitation of the data collection process of the MSLT. Star-CCM+ does have the capability to output data reports based on the mean of a user defined number of runs and should this be desired, future work opportunities include integrating this functionality into the MSLT.

4.4.4.6 Turbulence Settings

A potential limitation to the MSLT is in its usage of turbulent flow settings for the base models, regardless of inlet velocity. This represents a significant departure from the literature in that the simulations are set to use K-Omega Turbulence rather than laminar settings within the fluid continua definition. Many of the simulations analyzing microchannel fluid flow across the literature assume perfectly developed even and continuous flow into a single channel which is not a realistic setting to the way that cold plates will be used in the practical application. The water in the inlets is often in the turbulent regime based on inlet velocity hydraulic diameter of the inlet (as it is for the base case used for validation) before undergoing a sharp 90 degree turn entering into the inlet plenum, and contraction into the channels at sharp angles for the start of the channels. Any feature introducing flow disruption is adding to the potential for turbulence for the fluid and while the nominal channel Re is typically in the laminar regime for microchannels, the flow disruption leading up to the entrance for each microchan-

nel is significant enough to characterize the flow as turbulent. Additionally, the K-Omega turbulence model is used, which performs best when the flow is near the transition regime from laminar to turbulent. This was seen in the validation studies when building the base simulation files. The convergence and performance using the K-Omega model was generally good compared to experimental data and performed similarly to the laminar flow models. The K-Omega turbulence model was chosen over the laminar model to encapsulate a wider range of flow conditions to include transitional regions and increased flow disruption. Therefore, while the models are built and validated using the K-Omega turbulence model, there is a potential that very low inlet velocity rates may provide more accurate results using a laminar setting. However, if there is a desire to use a laminar flow model rather than a turbulent flow model, this can be adjusted by accessing the settings within the base simulation models, a matter further discussed in Appendix A.

4.4.4.7 Solution Integration to Real World System

Any design developed using the MSLT will need to be integrated into a real world system for practical use. The usage of geometric variability to include inlet dimensions in addition to cold plate dimensions as a whole was the primary accommodation included for testing a solution that could be adaptable and used in a variety of practical implementations. Additional considerations were the usage of turbulent models as discussed above. However, there are a number of other practical aspects to cold plate usage not factored into the base model simulations. These include variability of inlet location or entry angle, more realistic environmental boundary conditions, integration of multiple heater surfaces, and integration of thermal interface considerations such as thermal resistance between the cold plate and the heat generating component.

5 Model Validation

5.1 Base Model Description

An example of a straight microchannel cold plate found in the literature was used as a base case to validate the simulation models used in the simulation library. Lan et al. (2021) studied straight and interrupted flow through microchannels across a range of Re from approximately 350 to 1400. While they also studied a variety of geometries with oblique fins and secondary flow paths, the experimental and numerical setup that was modeled was the straight channel etched cold plate with straight uninterrupted microchannels. This model and experimentation was chosen as a validation model due to the data made available via publication. Specifically, Lan et al. (2021) provided temperature plots along the length of the channel for one of the flow cases. This was helpful to validate more granularly that the flow trends seen by the simulations were accurate. Additionally, they used water as the working fluid and conducted both experimental and numerical analysis that was in good agreement.

5.1.1 Lan Model Parameters

The baseline model simulated, built and experimented on by Lan et al. (2021) was a block of H62 brass ($k_{solid}=108$ W/m-K, $c_{p,solid}=381$ J/kg-K) with 15 parallel straight channels etched into it that were 20 mm [l] x 800 μm [w] x 1200 μm [h] each. Fluid flow was varied between 122 and 1575 ml/min and the flow rate with the most data given, including the temperature along the length of the microchannel, was 628 ml/min and is shown in Figure 24 by Lan et al. (2021). The straight channel base cases are represented by the black squares and black dashed line (data labeled RS). The red and blue lines are for alternate geometries explored by Lan et al. (2021).

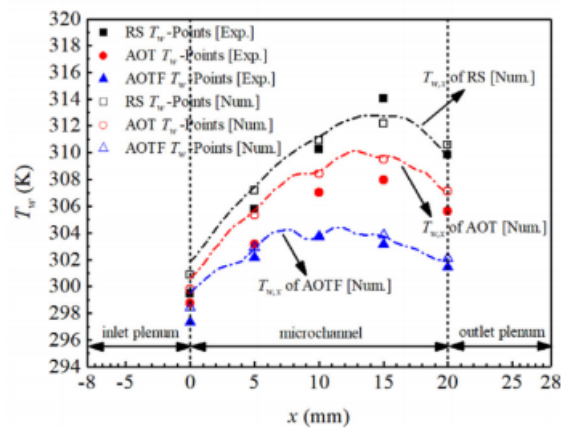


Figure 24: Lan et al. (2021) Graph of Wall Temperature Averages

A heat flux of 31.25 W/cm² was used over a 20 mm x 20 mm footprint for a total power of 125 W and they reported results of the wall temperature along streamwise direction ($T(x)$), Average wall temperatures vs Re, fluid bulk temperatures (x), $Nu(x)$, Nu_{avg} against Re, Thermal Resistance vs Re, and ΔP vs Re for the variety of geometries and fluid flow rates studied (Lan et al., 2021). Thermocouples were placed at 5 locations along the length of the channels, at 5 mm intervals from 0 to 20

mm. In order to replicate their experimental and simulation setup, certain assumptions were required to be made from the data that was available in the paper. Much of the geometry of the inlet and outlet manifold and plenum was not fully described but from the graphs reporting temperature along the length of the channel (including Figure 24), they can be assumed to be 8 mm long, the same depth as the channels (1.2 mm) and 23.2 mm wide (same width as the channels plus fins). The total depth of the copper block and location of the thermocouples was assumed as well, however, the temperatures reported by Lan et al. (2021) were wall temperatures extrapolated using 1-D heat conduction from the location of the thermocouple. For the simulations run in this study, temperatures were taken from the bottom of the channel wall directly and therefore didn't require extrapolation from the location of the thermocouple, diminishing the importance of the location of the thermocouples and the total thickness of the brass block. Finally, the inlet temperature of the water was never explicitly stated, however in the results graphs, it is reported as Bulk Fluid Temperature = 293 K (Lan et al., 2021).

5.2 Simulation Setup

From the geometry described by Lan et al. (2021) used in their experimental studies, I modeled a microchannel cold plate to best replicate the conditions used in an attempt to validate the base level of the model created. The general geometry of the model is shown in Figure 25.

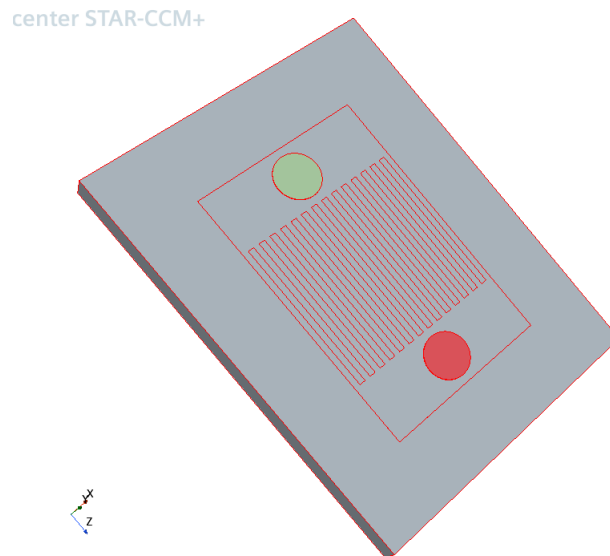


Figure 25: Model Geometry for Microchannel Model

The parameters used to define the geometry, meshing, and physics of the simulation are described in detail in the following sections.

5.2.1 Geometry and Boundary Conditions

The plate was modeled to be 54 mm long, 41 mm wide and due to the depth of the plate not being clearly defined as referenced earlier, a plate depth of 3.6 mm was assumed. The most data was available for the straight channel width at 0.8 mm, fin width of 0.8 mm and channel depth of 1.2 mm. I

modeled the heating surface as a constant heat flux applied directly at the bottom of the cold plate with a 20 mm by 20 mm patch outputting 31.25 W/cm^2 centered on the bottom surface. This was a total heat rate of 125 W. The inlet and outlet plenums were modeled as the same depth of the channels (1.2 mm), 8 mm long and spanning the entire width of the channels and fins. The inlet boundary condition was a velocity flow rate of water at 0.37018 m/s and 293K to match the flow condition of 628 mL/min as reported by Lan et al. (2021) for the results reported in Figure 24. The outlet boundary condition was set to atmospheric pressure and 300K. All other system boundaries were set to adiabatic with the exception of the heater plate to model the insulated system. The vertical inlets and outlets were at a 90 degree angle to the inlet and outlet plenums, as shown in Figure 25. The outlet was extended 0.05 m using Star-CCM+ surface and volume extruders which extend the mesh in order to prevent pressure outlet issues.

5.2.1.1 Symmetric Model Setup Validation

In order to save computational power and speed up the simulation time, the simulation was halved at the centerline longitudinally along the channels. The model is symmetric about this plane, and therefore the model was cut in half and the internal boundaries set as symmetry planes. The half model is shown in Figure 26.

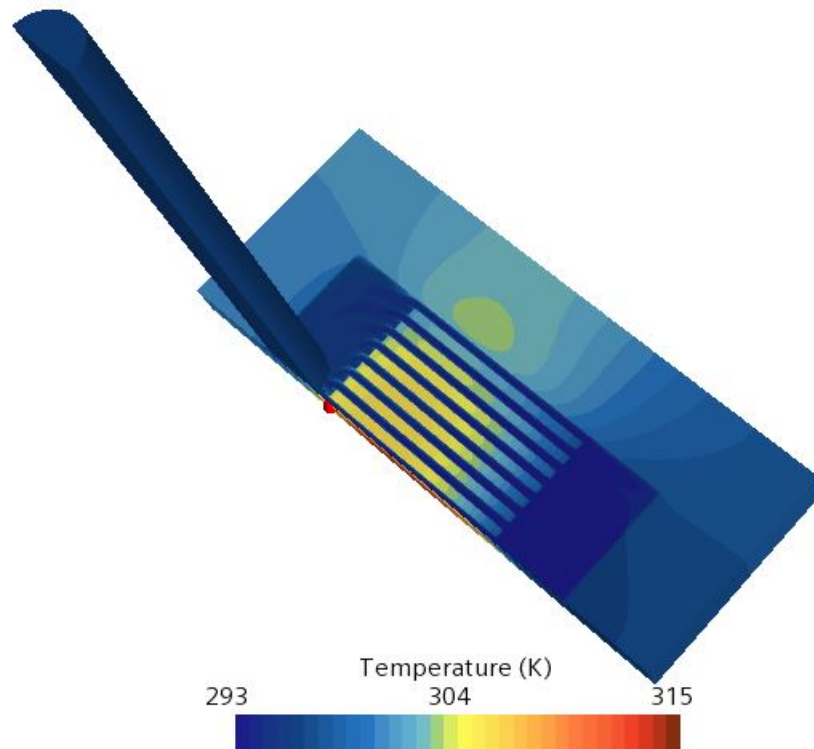


Figure 26: Symmetric Half Model

The half model displayed almost exactly the same results as the full model for the temperature distribution, and with approximately half the cells took less than half the time per iteration (3-4 sec/it compared to 9 sec/it). The temperature gradients for the full model and half model for the 628 ml/min run are shown in Figure 27. This graph shows the difference between the two models when the only thing changed is making it a symmetrical half model, versus a full model. However, the parameters to generate model accuracy were not fully honed at the time of this data gathering, and as such, the temperature distribution itself is not very accurate compared to the Lan et al. (2021) data. Further model refinements were undertaken and results are reported in Section 5.3.

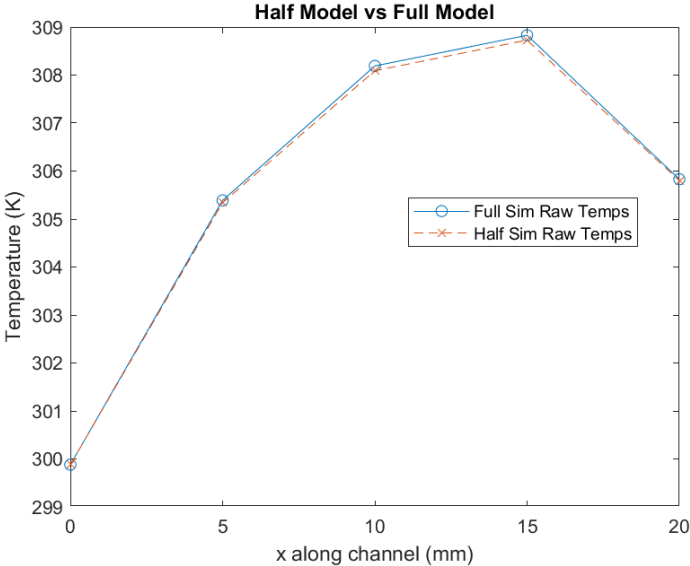


Figure 27: Half Model Temp Distribution vs Full Model Temperature Distribution

5.2.2 Meshing Parameters

The mesh is critical for any CFD simulation to getting accurate and reasonable results within the computing power of the available simulation. The meshers used within Star-CCM+ for both the fluid and solid regions were the polyhedral mesh. The polyhedral mesh type was used as recommended by SIEMENS Digital Industries Software (2021) for heat transfer and complex flow simulations. For validation, the base cell size of the mesh was 1/16 of the channel width or 0.05 mm for the fluid region and 1/8 of the channel width of 0.1 mm for the solid region. The surface remesher was utilized which is a default option within Star-CCM+. The surface remesher provides additional accuracy to a volume mesh by retriangulating the surface (SIEMENS Digital Industries Software, 2021). Due to the nature of internal fluid flow requiring increased accuracy near wall boundaries in order to get meaningful results, especially in problems surrounding thermal management, a prism layer mesher was also used to get more accurate results at the wall boundaries. This is described further in Section 5.2.2.1.

5.2.2.1 Prism Layer

Star-CCM+'s prism layer mesher increases the accuracy of the modeling near walls of an internal mesh model by creating orthogonal prisms at the boundary (SIEMENS Digital Industries Software, 2021).

The process followed in this section follows the recommendations of SIEMENS Digital Industries Software (2021). There are a number of equations laid out that govern the usage of the Prism Layer mesher. y^+ is a non-dimensional measurement of resolution at the wall of the model. It is based off the fluid material and thermal properties, velocity and model geometric characteristics. Because it is based on what is actually happening in the simulation, what value of y^+ a simulation will have cannot be pre-determined but rather the parameters necessary to get the simulation into a ballpark range can be estimated and validated after running the simulation (Siemens Digital Industries Software, 2017). The wall treatment used, and therefore the desired y^+ value can be defined by the user based on these recommendations, which are consolidated in Table 2, below.

Low y^+	10 - 15 Prism Layers	K-omega	Wall $y^+ \sim 1$
All y^+	2-3 Prism Layers	K-Epsilon and K-omega	Wall $y^+ \sim 5$
High y^+	2-3 Prism Layers	K-Epsilon	$30 < \text{Wall } y^+ < 50$
Laminar	5-20 Prism Layers	Laminar	N/A

Table 2: y^+ and Wall Treatment Recommendations

Because the prism layer is determined by total thickness, geometric expansion, and number of layers, the value for $y_{n,L}$ needs to be estimated to meet y^+ requirements, and the prism layer can be defined from there. $y_{n,L}$ which is the distance from the wall that the center of the first prism layer cell needs to be in order to meet y^+ requirements, listed above, can be initially estimated using the following formulas. Per guidance by Siemens Digital Industries Software (2017), these formulas should be used to determine initial prism layer parameters, and then the y^+ should be verified to meet criteria for the model being run.

$$y_{n,L} = \frac{y^+ \nu}{u_{\tau,L}} \quad (19)$$

where $u_{\tau,L}$ is the friction velocity at point L along the wall. $u_{\tau,L}$ is described by

$$u_{\tau,L} = \sqrt{\frac{\tau_{w,L}}{\rho_f}} \quad (20)$$

where $\tau_{w,L}$ is the wall shear stress at point L, and ρ_f is the fluid density. $\tau_{w,L}$ is described by

$$\tau_{w,L} = C_{f,L} \rho_f u_\infty^2 \frac{1}{2} \quad (21)$$

where $C_{f,L}$ is the skin friction coefficient. It is given for a flat plate by Siemens Digital Industries Software (2017) but for this application, the equation given by Incropera et al. (2007) in equation 22 for fully developed laminar flow in a circular pipe was used as a close approximation.

$$C_f = f/4 = 16/Re \quad (22)$$

Using the Reynolds number in the channels for the 0.8 mm base case, this gives a $y_{n,L}$ of 0.013 mm for $y^+ = 1$, or 0.065 mm for $y^+=5$. Since this is the center of the cell, the total thickness of the first layer needs to be double that or 0.026 mm for a $y^+ = 1$ or 0.13 mm for a $y^+ = 5$.

The final major parameter which is necessary to set, especially considering the small width of the microchannels, is the gap fill percentage. This dictates how far into the internal flow path that the prism layers can take up, maximally. Due to there being prism layer extension on both sides of the channel, the gap fill percentage was set to 0.4, allowing the prism layers to take up 40% of the channel width on either side. A stretching factor of 1.2 was applied (within the 1.1 to 1.5 range recommended). Starting with a first cell thickness of 0.026 mm and expanding each additional layer by 1.2, leaves a maximum of 7 layers for a total thickness of 0.33 mm to attempt a y^+ of approximately 1 for low y^+ wall treatment or 2 layers for a total thickness of 0.286 mm with 2 layers to attempt a y^+ of approximately 5 for all y^+ wall treatment. Due to the nature of the microchannels it is impossible to get a y^+ value of 30 to 50 and therefore a High y^+ treatment is inapplicable. Which wall treatment used is partially dictated by which turbulence model is used, as seen in Table 2 which is further explored in Section 5.2.3. A view of the mesh is shown in Figure 28. This is a cut away view from midway down the depth of the cold plate for a straight channel model.

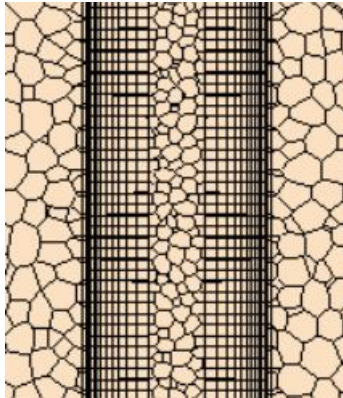


Figure 28: View of Mesh Showing Prism Layer and Tetrahedral Cells

In Figure 28 a single channel section is shown. The outer most layers of irregularly shaped cells on the left and right side of the image are part of the cold plate solid domain. The tightly layered rectangular prism layer cells lining the walls of the channel in the liquid domain with the polyhedral mesh of the liquid domain making up the center 20% of the channel liquid domain. The rectangular prism cells are layered near the wall to provide greater accuracy as to what is occurring near the wall.

5.2.3 Physics Modeling

The liquid and cold plate regimes were defined by models within Star-CCM+. The following model choices were chosen for the solid regime.

- Constant Density - Within the range of temperatures that the solids will be exposed to, the density will not change in a significant way. For the base model a density of 8430.0 kg/m^3 was used as reported by Lan et al. (2021) for their experimental setup for H62 Brass.
- Segregated Solid Energy - The options for energy solving are segregated and coupled. The segregated solid energy model de-couples the energy equations and solves them iteratively rather than as one system of equations, which saves solver time per iteration (SIEMENS Digital Industries Software, 2021). However, each iterative solution is not as close to convergence as each iterative solution for a coupled energy model.
- Steady - Any useful solution for a cold plate system will require a steady state solution, therefore steady modeling was done.
- Three Dimensional - Due to the nature of the model and system the model was conducted as a three dimensional model to capture the total effects.
- Material Properties - Specific heat ($c_{p,solid}$ was set to 381 J/kg-K and thermal conductivity (k_{solid}) was set to 108.86 W/m-K for H62 Brass as defined in the experimental set-up by Lan et al. (2021).

The following model choices were chosen for the liquid regime.

- Water - Water was chosen as the working fluid with an inlet temperature of 293 K and default material properties. Density was calculated using IAPWS-IF97 model properties.
- Segregated Flow and Segregated Fluid Temperature were used to decouple the energy conservation equation and allow for faster solver processing times (SIEMENS Digital Industries Software, 2021).
- Steady - Any useful solution for a cold plate system will require a steady state solution, therefore steady modeling was done.
- Three Dimensional - Due to the nature of the model and system the model was conducted as a three dimensional model to capture the total effects.
- Turbulent - The K-Omega turbulence model was chosen due to the directional changes and flow disruption involved in some of the flow cases. The decision to use the K-Omega turbulence model over the laminar flow models is discussed in Section 4.4.4.6.

5.2.3.1 Turbulence Models

The major options for Reynolds Averaged Navier Stokes Turbulence models given by Star-CCM+ are K-Omega and K-Epsilon turbulence. The difference between how these models solve for what is happening in the fluid flow are to do with the dissipation rate of turbulence (SIEMENS Digital Industries Software, 2021). In the K-epsilon model, an absolute dissipation rate or ϵ is used, versus a relative dissipation rate used in the K-Omega model (ω , which is relative to ϵ/k) (SIEMENS Digital Industries Software, 2021). The weakness of the K-Omega model to variations in the upstream conditions is corrected for by using Menter's modified model which effectively uses K-Epsilon modeling in the inlet/free-stream regions and K-Omega modeling to take advantage of the better near wall performance of that model (SIEMENS Digital Industries Software, 2021). This model choice for K-Omega

(SST (Menter) K-Omega) was activated while using K-Omega models within Star-CCM+. Using the guidelines set out by SIEMENS Digital Industries Software (2021), models were run at different combinations of wall treatment (low and all y^+), different turbulence models, and laminar models. These models were kept to the same parameters with the exception of the turbulence model chosen, and the prism layer characteristics used. The results, compared to the data reported by Lan et al. (2021) are shown in Figure 29.

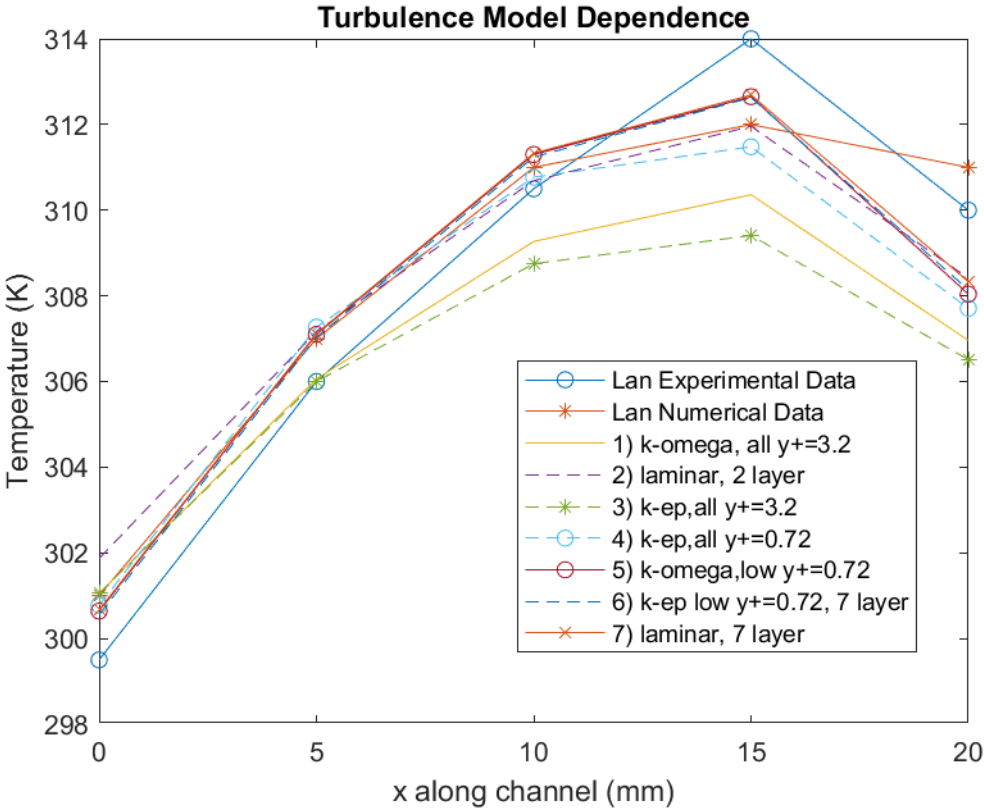


Figure 29: Model Turbulence Dependence

K-Omega models were expected to have better performance due to their increased capability to predict near wall performance. The majority of the increased flow resistance and heat transfer is happening in these near wall regions so the turbulence model with better predictive power is expected to be more accurate in this regime. The best performing models compared to the Lan et al. (2021) numerical and experimental data were the laminar models and the low y^+ models of both K-Omega and K-Epsilon turbulence models. The K-Omega turbulence model with low y^+ wall treatment was chosen because the physics modeling supports it as the more robust choice and the data showed concurrence. Since the equations laid out in Section 5.2.2.1 are to get an approximate y^+ value, the models shown in 5.3 were done using 10 prism layers with a prism layer thickness of 40% of the channel width. This was done to allow the same mesh to be used for all inlet velocity runs of the same geometry for the initial model validations with an approximate y^+ estimation. Since the channel geometry and inlet velocity are variable in the MSLT and those each have an effect on wall y^+ values, more refinement is included in the final tool simulation files to define the prism layer cell thicknesses and number of

layers as accurately as possible. This is explained in detail in Section 4.

5.3 Validation

With model parameters chosen, the model was validated against the Lan et al. (2021) experimental and numerical data.

5.3.1 Channel Wall Temperature Validation

The most specific data given by Lan et al. (2021), and why this paper was chosen for replication, was the streamwise temperature distribution of the bottom of the channel wall. Figure 30 and Table 3 show the numerical and experimental data reported by Lan et al. (2021) as well as the simulation data in the replicated model.

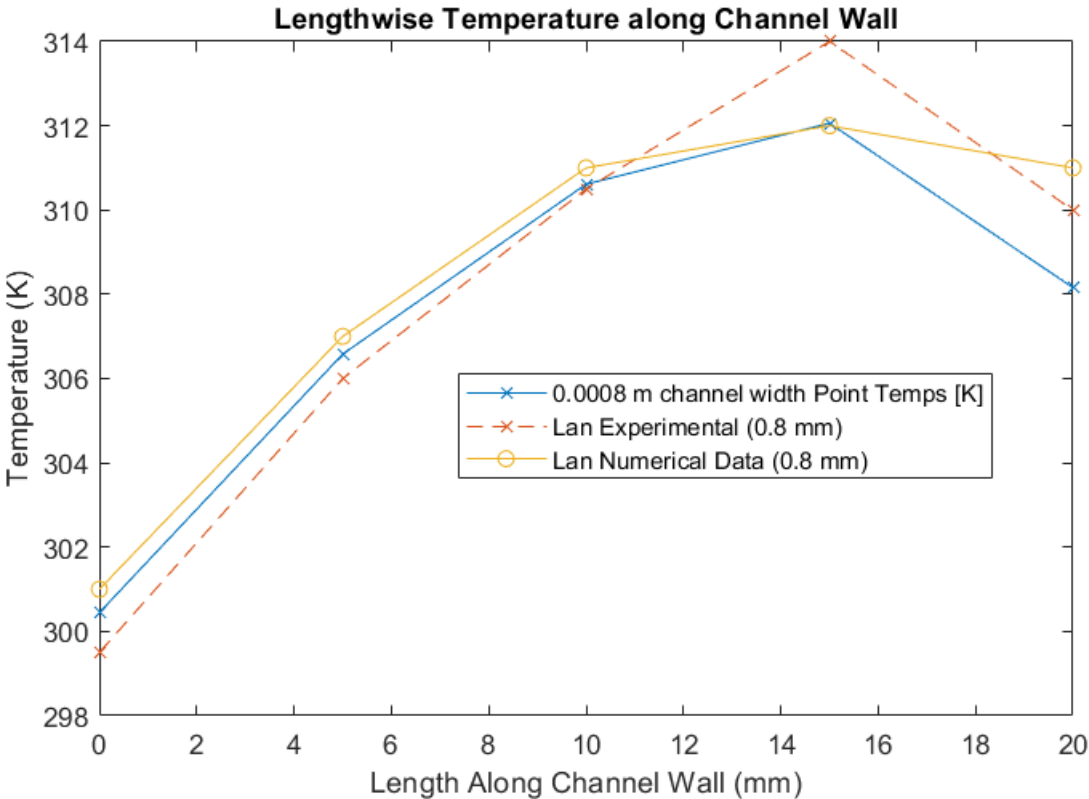


Figure 30: Point Temperatures Along Channel Wall

x along channel wall (mm)	Simulation Temperature (K)	Lan Experimental Temperature (K)	Lan Numerical Temperature (K)
0 mm	300.4 K	299.5 K	301 K
5 mm	306.6 K	306 K	307 K
10 mm	310.6 K	310.5 K	311 K
15 mm	312.1 K	314 K	312 K
20 mm	308.2 K	312 K	311K

Table 3: Temperature Along Channel Wall Validation Data

The data matches very closely from 0 to 10 mm along the length of the channel, at which point my simulation data matches more closely with the Lan et al. numerical data. The over prediction of performance (and under prediction of temperature) from the numerical data in both simulations can be due to imperfections in the cold plate itself causing fouling or less fluid flow along the length of the microchannels. The slope of the temperature matches Lan’s data almost exactly from 15 to 20 mm. This trend matching shows promising results for the accuracy of the model.

5.3.2 Average Wall Temperature Validation

An inlet velocity sweep was run to capture data along the range of channel Reynolds values. Average wall temperature was computed using a numeric mean of the five point temperatures collected from the channel wall. The results are shown in Figure 31.

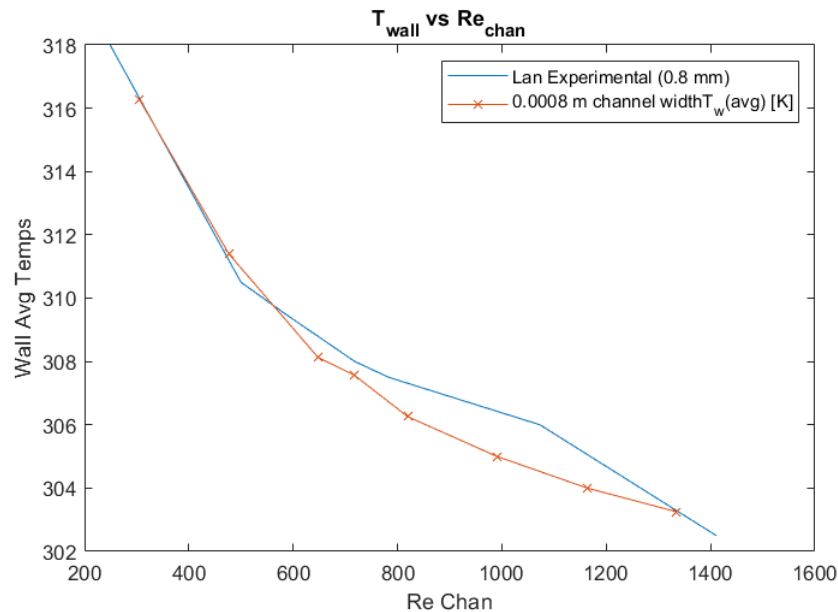


Figure 31: Average Wall Temperature vs Re

Overall, simulation results show good convergence with the reported experimental results by Lan et al. (2021) across the range of Re investigated.

5.3.3 Pressure Validation

Total pressure drop across the cold plate can be represented by (Qu et al., 2006; Lan et al., 2021; Steinke and Kandlikar, 2006)

$$\Delta P = \Delta P_{inlet} + \Delta P_c + \Delta P_{developing} + \Delta P_{fullydeveloped} + \Delta P_e + \Delta P_{outlet} \quad (23)$$

Each of the terms in this equation represent a pressure loss or gain at different points between the inlet of the cold plate domain and the outlet. ΔP_{inlet} is the pressure drop from the inlet to the plenum due to the 90 degree angle between the inlet and the cold plate plenum. ΔP_{outlet} represents a similar pressure drop on the exit of the working fluid from the plenum to the outlet due to the 90 degree angle change (Lan et al., 2021). ΔP_c is the contraction from the plenum to the channels and ΔP_e is the expansion pressure change from the channels to the plenum (Qu et al., 2006). $\Delta P_{fullydeveloped}$ represents the viscous and frictional losses that occur along the fully developed region of the channel ducts while $\Delta P_{developing}$ represent the losses that occur along the entry region of the channel ducts (Qu et al., 2006).

Total pressure drop across a system as represented by Equation 23 can be conceptually described as a summation of reversible pressure changes such as those which occur with velocity changes and irreversible pressure losses such as those which occur due to friction (Blevins, 1984).

$$(p_1 + \frac{1}{2}\rho u_1^2) - (p_2 + \frac{1}{2}\rho u_2^2) = \frac{1}{2}\rho u^2 K + \rho g(z_2 - z_1) \quad (24)$$

Equation 24 shows that the change in static pressure (p_1, p_2) plus the pressure due to velocity between two points (u_1, u_2) is equal to the irreversible losses which occur plus height based hydrostatic losses. In this formula, the constant K represents those static losses and is reported by Blevins (1984) for numerous cases. From equation 24, the different factors that make up equation 23 from the inlet of the cold plate to the outlet of the cold plate can be represented as functions of the generic constant K. K in each of these cases is a function of Re and geometry (Blevins, 1984).

5.3.3.1 Pressure Drop Due to Contraction

There is a pressure loss due to contraction of the flow and the subsequent velocity change of the fluid as it goes from the inlet plenum into the channels. This pressure loss is reflected in Equation 25 as a combination of the pressure change caused by velocity change (which is reversible) and the irreversible loss caused by the contraction itself. For initial case of $u_{inlet} = 0.37018m/s$ and $width_{chan} = 0.8mm$, the flow is developing the entire length of the channel (as calculated by Equation 10), and the $\Delta P_{fullydeveloped}$ is 0 since there is no fully developed portion of channel to account for. This, however, is dependent on the length and width of the channel and must be calculated for each geometry case. ΔP_c and ΔP_e account for contraction from the inlet plenum to the channels, and expansion from the channels to the outlet plenum, respectively. P_c for the laminar flow regime can be calculated using the following formulas presented by Qu et al. (2006) derived from Equation 24

(Blevins, 1984):

$$\Delta P_c = 1/2(\rho_f(u_m^2 - u_p^2)) + \frac{K_c}{2}\rho_f u_m^2 \quad (25)$$

u_m is the channel average velocity and u_p is the plenum average velocity, both assumed to be constant given the volumetric flow rate and cross-sectional area of the channels and the plenum, respectively. For the laminar flow regime, K_c , or the contraction loss coefficient is given as the loss coefficient for an inlet of the same geometry as the smaller duct (or channels in this case of contraction from the plenums to the channel inlets) (Blevins, 1984). K_c is presented by Qu et al. (2006) in Equation 26 for the laminar flow regime:

$$K_c = 0.6740 + 1.2501\alpha_c + 0.3417\alpha_c^2 - 0.8358\alpha_c^3 \quad (26)$$

Equation 26 is an approximation derived from experimental data presented by Blevins (1984). If the flow is turbulent, there is a different value for K_c that is reported by Blevins (1984) which takes into account flow from a plenum into multiple channels. In the turbulent regime $K_{c,turbulent}$ is calculated by Equation 27:

$$K_{c,turbulent} = \frac{1}{2}\left(1 - \frac{A_{ch}}{A_p}\right) \quad (27)$$

The difference between laminar flow pressure drop and turbulent flow pressure drop is due to flow separation that is more likely to occur at the entrance of the flow contraction due to turbulence (Blevins, 1984). Equation 26 does not take into account flow from a plenum into multiple channels and rather is the irreversible loss coefficient for an inlet of the size and shape of a single channel, however, due to the flow being in the laminar regime it is assumed to be smooth entering the channels and therefore have the same pressure losses as contraction into a single inlet (Blevins, 1984). This may or may not be the case for any given inlet and plenum geometry depending on the length of the plenum and how the flow develops prior to entering the channels and may be one source of error which is causing the simulation observed pressure drop to be higher than the theoretical pressure drop based on laminar flow.

If the aspect ratio as given by Equation 5 is greater than one, the aspect ratio used in the pressure drop equations must be the inverse (Steinke and Kandlikar, 2006).

5.3.3.2 Pressure Drop Due to Expansion

ΔP_e , which represents the pressure change due to expansion from the channels to the plenum, is also derived from Equation 24 (Blevins, 1984; Qu et al., 2006).

$$\Delta P_e = 1/2(\rho_{w,f}(u_p^2 - u_m^2)) + \frac{K_e}{2}\rho_{w,f}u_m^2 \quad (28)$$

u_p is the average plenum fluid velocity and u_m represents the average channel fluid velocity. K_e is the expansion coefficient which is presented by Blevins (1984) for abrupt expansion. This is the formula for the expansion coefficient regardless of Re due to the fact that the flow separation and eddy formulation does not occur when the flow is exiting the channels and combining into the outlet plenum

the same way it does when flowing from inlet plenum into the channels.

$$K_e = (1 - A_{ch}/A_p)^2 \quad (29)$$

and A_{ch} and A_p are the total cross-sectional areas of the channels and the plenums, respectively.

5.3.3.3 Pressure Drop Due to Friction Losses

The flow along the length of the channels will experience pressure losses due to friction as the fluid moves throughout the channel. The friction factor is dependent on whether the flow is fully developed or still developing. This is handled differently in the variety of studies that analyze the pressure drop along microchannels. Many researchers ignore the developing effects and assume the flow to be fully developed along the entire length of the microchannel, which may be the case for an idealized single channel simulation with a fully developed inlet condition, however is unlikely to be the case in any real world cold plate. Steinke and Kandlikar (2006) identified this discrepancy and noted in their literature review that studies that do not ignore entrance effects of developing flow have significantly less discrepancy between theoretical and experimental results than studies that ignore these effects. The theory and calculations are presented for both fully developed flow and developing flow here.

The friction factor, f , is a non-dimensional term which represents a ratio of shear stress at the wall to kinetic energy for a flow (Shah and London, 1978). It is defined by the local shear stresses which take into account the local velocity profiles within the fluid flow and therefore has been transformed into more usable formats for describing pressure drop, known as the apparent friction factor or f_{app} (Shah and London, 1978).

For laminar, fully developed flow in a rectangular duct, the following formula, as presented by Shah and London (1978) can be used as an approximation for the fully developed friction factor multiplied by Re (which is also equal to Po (Steinke and Kandlikar, 2006)), which is a constant based on aspect ratio

$$fRe = 24(1 - 1.3553\alpha_c + 1.9467\alpha_c^2 - 1.7012\alpha_c^3 + 0.9564\alpha_c^4 - 0.2537\alpha_c^5) \quad (30)$$

Equation 31 presented by Qu et al. (2006) is an approximation for flow in the developing region which is based off data presented by Shah and London (1978). Equation 31 takes the fRe , or Pouisselle number, presented here for fully developed flow, as well as aspect ratio and hydrodynamic entry length into account to determine the apparent friction factor of a given rectangular duct

$$f_{app} = \frac{1}{Re_{ch}} \left(3.44(L_d^+)^{-0.5} + \left(\frac{K(\infty)}{4L_d^+} + fRe_{ch} - 3.44(L_d^+)^{-0.5} \right) / (1 + C(L_d^+)^{-2}) \right) \quad (31)$$

where L_d^+ is a non-dimensional hydrodynamic entry length based purely on aspect ratio of a rectangular duct. Qu et al. (2006) presents the following equation based on data presented in Shah and London (1978):

$$L_d^+ = (0.06 + 0.07\alpha_c - 0.04\alpha_c^2) \quad (32)$$

There are a number of researchers data presented by Shah and London (1978) but the self-purported most accurate values used by Winginton and Dalton are used for the L_d^+ value in Equation 32.

In Equation 31 $K(\infty)$ and the coefficient C are based on aspect ratio of the channels (α_c). $K(x)$ refers to the Hagenbach factor which corrects the friction experienced by fluid flow in the developing region where as $K(\infty)$ refers to friction experienced by the fluid flow in the developed region. $K(\infty)$ is used as an approximation for both the developing region and fully developed region in the following equations (Steinke and Kandlikar, 2006).

Similarly to the values for L_d^+ being varied based on research data presented, there are a variety of analytical values presented for $K(\infty)$. $K(\infty)$, also known as the pressure defect term or incremental pressure drop number, refers to pressure loss attributed to the accumulation of wall shear (Shah and London, 1978). $K(\infty)$ refers to this value throughout the fully developed region, but value grows throughout the developing region (Shah and London, 1978). Shah and London (1978) presents data from multiple sources and claims that the correlations given by Miller and Han most closely fit well accepted experimental data. This data is fit by Equation 33 presented as an approximation by Qu et al. (2006).

$$K(\infty) = (0.6740 + 1.2501\alpha_c + 0.3417\alpha_c^2 - 0.8358\alpha_c^3) \quad (33)$$

C , for use in Equation 31 is defined by Qu et al. (2006) to fit the data presented by Shah and London (1978) as

$$C = (0.1811 + 4.3488\alpha_c - 1.6027\alpha_c^2)10^{-4} \quad (34)$$

5.3.3.4 Pressure Drop Due to Flow Direction Change at Inlet and Outlet

ΔP_{inlet} and ΔP_{outlet} are defined by Lan et al. (2021) as

$$\Delta P_{inlet+outlet} = 2 * K90(A_c/A_p)^2$$

for the 90 degree bend from the inlet to the plenum, and plenum to the outlet, with K90 being approximately 1.2. While the 90 degree directional change induces pressure losses that might be avoided with an in-plane inlet, many of the experimental setups across the literature included a inlet to plenum directional change of 90 degrees. Therefore, this setup was chosen to reflect similar setups across the literature.

5.3.3.5 Combined Formula for Pressure Drop in Straight Channels

This leaves a combined formula presented by Lan et al. (2021) as

$$\Delta P_{total} = \frac{\rho_w f u_{chan}^2}{2} \left[\left(\frac{A_c}{A_p} \right)^2 (2K90) + (K_c + K_e) + \frac{4f_{app}L}{D_h} \right] \quad (35)$$

where D_h is hydraulic diameter as described in Equation 4 and f_{app} is apparent friction factor as described by Equation 31. This formula is applicable in the laminar regime when the entire entry length of the channel is in the developing regime. If there is any part of the channel in the fully developed regime, then the term accounting for shear losses ($\frac{4f_{app}L}{D_h}$) is replaced by

$$\frac{4f_{app}L_{entry}}{D_h} + \frac{4fL_{fd}}{D_h}$$

where L_{entry} is the hydrodynamic entry length and L_{fd} is the fully developed region of the channel (or equal to channel length less the entry length, L_{entry}) (Qu et al., 2006). f in this term is the fully developed friction factor which can be found by dividing the result of Equation 30 by the channel Reynolds number.

The theoretical values calculated using the formulas above are presented graphically in Figure 32. The theoretical pressure drop is underpredicted, especially as the Reynolds number grows. This is likely due to the laminar nature of the equations. While the flow is technically in the laminar regime, based on the Reynolds number, the flow disruption caused by the inlet direction change, and the contraction into channels is likely to cause turbulent behavior and thus greater pressure drops. One specific example of this is that while not officially in the laminar regime, the flow is likely separating from the wall as it enters the channels and developing turbulent eddies along the wall (one of the phenomena that causes an increased pressure drop and the difference in values for K_c between the turbulent and laminar regimes) (Blevins, 1984). Additionally, Equation 23 does not account for frictional losses along the length of the plenums. This value is likely small as the velocity within the plenums is very small in comparison to the velocity within the channels, but it is likely leading to the underprediction as the Re of the simulation grows and the speed within the plenums grows with it. This value could be approximated by using an approach similar to Equation 31 to determine the apparent friction factor within the plenum and calculating the equivalent pressure drop within that region of flow, however this wouldn't be precise as the flow path isn't smooth or direct within the plenum region.

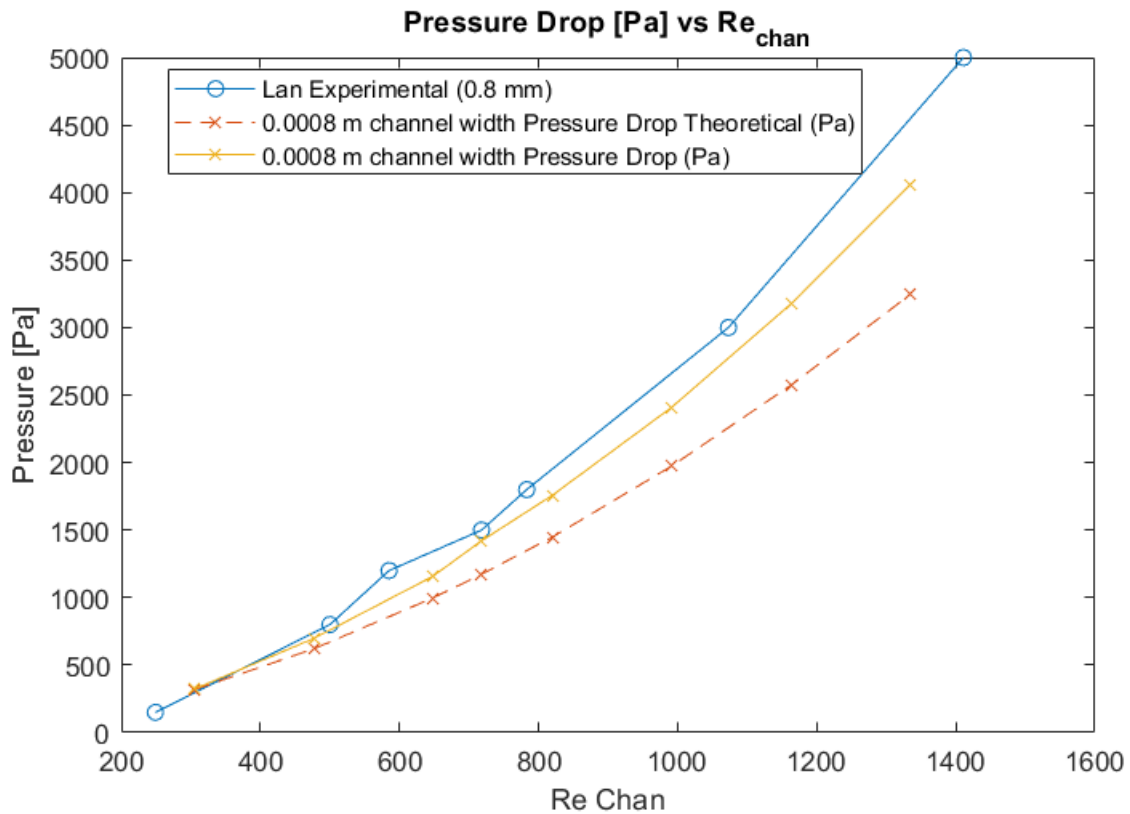


Figure 32: Numerical and Theoretical Pressure Drop

In Figure 32, the blue line is the experimental results reported by Lan et al. (2021), the yellow line is the results from the simulations run in Star-CCM+ and the red dashed line is the theoretical pressure drop calculated using the equations laid out in this section.

5.3.4 Nusselt Number Validation

The Nu_{avg} calculation was reported by Lan et al. (2021) using the following formulas.

The equations for h_{avg} and Nu_{avg} used are as follows from Lan et al. (2021)

$$h_{avg} = \frac{q}{A_{eff}(T_{w,avg} - T_{f,avg})} \quad (36)$$

$$Nu_{avg} = h_{avg}D_h/k_f \quad (37)$$

From Lee et al. (2012) A_{tot} is described as the total area to use for heat transfer in Equation 38, and is calculated by using fin efficiency and the surface area of the ‘fin’ which in this case is the walls of the microchannel. Many of the papers use this type of expression modeling the microchannel walls as adiabatic tipped fins and use fin efficiency correlations. In a normal cold plate setup, the tip of the fin would be considered conductive to the outside environment but since the boundary conditions of these simulations are defined such that all outside boundaries are adiabatic the adiabatic fin tip approximation applies.

$$A_{tot} = (N_{fin} + 1)length_{chan}(width_{ch} + 2\eta_{fin}height_{chan}) \quad (38)$$

where N_{fin} is the number of fins and therefore $N_{fin} + 1$ is the number of fin surfaces in contact with fluid flow and also equal to the number of channels. Using N as the number of channels, A_{eff} can be described as

$$A_{eff} = Nlength_{chan}(width_{chan} + 2\eta_{fin}height_{chan}) \quad (39)$$

And η_{fin} is described by Lienhard IV and Lienhard V (2019) and Incropera et al. (2007)

$$\eta_{fin} = \tanh(mheight_{chan})/mheight_{chan} \quad (40)$$

where m is calculated using formula 41, presented by Incropera et al. (2007)

$$m = \sqrt{height_{chan}P/k_sA_c} \quad (41)$$

where h is the heat transfer coefficient, P is the perimeter of the fin, k_{solid} is the cold plate solid k and A_c is the cross sectional area of the fin.

P is defined as

$$P = 2(height_{chan} + length_{chan}) \quad (42)$$

Due to the fact that there is a value for h inside of the arctan in the definition for m , which goes into fin efficiency and ultimately Nu_{avg} , h is difficult to solve for directly. A recursive function was

implemented in Matlab to solve for it iteratively, starting with a value of $10000 \text{ W/m}^2\text{-K}$ for h , and solving until the h value implemented matched the resulting h_{avg} . Figure 33 shows the results of the Nu_{avg} calculations.

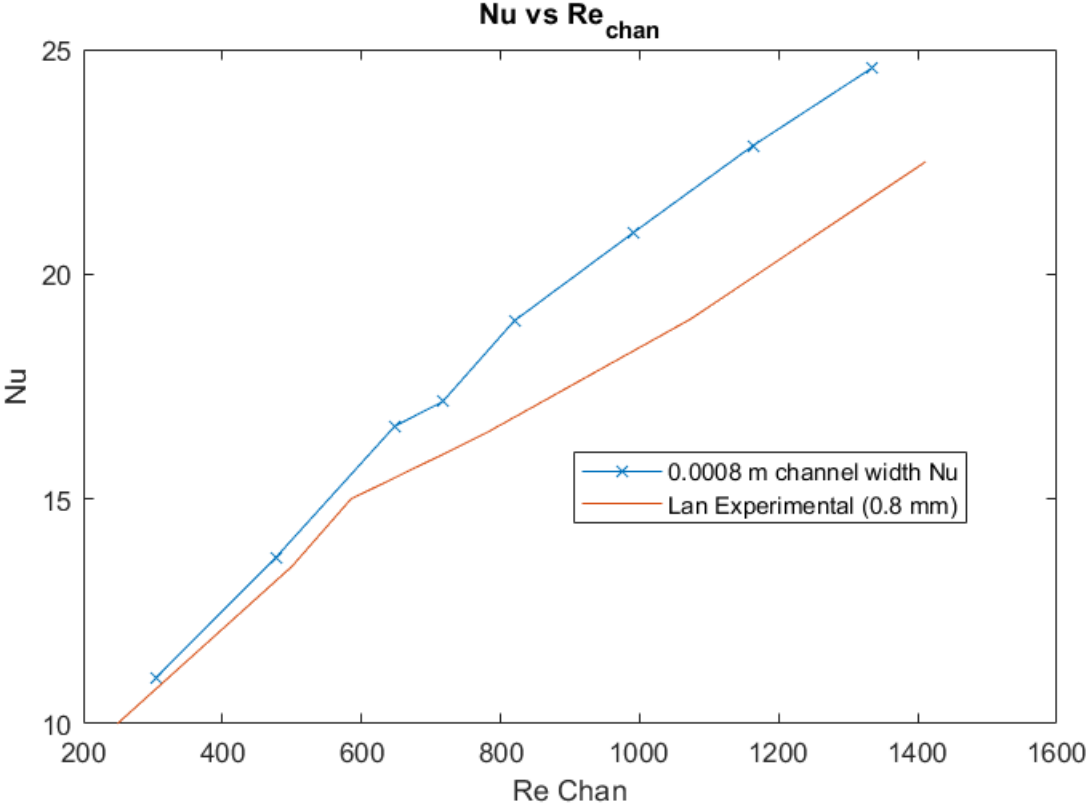


Figure 33: Average Nu vs Re

The simulation results shown in blue and the Lan et al. (2021) experimental results show good trend matching showing further validation of the model and Nu calculation methods.

5.4 Validation Lessons Learned

The validation shown in sections 5.3.1 through 5.3.4 shows good agreement with the results reported by Lan et al. (2021). This validates the model choices made to include the symmetric plane cutting, turbulence model choices, and meshing characteristics. These model choices serve as the baseline for future simulation runs, including different geometries included in the simulation library. Further validation and analysis for each geometry is included in subsequent sections.

6 Comparative Analysis of Features

To serve as a baseline of comparison between the geometries, each geometry was run at equivalent boundary, flow and heat application conditions. This was also to ensure an apples-to-apples comparison to the other sweeps run, with the appropriate number of channels, same inlet velocity/temperature and same heat condition.

For each of these simulations, the fin width was equal to the channel width and the channel depth was kept to a constant 1.2 mm. The straight channel sweep is the baseline to which the other models are compared. Each simulation was run delivering 31.25 W/cm^2 for a total of 125 W of heat flow into the system from the heater surface. All other external solid boundaries were adiabatic. The inlet was supplied with 0.4 m/s fluid flow of water at 293 K through the constant 3 mm radius inlet to keep the total volumetric flow rate of water constant across all simulations. The outlet was set to an atmospheric pressure condition.

Section 6.1 details each geometry individually, varying appropriate parameters to explore the nuances of that geometry. Section 6.2 compares the performances of the different geometries to one another. Section 6.3 provides a deeper investigation into the physical phenomena influencing the results

6.1 Baseline Sweep Variations

For the baseline sweeps, channel widths were varied from 0.4 mm to 1.2 mm wide, with the subsequent number of channels varying from 29 channels across to 9 channels across.

6.1.1 Straight Channel Baseline Sweep

No additional geometric augmentations were conducted with the straight channel baseline sweep other than varying channel width. Inlet velocities were also varied for the 0.6 to 1.2 mm channel widths. The cases run with initial results are shown in Table 4 and in Figures 41 and 42.

Channel Width	Number of Channels	Inlet Velocity	Pressure Drop (Pa)	Max Cold Plate Temp (K)
0.6 mm	19	0.1 m/s	234 Pa	328.1 K
0.6 mm	19	0.25 m/s	920 Pa	318.5 K
0.6 mm	19	0.4 m/s	1891 Pa	315.0 K
0.6 mm	19	0.55 m/s	3190 Pa	312.8 K
0.6 mm	19	0.7 m/s	4752 Pa	311.3 K
0.8 mm	15	0.1 m/s	174 Pa	333.1 K
0.8 mm	15	0.25 m/s	722 Pa	322.0 K
0.8 mm	15	0.4 m/s	1616 Pa	317.3 K
0.8 mm	15	0.55 m/s	2780 Pa	314.7 K
0.8 mm	15	0.7 m/s	4075 Pa	312.9 K
1.0 mm	11	0.1 m/s	165 Pa	336.2 K
1.0 mm	11	0.25 m/s	720 Pa	323.9 K
1.0 mm	11	0.4 m/s	1660 Pa	318.5 K
1.0 mm	11	0.55 m/s	2747 Pa	315.6 K
1.0 mm	11	0.7 m/s	4162 Pa	313.8 K
1.2 mm	9	0.1 m/s	152 Pa	340.8 K
1.2 mm	9	0.25 m/s	710 Pa	325.7 K
1.2 mm	9	0.4 m/s	1614 Pa	320.1 K
1.2 mm	9	0.55 m/s	2680 Pa	317.0 K
1.2 mm	9	0.7 m/s	4103 Pa	315.1 K

Table 4: Straight Channel Sweep Cases

In general, the maximum cold plate temperature was lower and the pressure drop was higher for decreased channel widths. Increased mass flow rate had a similar effect, with increased mass flow rate causing lower maximum cold plate temperatures and increased pressure drops. Further discussion is in Section 6.3.2.

6.1.2 Inline Pin Fin Sweep

The inline pin fin geometry was run at 30, 60, and 90 degree geometries, as shown in Figure 34 with the pin fin lengths, widths and fin spacing equal to the channel widths for channel widths from 0.4 mm to 1.2 mm.

The number of pins fins along the length of each channel was calculated by using

$$n_{fins} = \text{floor}(\text{length}_{chan} / (\text{length}_{fin} + \text{spacing}_{fin})) \quad (43)$$

where spacing_{fin} is the longitudinal distance between each of the fins.

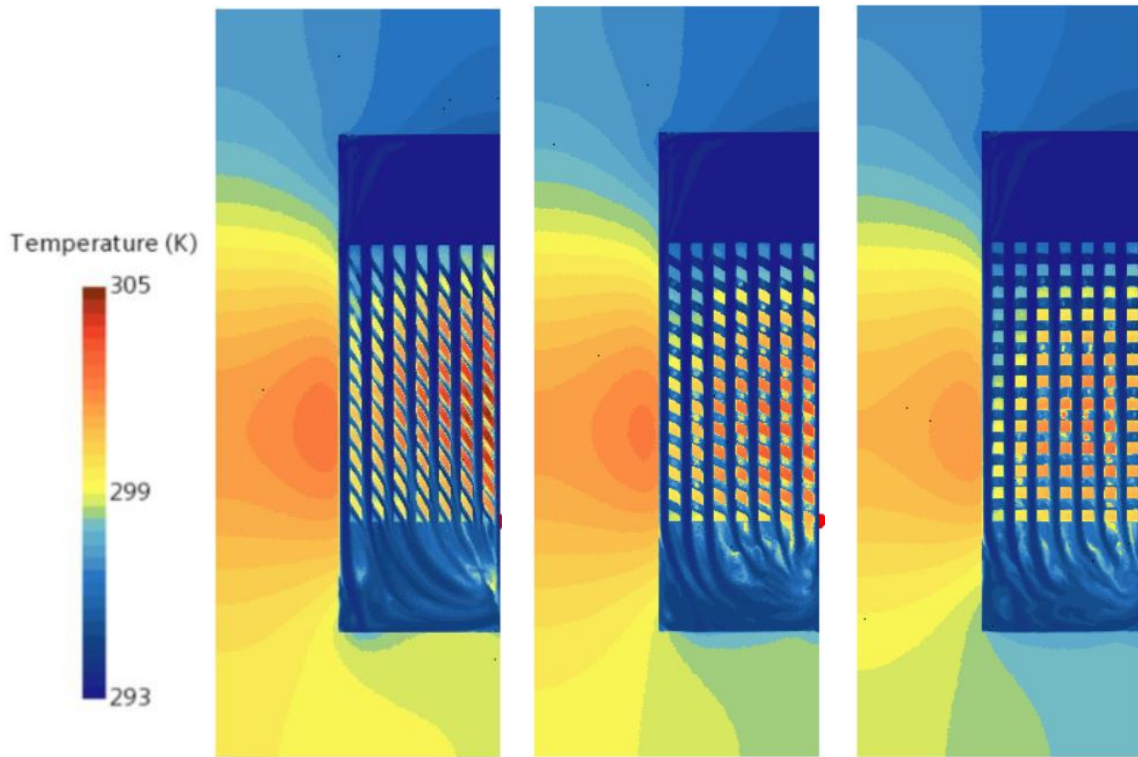


Figure 34: 30, 60 and 90 degree angled fins with 0.8 mm channel widths

The cases and initial results are shown in Table 5.

Channel Width	Number of Channels	Pin Angle (Degrees)	Pressure Drop (Pa)	Max Cold Plate Temp (K)
0.4 mm	29	30	3504 Pa	308.7 K
0.4 mm	29	60	3232 Pa	309.5 K
0.4 mm	29	90	3152 Pa	309.1 K
0.6 mm	19	30	2264 Pa	311.2K
0.6 mm	19	60	2231 Pa	311.9 K
0.6 mm	19	90	2366 Pa	311.5 K
0.8 mm	15	30	1684 Pa	314.5 K
0.8 mm	15	60	1838 Pa	313.9 K
0.8 mm	15	90	1965 Pa	312.7 K
1.0 mm	11	30	17756 Pa	315.0 K
1.0 mm	11	60	2005 Pa	314.9 K
1.0 mm	11	90	1974 Pa	313.6 K
1.2 mm	9	30	1638 Pa	317.4 K
1.2 mm	9	60	1798 Pa	316.6 K
1.2 mm	9	90	1978 Pa	315.9 K

Table 5: Pin Fin Sweep Cases

In general, the same trends were seen as with the straight channel, with increased channel width showing increased Maximum Cold Plate Temperature, and decreased pressure drop. There was no significant trend in the pressure drop across pin angles with the same channel widths. The fin angle for inline pin fins does not significantly affect the cross-sectional flow and there is not a significant surface area difference between each angled geometry. This is seen in Figure 44 and is further discussed in Section 6.3.3.

6.1.3 Zig-Zag Sweeps

Three different sweeps were conducted for the Zig-Zag Geometry to identify the mechanisms causing pressure drop variations. For the initial baseline zig-zag sweep, the zig offset was kept at 40% of the channel width and channel widths were varied from 0.4 mm to 1.2 mm with a consistent inlet velocity of 0.4 m/s. Zig height was maintained at 5 mm. For these sweeps, the whole zig-zag geometry was used rather than the half symmetric model as the model is not actually symmetric about the centerline for zig-zag geometry. Cases and initial results are presented in Table 6.

Channel Width	Number of Channels	Zig Offset (mm)	Pressure Drop (Pa)	Max Cold Plate Temp (K)
0.4 mm	29	0.16 mm	2574 Pa	311.8 K
0.6 mm	19	0.24 mm	2000 Pa	314.1 K
0.8 mm	15	0.32 mm	1744 Pa	315.9 K
1.0 mm	11	0.4 mm	1764 Pa	316.1 K
1.2 mm	9	0.48 mm	1956 Pa	316.7 K

Table 6: Zig-Zag Channel Width Sweep

Expected maximum cold plate temperature trends are seen with increased channel width leading to increased maximum cold plate temperatures. However, an interesting phenomenon is seen with the pressure drops. The pressure drop results are shown in Figure 35.

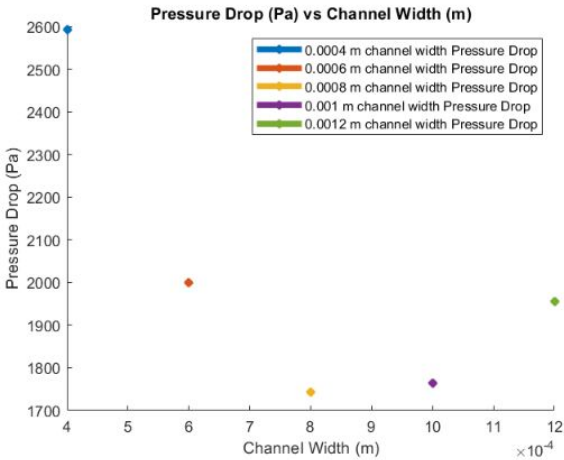


Figure 35: Surface Average Pressure Drop from Inlet to Outlet compared to Channel Width

With each other geometry, a general monotonic trend is seen showing increased pressure drop with decreased channel width. The parabolic trend shown in Figure 35 is a factor of aspect ratio, flow disruption, channel width, and channel velocity which each independently affect pressure drop. These phenomena are discussed in more detail in Section 6.3.4.

As a further exploration of the results seen in Figure 35, to tease out the relationship between horizontal flow disruption and performance, a sweep was conducted maintaining channel width at 1.0 mm and varying horizontal offset between 0.16 mm to 0.48 mm. The cases and results for the Zig-Zag Offset Sweep are presented in Table 7. This data is further discussed and plots are shown in Section 6.3.4. Data fluctuates slightly with each iteration as the solution converges, and in the case of absolute pressure, this fluctuation can have consequences if looking at modest changes, as explained in Section 4.4.4. In general, a limitation of model convergence is an oscillation about a stable pressure drop value which is small in absolute magnitude, but can be significant when looking at modest pressure drop changes such as the ones discussed in Table 7. Since the trend showed modest increase in pressure drop with increase in horizontal offset, the average of the last 100 runs for each simulation was used to get a more accurate picture of the pressure drop across the cold plate.

Channel Width	Number of Channels	Zig Offset (mm)	Averaged Pressure Drop (Pa)	Max Cold Plate Temp (K)
1.0 mm	11	0.16 mm	1668 Pa	317.7 K
1.0 mm	11	0.24 mm	1739 Pa	317.2 K
1.0 mm	11	0.28 mm	1757 Pa	317.0 K
1.0 mm	11	0.32 mm	1796 Pa	316.7 K
1.0 mm	11	0.36 mm	1818 Pa	316.5 K
1.0 mm	11	0.4 mm	1825 Pa	316.1 K
1.0 mm	11	0.48 mm	1971 Pa	315.0 K

Table 7: Zig-Zag Offset Sweep

For all factors remaining equal with the exception of horizontal offset, the pressure drop increases slightly with increased horizontal offset. Additionally, a modest but monotonic drop in Maximum Cold Plate Temperature is also seen with the increased flow disruption caused by increased horizontal offset.

In further exploration of this concept, a final zig-zag sweep was conducted maintaining constant horizontal offset of 0.32 mm for changing channel widths from 0.6 mm to 1.2 mm. The cases and results for the channel width with constant offset sweep are shown in Table 8.

Channel Width	Number of Channels	Zig Offset (mm)	Pressure Drop (Pa)	Max Cold Plate Temp (K)
0.6 mm	19	0.32 mm	2080 Pa	313.6 K
0.8 mm	15	0.32 mm	1737 Pa	315.8 K
1.0 mm	11	0.32 mm	1824 Pa	316.7 K
1.2 mm	9	0.32 mm	1695 Pa	318.5 K

Table 8: Zig-Zag Channel Width with Constant Offset

While maintaining a constant offset, pressure drop does not follow a monotonic trend for channel width due to competing factors of horizontal flow disruption, channel width, aspect ratio and channel velocity. This is further explored in Section 6.3.4.

6.1.4 Channels With Cavities Sweep

For the initial fan cavity sweep, the C value, or cavity offset, was kept to 0 and therefore symmetrical channels were used. Fan radii were set to default to 40% of the channel width to ensure that the geometry of the fin would not cross the symmetry plane. E , or the depth off the channel, was equal to the radius. The cases and initial results for the baseline cavity sweep are shown in Table 9.

Channel Width	Number of Channels	Fan Radius (mm)	Pressure Drop (Pa)	Max Cold Plate Temp (K)
0.4 mm	29	0.16 mm	4321 Pa	316.4 K
0.6 mm	19	0.24 mm	1906 Pa	312.7 K
0.8 mm	15	0.32 mm	1696 Pa	314.4 K
1.0 mm	11	0.4 mm	1658 Pa	316.9 K
1.2 mm	9	0.48 mm	1629 Pa	319.8 K

Table 9: Channels With Cavities Width Sweep

In general, with the exception of the 0.4 mm wide channel case, increased channel width lead to increased Maximum Cold Plate Temperatures and decreased pressure drops. There are a number of reasons for the discrepancy seen with the 0.4 mm wide case. The benefit of the cavities is in excess surface area in contact with the fluid flow and increased flow mixing, but with cavity size being tied to the channel width, the benefit may be too minimal with the 0.4 mm channel widths to cause flow disruption sufficient to lowering the maximum cold plate temperature.

6.2 Comparative Results

Pressure drop, Temperature Rise Factor (TRF) as defined by Equation 14, and maximum cold plate temperature are the basic metrics used to compare the performance of the cold plates to each other. For simplicity in display, the performance of the 60 degree angled pin fins was chosen as a representative fin case since there was not a significant difference in performance between the pin angle cases.

Figure 36 shows the TRF compared to the number of channels for each of the four geometries' channel width sweeps. For the results shown in Figure 36 the inlet velocity was 0.4 m/s and the parameters

were as described in the initial channel width sweeps for each geometry as described in Tables 4, 5, 6, and 9.

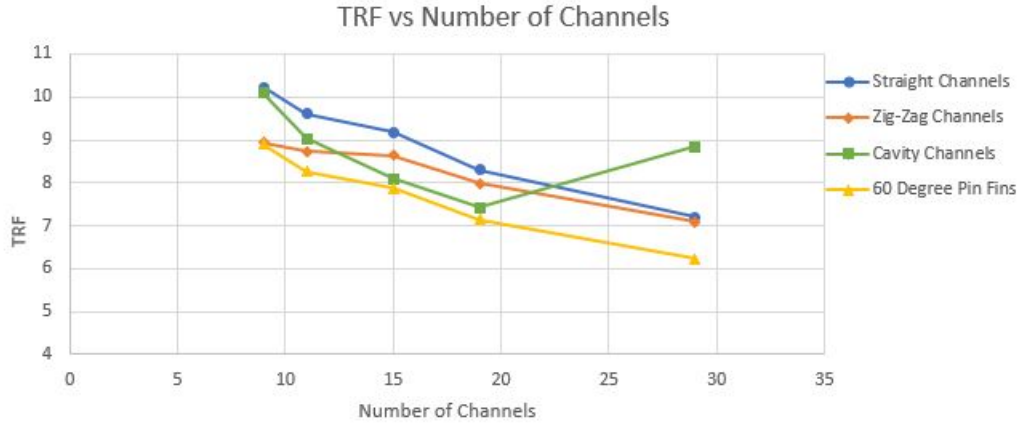


Figure 36: Temperature Rise Factor Compared to Number of Channels for Baseline Geometries

Figure 37 shows the maximum temperature in the solid cold plate domain for each geometry compared to the number of channels.

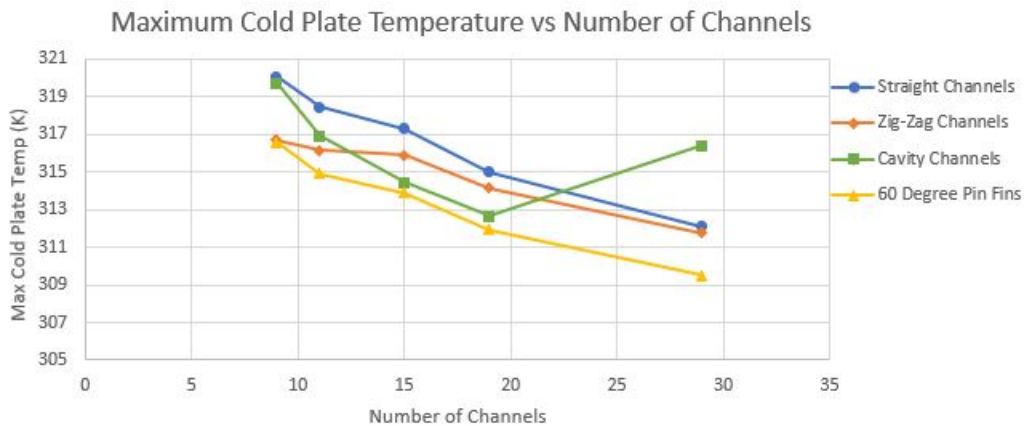


Figure 37: Maximum Cold Plate Temperature Vs Number of Channels

Generally, the TRF and Maximum Cold Plate Temperatures decrease with the number of channels, or with decreased channel width, for all geometries. In general, increased surface area leads to increased heat transfer surface contact with the working fluid. Due to the fact that the bulk of the heat transfer occurs within the layer directly in contact with the cold plate interface, increased surface area contact leads to increased heat transfer from the cold plate to the working fluid and decreased Maximum Cold Plate Temperatures.

There are a couple of notable deviations from this seen in Figure 36. The 0.4 mm channel width channel with cavities data point is reflecting a higher TRF. This is likely due to the cavities being too

small of a physical deviation to influence flow disruption but causing stagnation in heat transfer. Additionally, the zig-zag channels sweep is not showing a monotonically decreasing TRF with increased number channels. Because of the way that zig offsets were dependent on channel width for the zig-zag channel width sweep, there are competing factors at play as channel width decreases. The magnitude of flow disruption is decreased as channel width decreases, but the surface area is increased. These are competing factors to decreasing temperature rise.

Figure 38 shows the pressure drop from the inlet to the outlet across the entire cold plate compared to the number of channels for each geometry.

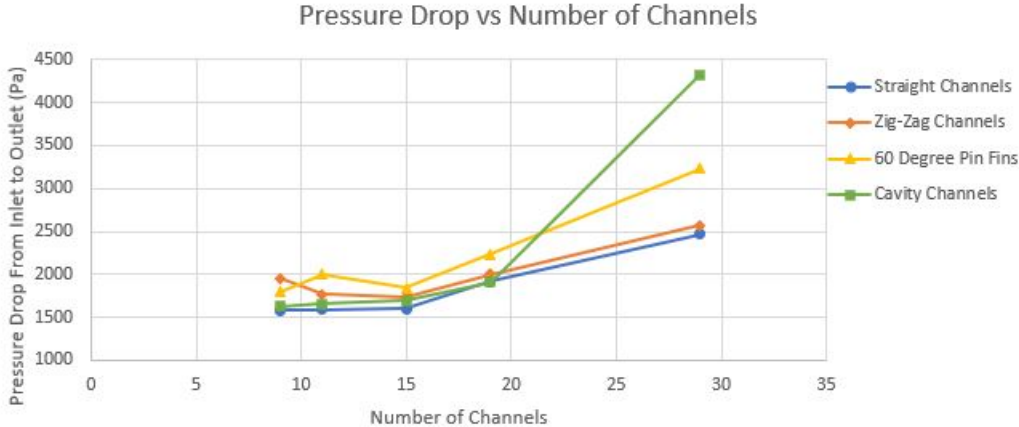


Figure 38: Total Cold Plate Pressure Drop (Pa) compared to the Number of Channels

Similar to TRF decreasing for increasing number of channels, increased pressure drop is generally seen for increased number of channels. With more surface area in contact with the fluid, the friction drag along the fluid flow path increases. A notable exception to this is the zig-zag channels. This almost parabolic pattern is explored in depth in Section 6.3.4 and is a product of competing factors of flow disruption, channel aspect ratio, channel velocity and surface area contact area.

As a metric of cold plate performance compared to cost, TRF vs pressure drop is plotted for each of the four main geometries in Figure 39.

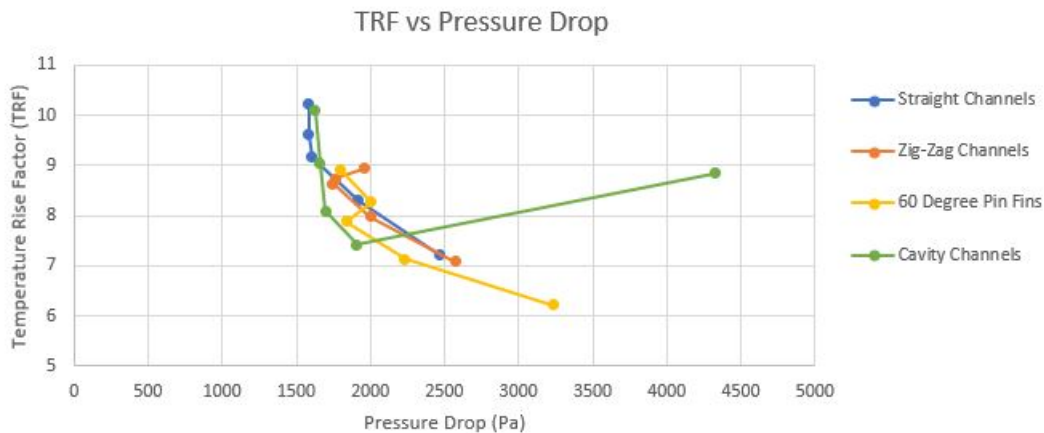


Figure 39: TRF vs Pressure Drop for baseline geometries

As seen in Figure 39, the enhanced geometric features almost universally performed better than the straight channels by producing a lower temperature rise factor and maximum cold plate temperature. However, this came at an equally universal pressure drop increase. This has been seen in virtually all studies presented on microchannel cold plates and geometric enhancements. In general, the pin finned channels performed best by producing the lowest amount of temperature rise. Channels with cavities, however, produced a lower TRF for all channel widths greater than 0.4 mm while maintaining a similarly low pressure drop as straight channels, so may be an option for exploration for cold plate designers looking to maintain a low pressure drop while enhancing heat transfer. Figure 39 serves as a cost benefit analysis and is reflective of the type of decision making data thermal engineers would need when assessing the merits of a cold plate design for their particular set-up. The non-monotonic nature of the trend lines of the zig-zag channels and pin-fins reflect some disparities in competing physical phenomena affecting pressure drop as further discussed below in section 6.3.

6.3 Physical Phenomena Influencing Results

The primary factors influencing the different performance of each geometry are explored in this section. Variations on the baseline sweeps run in Section 6.2 were used to explore the physical phenomena causing the results seen.

6.3.1 Effect of Surface Area on Heat Transfer

Effective heat transfer between the solid substrate of the cold plate and the working fluid itself relies on forced convection from the working fluid boundary with the cold plate surfaces. The heat transfer occurs within the thermal boundary layer of the working fluid at the cold plate walls. Smaller microchannels allow for more surface area in contact with working fluid for the same volumetric area taken up by the cold plate. This general trend with a couple of discrepancies can be seen in Figure 37. With smaller microchannels and consequently more microchannels available across the same size cold plate, maximum cold plate temperatures decreased. Additionally, the geometries of the channels themselves allow for more fin surface area within the cold plate, even for the same channel widths and thicknesses. Straight channels have, by default, the least amount of fin surface area for any given

channel width. Zig-Zag channels have slightly more surface area due to the length of the flow path of the channel being slightly longer due to channel re-direction along the same channel laydown length of 20 mm long. The channels with semi-circular cavities have excess surface area in the form of the semi-circular divets providing more surface area compared to the equivalent straight section the cavities replace. Finally, the pin fins have significantly more surface area in contact with fluid flow especially at lower channel widths which contain many more pins. Figure 40 shows the relationship between TRF and surface area in contact with the fluid flow. The surface area is defined as the area within the channels region in contact with the fluid to include the sides of the channel walls and the channel floor. The plenum areas are not included as they are the same for all similar cases and not geometry dependent and the bulk of the heat transfer occurs along the channel regions.

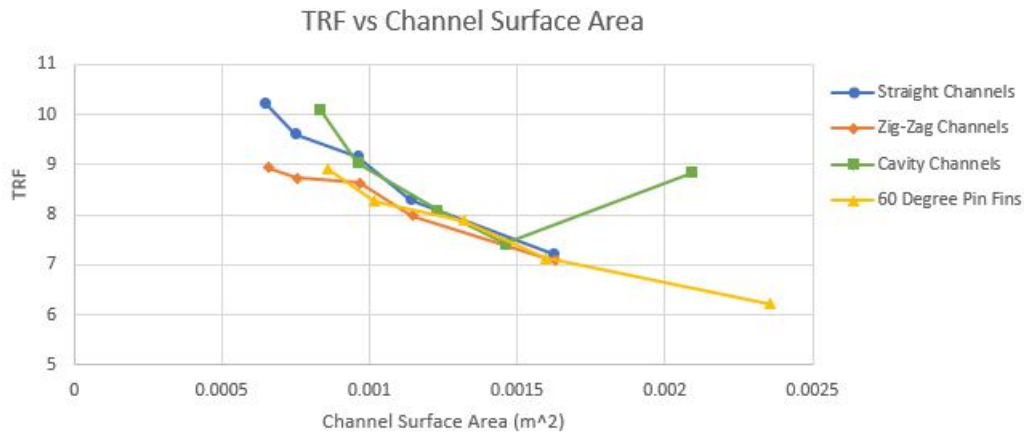


Figure 40: Relationship Between TRF and Surface Area

Generally, with the exception of the 0.4 mm channels with cavities data point, decreased surface area is met with increased TRF and vice versa with the geometries that offer increased surface area (such as the pin fins) offering decreased Temperature Rise. These runs are comparing the channel width sweeps for each geometry and therefore have equivalent fluid flow and heating conditions.

6.3.2 Effect of Flow Speed on Heat Transfer

With increased inlet flow speed comes an increase in heat transfer to the working fluid, and lower cold plate temperatures. This is seen in many studies with increased Channel Reynolds number due to overall increased mass flow rate for the same geometries leading to increased Nusselt numbers and lower component temperatures. This is due to the fact there is more advection occurring throughout the system. Working fluid moving at a quicker rate has a physical ability to advect more heat through the system than working fluid moving at a slower rate. Inlet velocity and therefore mass flow rate was varied for straight channels at widths from 0.6 mm to 1.2 mm with fin widths equal to channel widths. The results are shown in Figure 41. The heat transfer, boundary conditions and channel number correlations were kept the same as for the baseline sweep (125 W heat on heater surface, channel number varying by channel width to keep approximately the same overall plenum width).

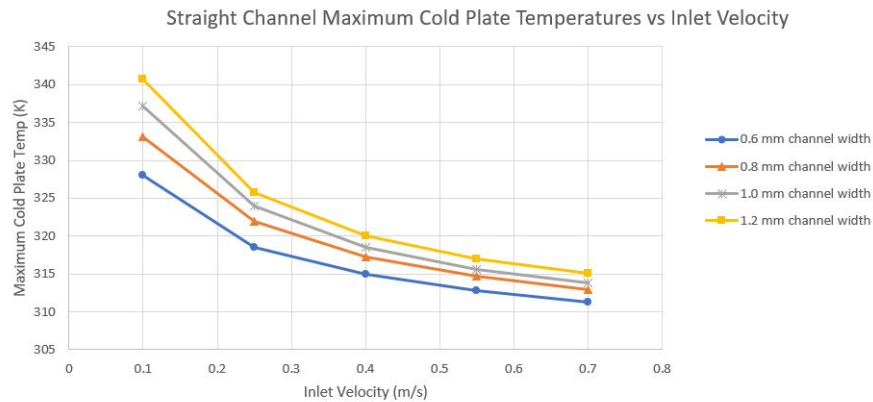


Figure 41: Maximum Cold Plate Temperatures vs inlet velocity for straight channels of different widths

The trend can be seen across all channel widths, that increased mass flow rate leads to decreased maximum cold plate temperature. This comes at the same expected increased pressure drop for increased mass flow rate as discussed in validation Section 5.3.3.3. Pressure drop compared to inlet velocity for the various channel widths can be seen in Figure 42.

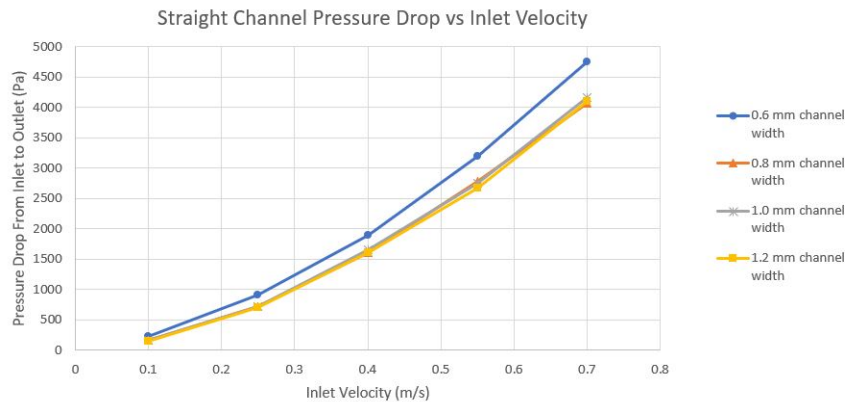


Figure 42: Pressure Drop vs Inlet Velocity for Straight Channels of Different Widths

Pressure drop increases with increased flow speed but is generally similar for channel widths 0.8 mm to 1.2 mm. This is likely due to total cross-sectional area disparities. Increased channel width has typically led to decreased pressure drop, however, in this sweep, with increased channel width comes varying channel velocities due to the fact that total channel cross-sectional area is not maintained. This allows for some of the larger channels to have faster channel velocities which therefore leads to increased friction drag in the channel. The increased surface drag of more surface area in contact with the working fluid of smaller channels is at odds with the increased friction drag caused by increased channel velocities and causes similar pressure drops.

To explore this further, total cross-sectional area was maintained by exploring the pressure loss for cold plate with 25 0.48 mm channels. Table 10 shows the comparison between the 15 channel wide

cold plate made up of 0.8 mm channels and the 25 channel wide cold plate made up of 0.48 mm channels. Each has the same total channel cross sectional area, meaning average channel velocity is equivalent.

Number of Channels	Channel Width	Inlet Velocity (m/s)	Pressure Drop (Pa)
15	0.8 mm	0.4 m/s	1616 Pa
25	0.48 mm	0.4 m/s	2194 Pa

Table 10: Pressure Drop for Constant Total Channel Cross-Sectional Area

The pressure differences seen across these channel widths helps to show that when constant cross-sectional area, and therefore constant channel velocity, is maintained, other factors such as aspect ratio, and increased surface drag dominate and show that smaller channel widths leads to increased pressure drop. This leads to an area for optimization because while pressure drops were similar for 0.8-1.2 mm channel widths in the initial setup shown in Figure 42, smaller channel widths universally showed lower maximum cold plate temperatures as seen in Figure 41. Therefore, there can be an optimization to explore the space decreasing pressure drop but maintaining decreased maximum cold plate temperatures depending on the needs of cold plate designers and system setup.

6.3.3 Effect of Flow Disruption on Heat Transfer

The concept of flow disruption to enhance heat transfer is not unique to using micropins in microchannel cold plates as discussed in Section 2.2.2.3. Many researchers have applied this concept of flow disruption in various heat dissipation media at all scales with success. Manca et al. (2011) analyzed fluid flow through 10 mm wide channels with different shaped protruding ribs. Due to the large size of the channels, the analysis was also conducted at very large and definitely turbulent Reynolds numbers. One area of study in a variety of types of heat exchangers is the use of turbulators. Vaisi et al. (2020) found that turbulators increase heat transfer for shell and tube heat exchangers across the laminar and turbulent regime and that they also enhance heat transfer by increasing local flow velocity without increasing overall inlet velocity or mass flow rate.

Della Torre et al. (2019) studied the application of turbulators and offset-strip fins to disrupt fluid flow in a plate heat exchanger, noting that the turbulators and offset-strip fins enhance heat transfer by disrupting the boundary layer and inducing mixing in the fluid. Air injection is also a popular technique used by researchers, with the aim of disrupting the fluid flow and causing increased mixing in the fluid flow. Moria (2021) used both air injection and twisted tape turbulators in vertical tubes to analyze the effect of heat transfer to the fluid flowing through the tubes. By analyzing the flow in transparent tubes they were able to visually see the effects of the bubbles and turbulators on the flow in addition to the heat transfer measurements that most experimental researchers used. They found that the mixing caused by the bubbles and the turbulators increased heat transfer in the fluid streams (Moria, 2021). Khorasani and Abdolrahman (2017) studied the injection of air bubbles into a shell and tube type heat exchanger and saw increased effectiveness with the air injection due to flow disruption and increased turbulence within the flow. While most studies assessing heat transfer for cooling technologies focus on a forced convection scenario, Kitagawa et al. (2008) looked at natural convection along a heated plate and the effects that sub-millimeter bubble generation into the fluid had

on it. The bubbles increased mixing near the wall which increased the natural convection cooling of the plate.

For this reason, an offset pin fin geometry was generated after the inline pin fin geometry was generated. The flow disruption phenomenon was studied and very acutely evident between the inline pin fins and the offset pin fins. The comparison between those two geometries is used here to illustrate the effects of flow disruption. For inlet velocities of 0.4 m/s, 0.8 mm channel and fin widths and 45 degree angled fins, the inline fin geometry and offset fin geometry are shown in Figure 43.

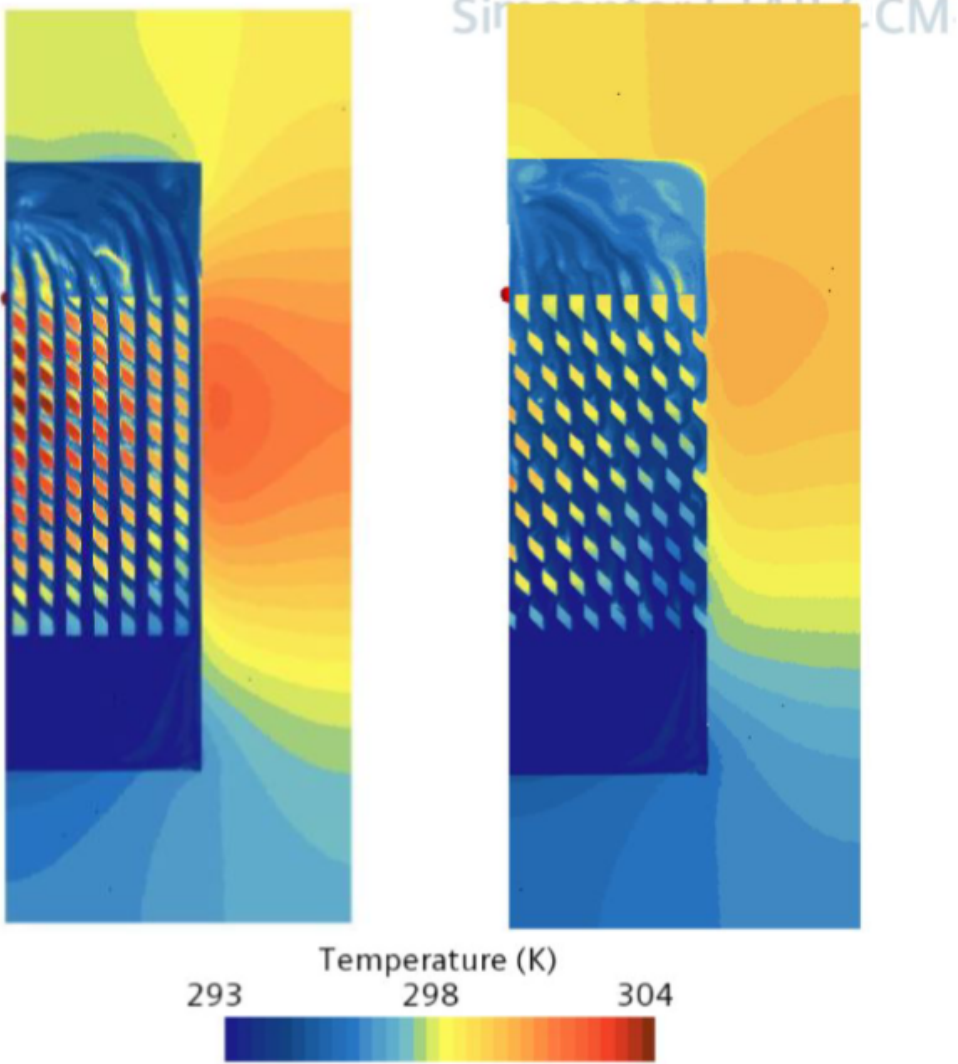


Figure 43: 45 Degree Angled Fins at 0.8 mm fin width and channel width in Inline Geometry (L) and Offset Geometry (R)

Results for the inline pin geometry compared to the offset pin geometry are shown in Table 11.

Geometry	Channel Width	TRF	Pressure Drop (Pa)	Max Cold Plate Temp (K)
Inline Pins	0.8 mm	8.10 mm	1775 Pa	314 K
Offsets Pins	0.8 mm	6.54 mm	4204 Pa	310 K

Table 11: Inline Pins vs Offset Pins Results for 0.4 m/s Inlet Velocity

The maximum cold plate temperature for the offset fin geometry was 310 K while the maximum cold plate temperature for the inline fin geometry was 314 K. Using Equation 14, the TRF for the offset fin geometry was 6.54 compared to the 8.10 seen by the inline finned geometry, or 19% improvement in TRF.

This comes at the expense of the pressure drop expected by the disruption of fluid flow, which is explored more in Section 6.3.4. The pressure drop across the plenums for the offset fin was 4204 Pa compared to 1775 Pa for the inline fins, a significant increase. While a benefit of microchannels is an increase in surface area compared to the bulk fluid flow, the offset fins, which have an increase in performance over the inline fins of almost 20% with 22% less surface area, points to the positive impact of flow misdirection in the effectiveness of the cold plate. Figure 44 shows that the flow is being disrupted as it goes along the course of the cold plate.

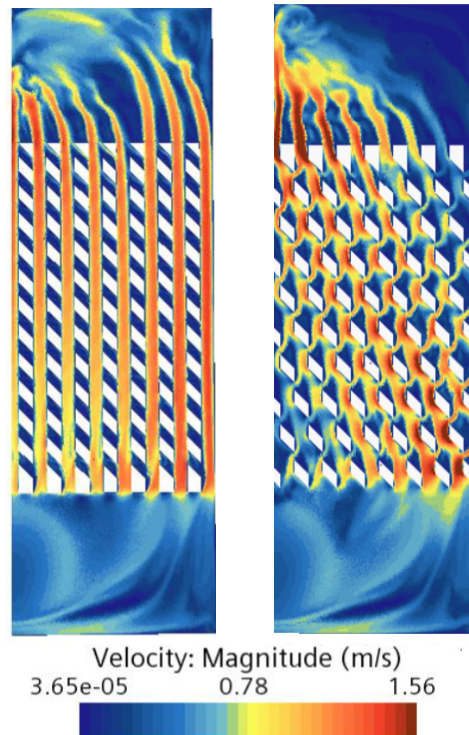


Figure 44: Velocity for the Inline Fins (L) and Offset Fins (R) at 45 Degrees (inlet velocity is 0.4 m/s)

In the inline fin geometry, very little secondary flow is happening between the fins, because there is no mechanism causing the flow to be misdirected. As can be seen by the minimal flow velocity in between the channels, there is very little secondary fluid flow occurring.

With equal heating conditions, boundary conditions and working fluid inlet velocity and temperature, the primary differences between the offset and inline geometries are: 1) The offset fin geometry has less finned surface area compared to the inline fin geometry and 2) The inline fin geometry has less flow disruption and secondary flow than the offset fin geometry. Theoretically, with more available surface area to heat the bulk fluid, the inline pin geometry would allow more heat dissipation from the cold plate material. However, much of that additional surface area only comes into contact with mostly stagnant water and therefore there is not much mixing occurring between the colder inlet flow working fluid and the warmer water in between the fins. This is evident in the innermost fin row where the water towards the end of the fluid flow path between the fins heats up significantly in comparison to the rest of the fluid regions. Therefore, the impact of additional surface area is largely negated due to minimal flow over the additional available surface area. It is not completely negated, however, due to the fact that the inline fin geometry still performed better than the straight channel geometry with the same inlet and heating conditions (TRF approximately 11.6% better). Therefore, the biggest factor at play between the inline fin and the offset fin geometries must be the flow re-distribution.

As many authors have pointed out, disrupting fluid flow can lead to more heat transfer between the walls of the cold plate and the bulk fluid for a number of reasons. In the bulk fluid moving through the channel regions the heat transfer occurs in the thin boundary region between the wall and the fluid. This boundary region gets thicker as the fluid flow develops along the length of the channel, and this thickening boundary layer increases the thermal resistance between the fluid and the cold plate walls (Bau, 1997). Disrupting this boundary layer and creating a new re-developing boundary layer can decrease the thermal resistance and allow more heat transfer from the walls to the fluid. Another phenomenon seen by flow disruption is increased mixing. Much like air injection and ribs in channels, this increased mixing allows for more of the bulk fluid to come into contact with the channel walls, and therefore be a part of the actual heat transfer occurring. Figure 45 shows the results of flow disruption.

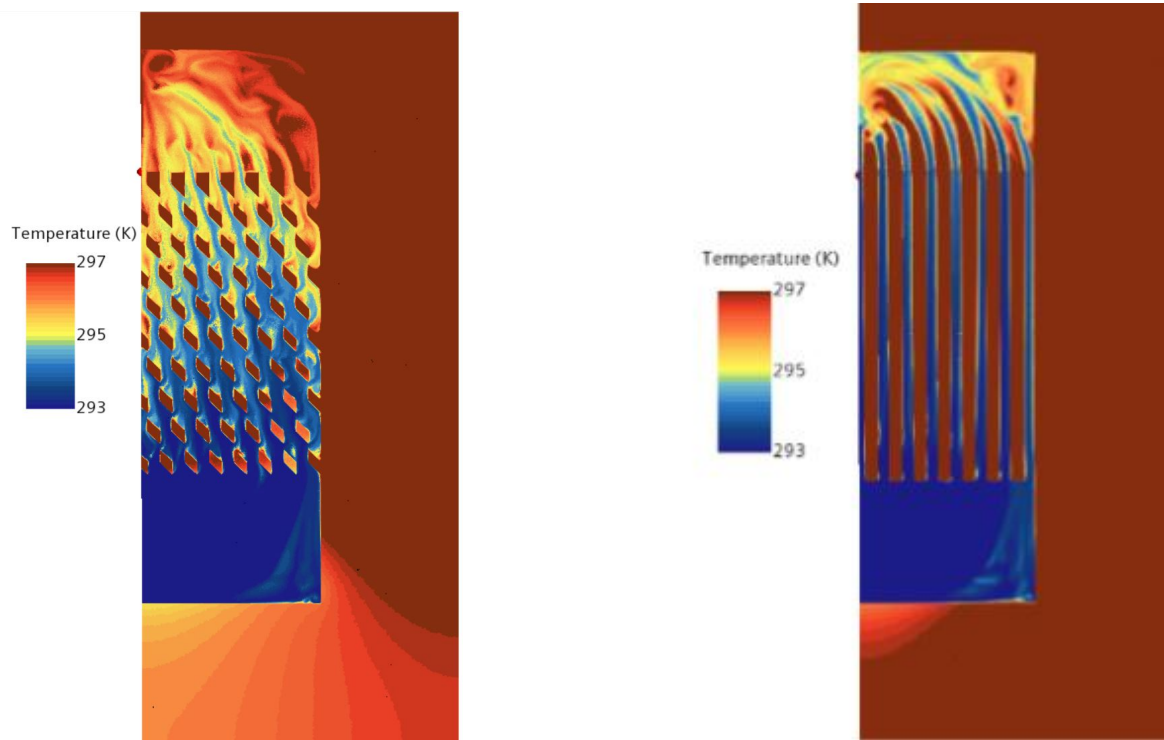


Figure 45: Offset Fins and Straight channels with 0.8 mm channels, 0.8 mm fin width and 0.4 m/s inlet velocity

The bulk fluid flow is largely at 293K in the straight channels and very little heat transfer is occurring aside from the heat transfer occurring in the immediate vicinity of the channel walls. This is one of the reasons that for the same geometry, smaller channels lead to better overall heat transfer - a greater percentage of the fluid flow is made up by the near-wall layer where energy is transferring from the wall to the fluid. The flow re-direction of the offset fins causes more of the bulk fluid to be in contact with the wall surfaces. In addition to this, the mixing causes warmer liquid to interact with the cooler liquid away from the walls and transfer energy as well, leading to greater overall heat transfer from the cold plate to the working fluid, and lower maximum cold plate temperatures.

6.3.4 Effect of Flow Disruption on Pressure Drop

As seen in most performance studies for microchannel cold plates, features that minimize temperature rise additionally increase pressure drop. The pressure drop phenomena is explored via variations in the zig-zag channels. The zig-zag turns are also referred to as miters or mitered regions in fluid dynamics literature.

6.3.4.1 Pressure Drop in Mitered Regions

In the mitered regions of the zig-zag geometry, there are pressure losses associated with the change in direction of the water flow path. In fitting with the model proposed in Equation 23, where the pressure drop from one plenum inlet to another is made up of a series of physical effects causing pressure loss,

each change of direction, or miter, can be summed up to add to the overall pressure drop experienced across the length of the channel. Pressure drop occurs at each miter due to the disruption of the flow. This flow disruption is characterized by the separation of the flow from the wall, the effects of said flow disruption on the flow path beyond the bend and the effects of the flow disruption on the flow path upstream of the bend (Blevins, 1984). $K_{\theta,circ,turbulent}$ for turbulent flow in a circular pipe is described by Equation 44, approximated with a line of best fit from tabular data provided by Blevins (1984).

$$K_{\theta,circ,turbulent} = -1E^{-8}\theta^4 + 1E^{-6}\theta^3 + 0.0001\theta^2 - 0.003\theta + 0.042 \quad (44)$$

where θ is the angle off of the flow path that the bend takes in degrees. $K_{\theta,circ,turb}$ is adjusted for the appropriate Reynolds number for anything less than $Re=2 * 10^5$ by

$$K_{\theta,circ,laminar} = K_{\theta,circ,turbulent} \left(\frac{2 * 10^5}{Re} \right)^{0.2} \quad (45)$$

$K_{\theta,circ,laminar}$ is then corrected by an aspect ratio correction factor, β , to generate $K_{\theta,rect,laminar}$. The aspect ratio correction factor is a function of aspect ratio, and a ratio of an equivalent radius of curvature of the miter bend to the width of the duct. Pressure drop due to each miter bend is expressed by (Blevins, 1984).

$$\Delta P_{miter} = \frac{1}{2} \rho u_m^2 K_{\theta,rect,laminar} \quad (46)$$

Since the pressure drop due to the miter calculated in Equation 46 is based on a relatively long inlet and outlet of straight pipe and therefore not designed for compounded bends, this is likely to be an underprediction of pressure loss as the flow is not expected to stabilize before getting further disrupted by the next bend as in the case with the bent geometries developed for and reported on here.

In this scenario, absent any effects of the bends in the channels, the total pressure drop between plenums was expected to increase as the channel width decreased, as seen by the straight channel models. This is primarily due to the apparent friction term (f_{app} , described by Equation 31). The apparent friction factor is a non-dimensional term that describes pressure drop due to the shear stress between the fluid flow and the wall.

The effects of physical phenomenon on the pressure drop were teased out by additional variations studied within the zig-zag channels.

The initial sweep results reported in Section 6.2 had horizontal offsets of each zig-zag set to 40% of the channel width; therefore, the flow path of the larger channel widths also included more a greater magnitude of horizontal disruption to the flow.

Figure 46 shows the difference in offset between the various geometries.

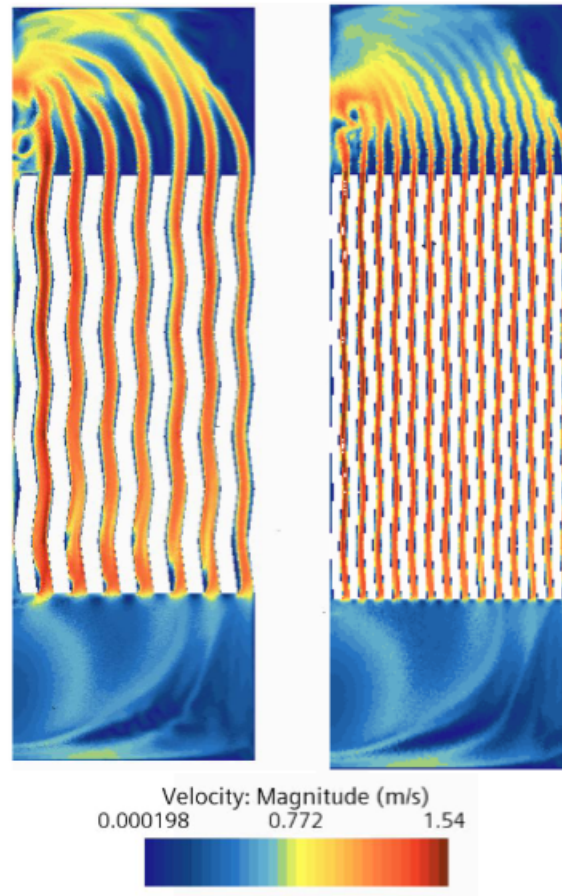


Figure 46: Zig-Zag geometry with 0.4 mm channel width and 0.16 mm horizontal channel offset (L) and 0.8 mm channel width and 0.32 mm horizontal channel offset (R)

The mechanisms that are influencing the pressure drop from the theoretical point of view for the zig-zag geometry are aspect ratio, angle of flow offset, and channel velocity (and subsequently channel Re). Each of their effect on pressure drop within the miter regions is detailed here. They do not necessarily have the same impact in straight channel sections and therefore these terms may have other impacts in the rest of the pressure drop equation:

- Aspect Ratio - as aspect ratio of the channels increases, factor β used to correct for the difference between circular duct flows and rectangular duct flows, decreases. In general a larger aspect ratio (channel width to channel depth) leads to a lower β , and therefore a lower irreversible pressure loss coefficient. All things being equal channel width increasing leads to lower pressure drop.
- Angle of flow disruption - As angle of flow disruption increases, the irreversible loss coefficient

increases. For larger horizontal offsets with the same zig-zag height, the angle of flow disruption increases and therefore pressure drop increases.

- Channel Velocity - As channel velocity increases, the pressure drop due to mitered regions also increases as the irreversible loss coefficient is multiplied by $chan_{vel}^2$. However, channel velocity is not directly tied to channel width because the number of channels also changes and total cross-sectional area was not maintained nor was it a monotonic trend between channel velocity and channel width.
- Channel Re - While channel velocity plays a role in channel Re, the channel Re increases monotonically for this sweep as channel width increases due to the increasing hydraulic diameter with wider channels. Higher channel Re leads to a higher irreversible loss coefficient.

For the zig-zag sweep where horizontal channel offset was kept at 40% channel width for channel widths between 0.4 mm to 1.2 mm, the pressure drop due to the zig-zags increased. This is due to the fact that the angle of flow disruption and channel Re both increased as the channel widths increased. Additionally, while aspect ratio provided a counter to that effect in that as aspect ratio increases absent of other changes, pressure drop decreases, the effect of the angle of flow disruption and channel Re were greater. The physical phenomenon that causes increased pressure drop for bends in the flow path is flow disruption which leads to increased shear in the liquid (Blevins, 1984). This is why greater angle directional changes as well as greater fluid velocity and Re within the channels leads to more pressure drop. The flow is already more susceptible to disruption at higher fluid velocities. Additionally, the theoretical pressure drop due to the bend takes into account the dynamic pressure of the fluid running through the component at hand and reports the pressure drop due to the component as a fraction of that (Blevins, 1984). This dynamic pressure is higher with a higher channel velocity. However, this pressure drop due to the component is not intended to replace in the equation the pressure drop due to flow friction, but rather augment for changes seen in the flow in excess of what would be seen in a straight pipe. This increase in pressure drop from the miters as channel width increased met the phenomena of pressure drop decreasing as channel width increased in straight pipes to lead to the results shown in Figure 35. There exists a minimum pressure drop where the increased pressure drop due to the angular offset of the channels is not overpowering the decrease in pressure drop that comes with wider channels. For the sweep described by Figure 35, this minimum is at 0.8 mm.

In order to determine the effects of just varying horizontal disruption absent of other effects that changing channel size had on pressure drop, channel width was held constant at 1 mm and horizontal offset was varied from 0.16 mm to 0.48 mm. Pressure drop results (averaged across the last 100 simulation iterations) are shown in Figure 47.

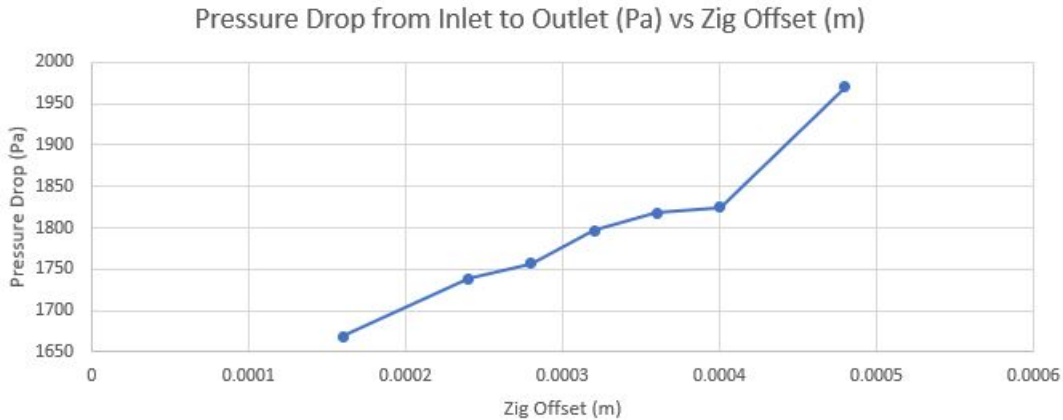


Figure 47: Pressure Drop varying horizontal flow path offset for 1 mm channel width

The pressure drop results for varied horizontal offsets and a constant 1 mm channel width showed a trend that supports the theory that increased flow disruption causes increased pressure drop. However, as evidenced by Figure 35, in varying channel width without controlling horizontal offset, there was not a trend matching the pressure drop trend as channel width increased seen by straight channels. This is due to the effects of the bends on the fluid flow. This supports the parabolic shape seen in the channel width sweep shown in 35.

Similar phenomena can be spoken to for the sweep results described by Figure 47. The figure shows the expected trend of pressure drop increasing due to angular offset of the zig-zags increasing. By holding channel width constant, aspect ratio, channel velocity, channel Re , and β (the correction factor for rectangular ducts versus circular ducts) were all held constant - thus teasing out the impact that angular disruption to the flow path has on the pressure drop due to the miter. Additionally, by keeping channel widths constant, all factors in the original pressure drop equation should stay the same with the exception of slight variations in channel length. The overall pressure drop seen in the simulations mirrors the expected trend where the only significant pressure drop change is due to the miters, which increases as the angle of disruption increases.

This confluence of factors having competing effects on pressure drop is further supported by the results seen in the final zig-zag sweep run to tease out these differences. In this sweep, the inlet temperature and velocity was kept constant, as well as the horizontal offset. This means that the angular disruption was kept constant across all runs. The channel width, however, was varied from 0.4 mm to 1.2 mm. With the factors identified that affect the pressure drop across the channels, the expected impacts are:

- As channel width increases, aspect ratio increases. Expected impact: lower pressure drop due to apparent friction term and β correction factor in bends
- As channel width increases, channel velocity changes for this setup due to the slight variations in total cross-sectional channel area. The channel velocities decrease from 0.4 mm to 0.8 mm and increase in the 1.0 mm and 1.2 mm runs. Increased channel velocity leads to increased pressure drop due the increased dynamic pressure of faster flow (and the channel velocity is a prefactor in almost every pressure drop term since they are reflected as a fraction of overall

dynamic velocity).

- As channel width increases, channel Re increases. This leads to a decrease in the apparent friction term, but an increase in the pressure drop due to each bend. This is due to greater flow disruption occurring for the same disturbance at higher Reynolds numbers.

The pressure drop increase due to a single bend for these flow conditions is plotted in Figure 48 for each channel width. While the horizontal offset is the same, the factors listed above highlight that there are factors at play that contribute to both increase and decrease in pressure drop as the channel widths get bigger. This results in a trend line that is not strictly monotonic for the pressure drop due to the miter shown in Figure 48.

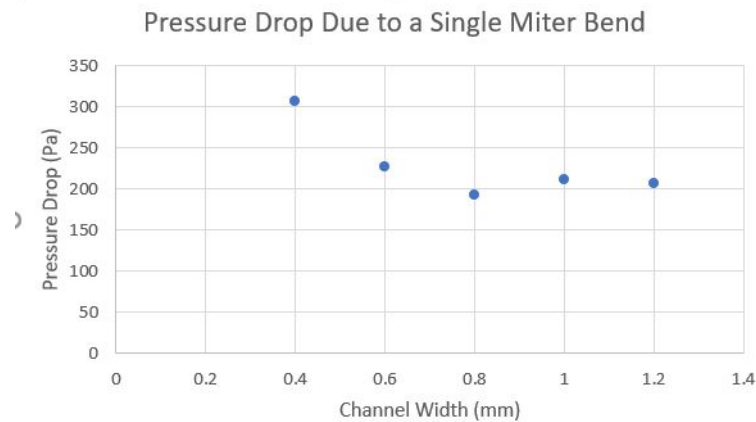


Figure 48: Theoretical Pressure Drop due to One Bend for Varying Channel Widths with Same Bend Offset

This general trend is reflected in the overall pressure drop seen by the mitered channels shown in Figure 49. This shows good concurrence with the theory of pressure drop in channels and around bends that the pressure drop due to a single miter roughly matches the pressure drop accumulations along the length of a channel with multiple bends of the same geometry.

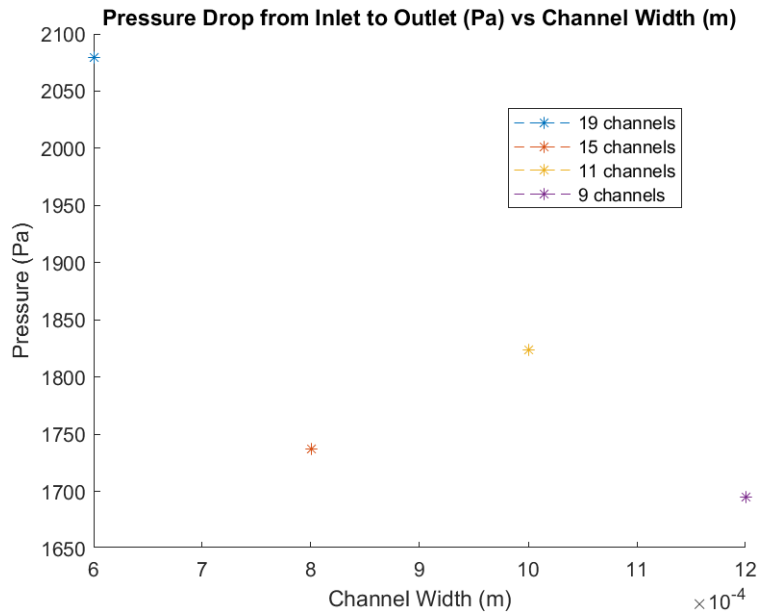


Figure 49: Pressure Drop from inlet to outlet across cold plate with varying channel widths and constant horizontal offset

This pressure discussion matters in the greater context of understanding what exactly is happening with the fluid flow in order to draw conclusions around how to minimize temperature rise while also minimizing pressure drop. Understanding the deviations from expected trends helps to tease out the physicality between what is happening with the fluid flow.

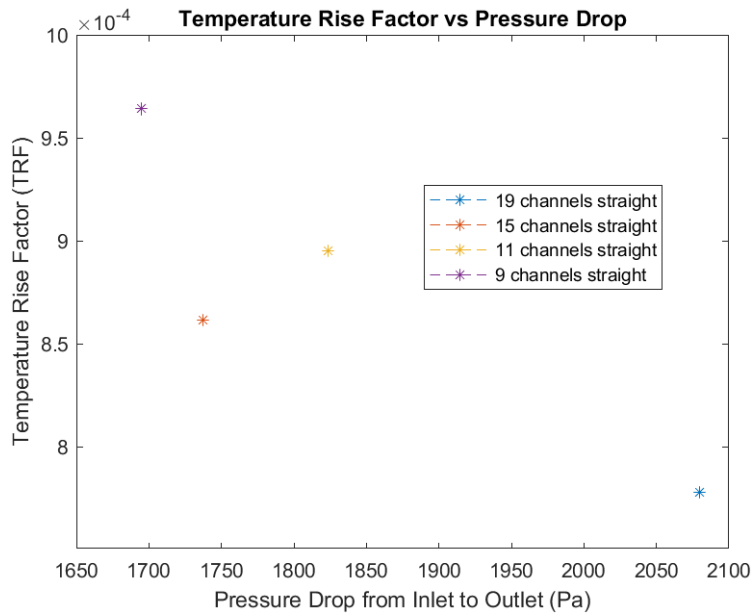


Figure 50: Temperature Rise Factor vs Pressure Drop for Constant Offset and Varying Channel Widths

Figure 50 places this pressure drop conversation back into its relevant contextual place by showing the pressure drop compared to the TRF showing the cost of higher performance.

7 Example Usage of MSLT

A simple example is outlined here from start to finish in order to show usage of the MSLT. This section includes figures and results to demonstrate the usage of the MSLT for informational and familiarity purposes, but much more detailed instructions including diagrams which define geometric parameters are found in Appendix A. In this case, 2 geometries are compared with 3 inlet velocity data points run at each geometry. A straight channel geometry case with water as the working fluid utilizing the half model is run first.

First, MSLT_INTERACTIVE.mlx is opened. The computer parameters are input:

Insert Computer and Run Time Setup Data Here:

Remote Server User Name	kelli
Remote Server IP address	[REDACTED]
Remote Server Directory for Files	../media/backUp6TB_2/1
POD License Key	[REDACTED]
Star-CCM+ Run Command	starccm16
Project Name	STRAIGHT_EXAMPLE_3
Number of Compute Processes (integers only)	38
<input checked="" type="checkbox"/> Save Simulations?	
<input checked="" type="checkbox"/> Passwordless connection enabled?	

Figure 51: Computer Setup Parameters Example

The project name for this example is 'STRAIGHT_EXAMPLE_3'.

Straight Channel Geometry, Half Model and Water as the working fluid options are chosen. Additionally, Cold Plate Material Properties are entered. The working fluid properties are left as is, but will not have any input in the simulation runs because water is selected as the working fluid.

Select a geometry from the drop down menu. Check any parameters you would like to change from the default. To include as a range, enter different values for min and max and include how many resolution data points you would like to include. To keep constant (but different from simulation default), set min and max to same desired value and set resolution to 1. IMPORTANT: Do not check any value you do not wish to change from default.

Geometry

Working Fluid

Model Size

Heat Transfer Discrepancy Threshold (%)

Define Cold Plate Material Properties. Whatever values are shown here will be used in the simulation for the solid cold plate domain.

Solid Density (kg/m³)

Solid Cp (J/kg-K)

Solid k (W/m-K)

Define Working Fluid Material Properties if anything other than Water is chosen

Working Fluid Density (kg/m³)

Working Fluid Cp (J/kg-K)

Working Fluid k (W/m-K)

Working Fluid Turbulent Prandtl Number (dimensionless)

Working Fluid Dynamic Viscosity (Pa-s)

Figure 52: Model Setup Parameters Example

Geometry and boundary conditions are entered to get desired sweep design. In this case, one geometry is tested in 3 different inlet flow conditions, ranging from 0.4 m/s to 0.7 m/s inlet velocity.

Check any parameters you would like to change from the default. To include as a range, enter different values for min and max and include how many resolution data points you would like to include. To keep constant (but different from simulation default), set min and max to same desired value and set resolution to 1.

<input checked="" type="checkbox"/>	inlet velocity (m/s)	Minimum Value	<input type="text" value="0.4"/>	Maximum Value	<input type="text" value="0.7"/>	Resolution (how many data points - integers only)	<input type="text" value="3"/>
<input checked="" type="checkbox"/>	channel width (mm)	Minimum Value	<input type="text" value="0.8"/>	Maximum Value	<input type="text" value="0.8"/>	Resolution (how many data points - integers only)	<input type="text" value="1"/>
<input checked="" type="checkbox"/>	channel height (mm)	Minimum Value	<input type="text" value="1.2"/>	Maximum Value	<input type="text" value="1.2"/>	Resolution (how many data points - integers only)	<input type="text" value="1"/>
<input checked="" type="checkbox"/>	channel length (mm)	Minimum Value	<input type="text" value="30"/>	Maximum Value	<input type="text" value="30"/>	Resolution (how many data points - integers only)	<input type="text" value="1"/>
<input checked="" type="checkbox"/>	fin width (mm)	Minimum Value	<input type="text" value="0.8"/>	Maximum Value	<input type="text" value="0.8"/>	Resolution (how many data points - integers only)	<input type="text" value="1"/>
<input checked="" type="checkbox"/>	number of channels (integers only)	Minimum Value	<input type="text" value="15"/>	Maximum Value	<input type="text" value="15"/>	Resolution (how many data points - integers only)	<input type="text" value="1"/>
<input checked="" type="checkbox"/>	inlet radius (mm)	Minimum Value	<input type="text" value="3"/>	Maximum Value	<input type="text" value="3"/>	Resolution (how many data points - integers only)	<input type="text" value="1"/>
<input checked="" type="checkbox"/>	inlet temperature (K)	Minimum Value	<input type="text" value="293"/>	Maximum Value	<input type="text" value="293"/>	Resolution (how many data points - integers only)	<input type="text" value="1"/>
<input checked="" type="checkbox"/>	heat flux (W/m ²)	Minimum Value	<input type="text" value="400000"/>	Maximum Value	<input type="text" value="400000"/>	Resolution (how many data points - integers only)	<input type="text" value="1"/>
<input checked="" type="checkbox"/>	Gauge pressure out (Pa)	Minimum Value	<input type="text" value="0"/>	Maximum Value	<input type="text" value="0"/>	Resolution (how many data points - integers only)	<input type="text" value="1"/>
<input checked="" type="checkbox"/>	Plate Thickness (mm)	Minimum Value	<input type="text" value="3.6"/>	Maximum Value	<input type="text" value="3.6"/>	Resolution (how many data points - integers only)	<input type="text" value="1"/>
<input checked="" type="checkbox"/>	Plate Width (mm)	Minimum Value	<input type="text" value="60"/>	Maximum Value	<input type="text" value="60"/>	Resolution (how many data points - integers only)	<input type="text" value="1"/>
<input checked="" type="checkbox"/>	Heater Length (mm)	Minimum Value	<input type="text" value="30"/>	Maximum Value	<input type="text" value="30"/>	Resolution (how many data points - integers only)	<input type="text" value="1"/>
<input checked="" type="checkbox"/>	Heater Width (mm)	Minimum Value	<input type="text" value="30"/>	Maximum Value	<input type="text" value="30"/>	Resolution (how many data points - integers only)	<input type="text" value="1"/>
<input type="checkbox"/>	Plenum Width (mm)	Minimum Value	<input type="text" value="23.2"/>	Maximum Value	<input type="text" value="23.2"/>	Resolution (how many data points - integers only)	<input type="text" value="1"/>
<input type="checkbox"/>	Plenum Length (mm)	Minimum Value	<input type="text" value="23.2"/>	Maximum Value	<input type="text" value="23.2"/>	Resolution (how many data points - integers only)	<input type="text" value="1"/>
<input checked="" type="checkbox"/>	Plate Length (mm)	Minimum Value	<input type="text" value="64"/>	Maximum Value	<input type="text" value="64"/>	Resolution (how many data points - integers only)	<input type="text" value="1"/>

Figure 53: Geometry and Boundary Condition Setup Parameters Example

The 'Run' button is clicked and a .java file is generated with the project name: 'STRAIGHT_EXAMPLE_3.java'. Because the 'Passwordless' radio button was checked in the computer setup parameters, the .java file is automatically copied over to the *remote_directory*. A command is generated and displayed in Matlab.

```

Run

ans = "STRAIGHT_EXAMPLE_3.java"

Enter following commands into command line of home directory on remote server
cp DEFAULT.dmprj STRAIGHT_EXAMPLE_3.dmprj;starccm16 STRAIGHT_EXAMPLE_3.dmprj -batch STRAIGHT_EXAMPLE_3.java -dmnoshare -passtodesign "-power -podkey '

```

Figure 54: Command Generation Example

The command can be copied by right clicking and selecting 'Copy Output'. The command is pasted

into a shell connected to the remote server in the *remote_directory* location. For security purposes the license key and IP address have been blacked out in the following image.

```
kelli@ -SYS:~$ cp DEFAULT.dmprj STRAIGHT_EXAMPLE_3.dmprj;starccm16 STRAIGHT_EXAMPLE_3.dmprj -batch STRAIGHT_EXAMPLE_3.java -dmnoshar
e -passtodesign "-power -podkey -licpath 1999@flex.cd-adapco.com" & disown
```

Figure 55: Command Entered into Remote Server Command Shell

This command will cause Star-CCM+ to execute the Design Manager project named STRAIGHT_EXAMPLE_3.dmprj. This will run 3 simulation runs, varying the inlet velocity with each run. In order to check if the simulation is done running, the proper information is entered into the next section and the ‘Check if Sim is Done Running’ button is clicked. This button will attempt to copy the CSV output file from the Design Manager project on the Remote Server over to the client server. If the file is available and copied over, then the Design Manager project is done running, and the message ‘IS DONE’ is displayed.

When time has passed and you would like to check on the simulation example, enter the project information here and click ‘Check if Sim is Done Running’. This will also copy the CSV of results and output images to the local folder for later post-processing.

Remote Server User Name

Remote Server IP address

Remote Server Directory for Files

Current Project

IS DONE

Figure 56: Checking on Project Completion Example

In order to see the difference between the straight channel geometry and the same conditions applied to a Pin Fin geometry, a new project is created ‘PIN_EXAMPLE_3’.

Insert Computer and Run Time Setup Data Here:

Remote Server User Name

Remote Server IP address

Remote Server Directory for Files

POD License Key

Star-CCM+ Run Command

Project Name

Number of Compute Processes (integers only)

Save Simulations?

Passwordless connection enabled?

Figure 57: Second Project Computer Parameters Setup Example

This time the Fin Geometry is selected. Nothing was changed within the user interface since gener-

ating the Straight Channel Geometry, but nonetheless parameters should be double checked to ensure they are correct.

Select a geometry from the drop down menu. Check any parameters you would like to change from the default. To include as a range, enter different values for min and max and include how many resolution data points you would like to include. To keep constant (but different from simulation default), set min and max to same desired value and set resolution to 1. IMPORTANT: Do not check any value you do not wish to change from default.

Geometry

Working Fluid

Model Size

Heat Transfer Discrepancy Threshold (%)

Define Cold Plate Material Properties. Whatever values are shown here will be used in the simulation for the solid cold plate domain.

Solid Density (kg/m³)

Solid Cp (J/kg-K)

Solid k (W/m-K)

Figure 58: Pin Fin Model Parameters Example Setup

All parameters are verified for the generic setup and ensured that they are the same as desired. Unique Pin Fin parameters are entered.

Pin Fin Specific Parameters

Pin Angle (degrees)
 Minimum Value Maximum Value Resolution (how many data points - integers only)

Fin Spacing (mm)
 Minimum Value Maximum Value Resolution (how many data points - integers only)

Fin Length (mm)
 Minimum Value Maximum Value Resolution (how many data points - integers only)

Figure 59: Pin Fin Parameter Selection Example

The Run button is selected again to generate a new .java file, this time named 'PIN_EXAMPLE_3.java'. The command generated is copied and entered into a server connected command shell as in Figure 55. To check for simulation completion, the new project name is entered into the next section.

When time has passed and you would like to check on the simulation example, enter the project information here and click 'Check if Sim is Done Running' also copy the CSV of results and output images to the local folder for later post-processing.

Remote Server User Name

Remote Server IP address

Remote Server Directory for Files

Current Project

IS DONE

Figure 60: Checking for Project Completion Example

Chosen results are plotted for the straight channel, in this case TRF compared to inlet velocity by making the appropriate selections. This case was chosen to show the impact of changing just the base model geometry on the results. The inline pin fin geometry had lower TRF and maximum cold plate temperature values, with higher pressure drop between the inlet and the outlet.

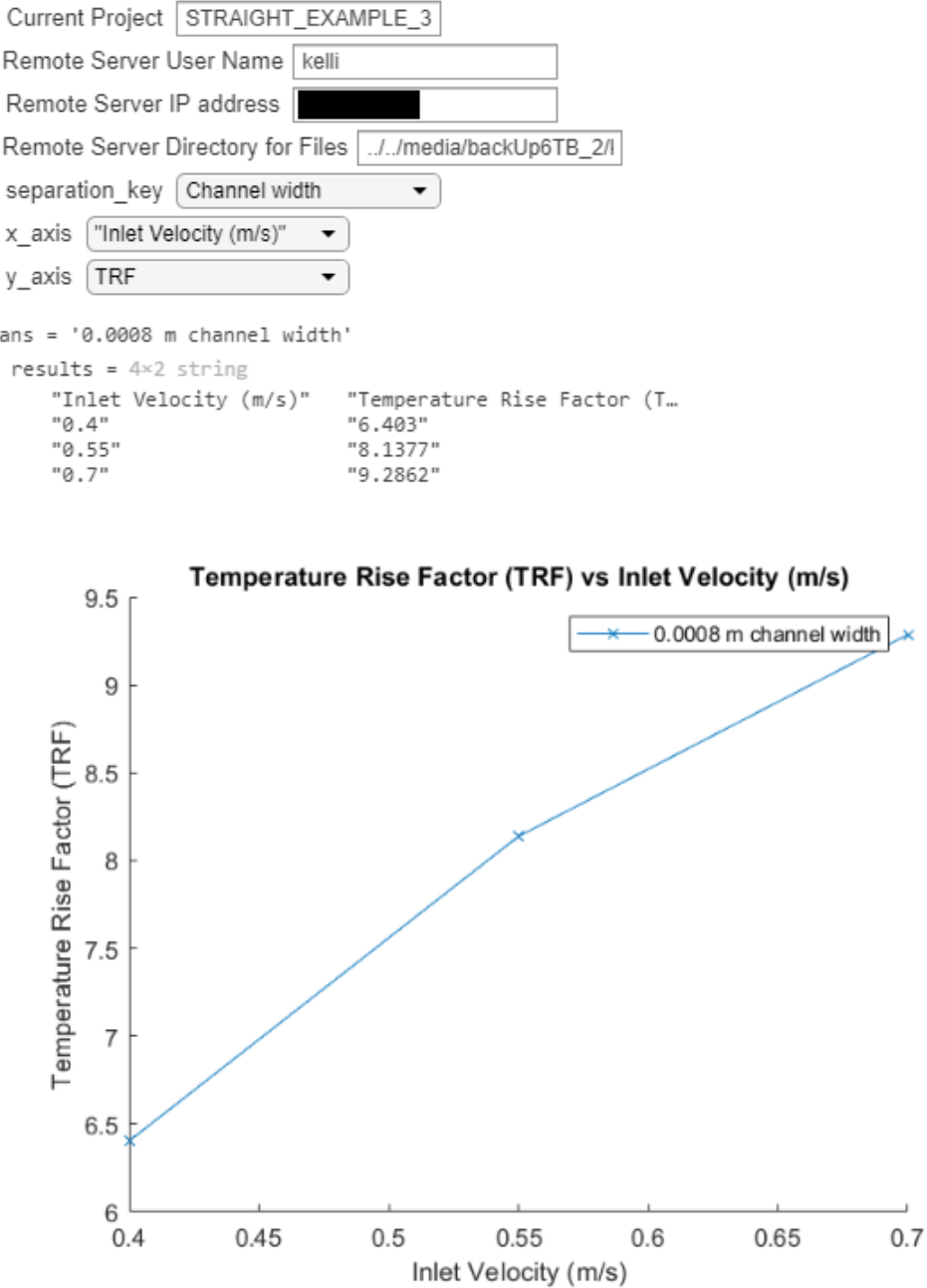


Figure 61: Straight Channel Example Graph Generation

In order to overlay the results of the Pin Fin sweep onto the graph, the project title is changed, and the appropriate selections are made.

Current Project
Remote Server User Name
Remote Server IP address
Remote Server Directory for Files
separation_key
x_axis
y_axis
ans = '0.0008 m channel width'
results = 4x2 string
"Inlet Velocity (m/s)" "Temperature Rise Factor (T..."
"0.4" "5.9658"
"0.55" "7.3983"
"0.7" "8.6371"

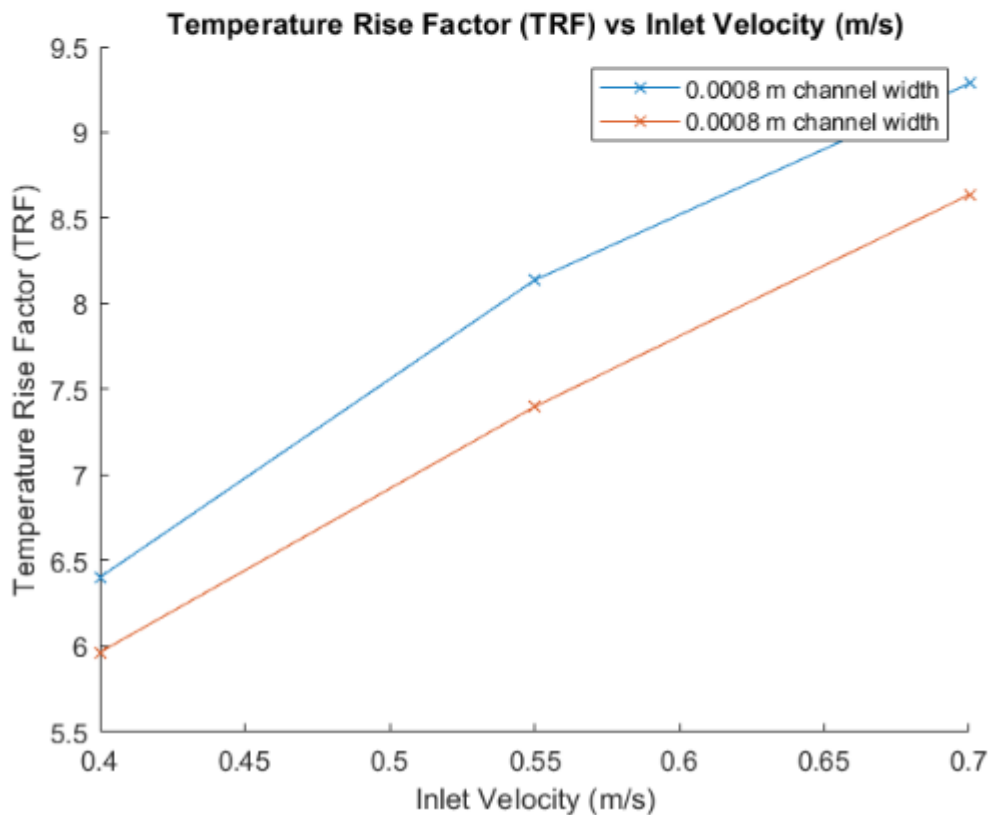


Figure 62: Overlay of Pin Fin Data with Straight Channel Data for Example Data Comparison

In this case it is easy to see that the Pin Fin geometry with the same parameters had a lower TRF for each inlet velocity and therefore had better temperature performance. Other graphs can be generated to see how the cold plates compare in other ways. Figure 63 shows how the two geometries compare in terms of pressure drop.

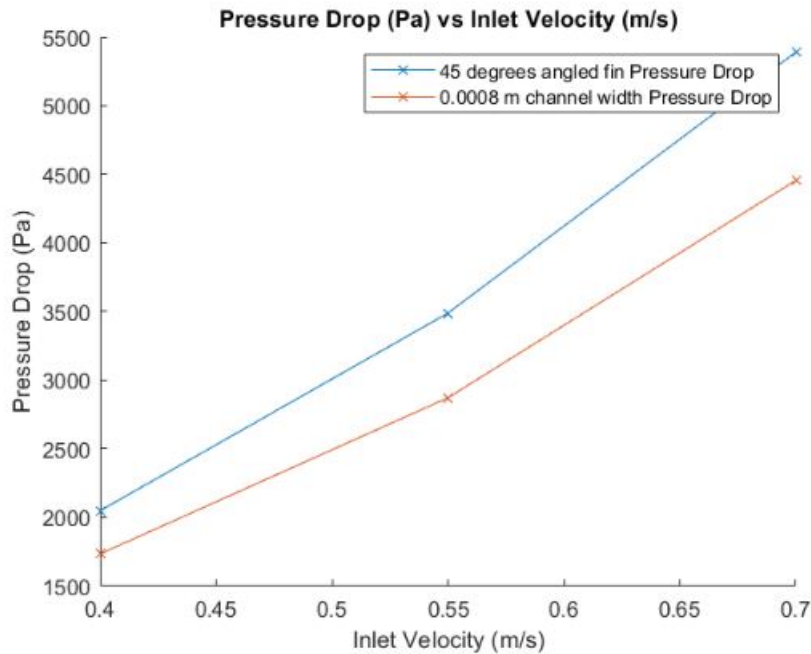


Figure 63: Pressure Drop Comparison Example Graph

Of note, the Clear Graph button was selected prior to making new axis selections to clear the data.

Planar cutouts showing temperature, fluid velocity, and the mesh were extracted from each run by Star-CCM+ and transferred to the local client when the results were copied over. These are in subfolders for each project and can also be displayed in the user interface by selecting the desired Design and plot. Figure 64 shows an example of the Pin Fin Design 1 Velocity plot.

The chosen image is shown here - other images are available in the subfolder for the current project, separated by Design.

Type of Figure
 Design Number

Simcenter STAR-CCM+

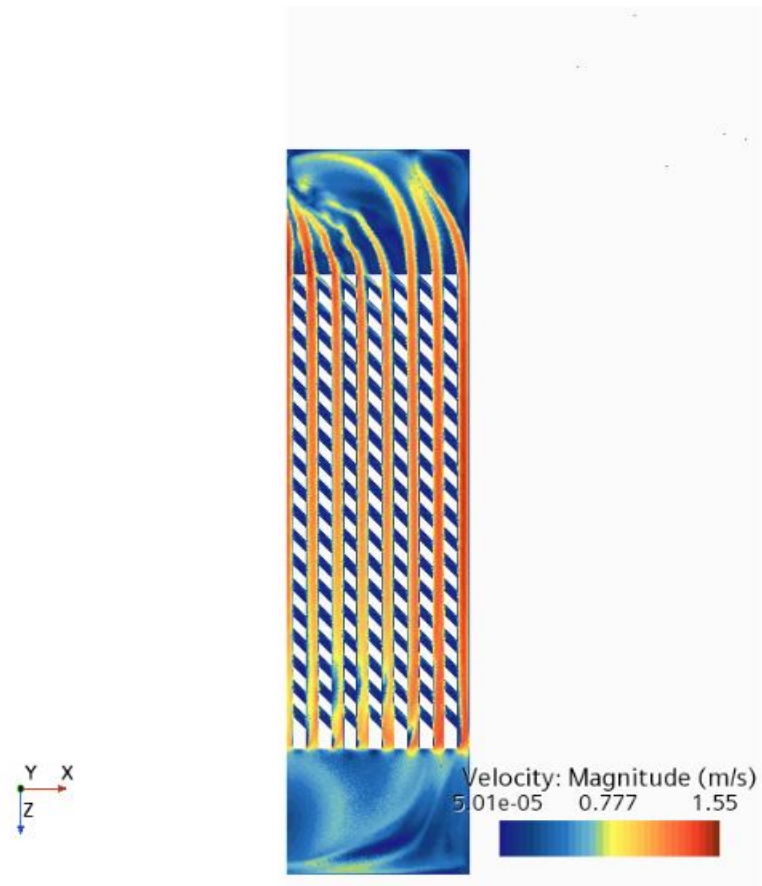


Figure 64: Example of Generated Velocity Image

8 Conclusions and Future Work

The goal of this study was to develop an effective tool for cold plate designers to provide them with the ability to analyze and optimize cold plate design for their given thermal management problem. This tool, the Microchannel Simulation Library Tool, aims to bring the input and post-processing of variable models to a more user-friendly level for cold plate designers to have access to a library of CFD simulations without having to rebuild, and revalidate each model in a time consuming process. In order to do this, four categories of geometric augmentation were chosen as library features and a robust validation of the base straight channel simulation case was conducted. Trend analysis was also explored for each of the geometric enhancements to both validate that the results seen were physically sensible and to provide future users with an intuition as to the effects of each of the different geometries on cold plate performance. Finally, performance metrics were generated to provide sensible means of comparison for the cold plate results generated by using this tool.

The base sweeps run on each of the geometries showed a general decrease in maximum cold plate temperature as channel width decreased and consequentially number of channels increased. This was due to a higher percentage of the bulk fluid flow through the cold plate being a part of the boundary layer between the fluid domain and the cold plate surfaces where the heat transfer occurs axially into each channel. Augmentations that increased surface area such as the inline pin fins showed lower maximum cold plate temperatures compared to cold plates with the same geometric scaling and less total surface area exposed to fluid flow. However, the effect of flow disruption was an even greater impact to decreasing maximum cold plate temperature. The offset pin fin geometry had less exposed surface area from the pin fins, but showed significantly lower temperatures. This is due to the redeveloping boundary layers caused by flow redirection and the increased mixing that is caused by forced flow redirection. The effect of flow re-direction was of greater significance than the effect of increased fin surface area. However, each enhancement was met with an increase in pressure drop across the cold plate. The similar results seen across geometric enhancements in the exploration of baseline geometries, highlighted in Figure 39, represent an opportunity for further exploration of what is physically occurring in microchannel cold plates using the MSLT.

The trade-off between performance and pressure drop is what necessitates a tool that can be tailored to an individual thermal management problem at hand. Increased pressure drop can cause a problem when integrating a cold plate design into a system because of increased pump demands. If the pressure drop is too high, the cooling water system available may not be able to meet adequate flow rates for cooling based on the increased fluid resistance across the plate. Additionally, it is typically desirable to avoid higher pressure liquid systems in the vicinity of electronics as higher pressure flow rates increase the chances of leakage or burst which could damage the electronic components. It also physically uses more energy to pump water at a higher pressure rate, so higher pressure demands can very directly be seen as a cost to high flow rate systems. Over-designing a solution with the most effective cold plate in terms of cold plate maximum temperatures may come at too high of a pressure drop cost for some systems and therefore a solution which provides adequate cooling may be the best fit for a given design problem. The Microchannel Simulation Library Tool can also be of benefit to design engineers who are working the thermal management side of a component in an environment where the component itself is changing. Allowing a quick and simple way to change metrics and get analysis results takes away much of the challenge of having changing boundary conditions, dimensions, and requirements in a component whose design is still developing. This allows thermal management to

be a much more integrated part of the design process rather than an after the fact problem to solve. Furthermore, the different levels of accessibility of the tool, from a basic user interface to the ability to apply the framework to expanded geometries and applications provides for flexibility depending on the needs of the user.

Future opportunities based on this work include:

- **Validation:** Experimental validation was conducted based off one experimental case for a sweep of Re for straight microchannels only. Further validation of each geometry can be conducted and any discrepancies addressed within the base case models. The geometric limitations of accuracy on this model were not explored, and this presents an opportunity for size limitation validations. It is expected that geometric changes on the same order of magnitude as the current model parameters will provide accurate results, but validation is necessary to provide further confidence in results when the sizes are changed significantly from the geometric parameters validated in this study.
- **Exploration of turbulence:** The models are based on K-Omega turbulence models while the size of the microchannels puts them in the laminar regime for most flow rates. However, due to the flow disruption introduced by the inlets, plenums, flow contraction, and model geometric parameters, turbulent characteristics are to be expected. Validation showed good concurrence with the experimental data when using the K-Omega turbulence model with low y^+ wall treatment as well as with the laminar flow regime models. The K-Omega turbulence model was selected, however, to encapsulate a wider range of flow rates and flow disruptions. An exploration of transition and when the laminar flow regime should be used in comparison to a turbulent flow regime would make model results more accurate across all flow rates.
- **Scale Augmentation:** The current geometric models are designed for a small cold plate with microchannel lengths on the order of 20 mm long. This can be expanded and the new sizes validated to provide greater confidence in expanded use of the MSLT.
- **Extended Geometric Enhancements:** The framework can easily be augmented to include more geometric enhancements as seen fit for increasing effectiveness of cold plates. In addition to varied features other than zig-zag channels, channels with cavities and oblique fins, specific enhancement opportunities include:
 - **Number and location of hotspot designation:** The current tool allows for a singular hotspot centered on the cold plate. Augmenting to reflect more targeted heat flux coming from varied positions in an electronic component may provide more accurate analysis for specific design problems.
 - **Counterflow cooling:** Many microchannel cold plates are designed with counterflow cooling providing liquid cooling on two sides of a component. Right now this cold plate is designed to have a single flow direction on one side of a component, but that capability can be expanded.
- **Targeted cooling:** Currently the tool provides analysis based on inputs, with optimization capable by the user running new sweeps based on the data seen in the design. However, feedback within the tool which provides for localized enhancing features (such as fins causing flow redirection) targeted to the hotspots identified initially would allow the tool to provide a more robust

optimized solution to designers with less input required. Additionally, the ability to implement a non-uniform distribution of features may allow for desired cooling affects with lower pressure drop (Ramakrishnan et al., 2018).

- System integration and implementation: Any design developed using the MSLT will need to be integrated into a system for practical use. Certain decisions were made to account for this, including the geometric variability of the inlet and outlets, the usage of turbulent models, and the variability of the heater surface dimensions. However, there are a number of other augmentations to the base models that could be considered. These include variability of inlet location or entry angle, more realistic environmental boundary conditions, integration of multiple heater surfaces, and integration of thermal interface considerations such as thermal resistance between the cold plate and the heat generating component.

Providing a tool which has been validated, and its basic capabilities explored, will allow future electronic component designers to identify possible solutions to their thermal management problems in a quick, reproducible and adaptable way. By simplifying the usability of CFD to a library focused on a specific type of solution, the powerful functionality of a CFD simulation becomes accessible to designers with little to no experience using or modeling with it.

References

- Abdulqadur, A. A., H. M. Jaffal, and D. S. Khudhur (2019). Performance optimization of a cylindrical mini-channel heat sink using hybrid straight–wavy channel. *International Journal of Thermal Sciences* 146, 106–111.
- Bar-Cohen, A. and W. Rohsenow (1984). Thermally optimum spacing of vertical, natural convection cooled, parallel plates. *Journal of Heat Transfer* 106, 116–123.
- Bau, H. (1997). Optimization of conduits' shape in micro heat exchangers. *International Journal of Heat and Mass Transfer* 41, 2717–2723.
- Bejan, A. and E. Sciubba (1992). The optimal spacing of parallel plates cooled by forced convection. *International Journal of Heat and Mass Transfer* 35(12), 3259–3264.
- Blevins, R. D. (1984). *Applied Fluid Dynamics Handbook*. Van Nostrand Reinhold Company.
- Chen, C., S. Yang, and M. Pan (2021). Microchannel structure optimization and experimental verification of a plate heat exchanger. *International Journal of Heat and Mass Transfer* 175.
- Chen, X. and X. Wang (2020). Microchannel cold plate heat transfer and flow resistance characteristics calculation and structure optimization. *Journal of Physics: Conference Series* 1676, 012204.
- Cova, P., D. Santoro, D. Spaggiari, F. Portesine, F. Vaccaro, and N. Delmonte (2020). CFD modeling of additive manufacturing liquid cold plates for more reliable power press-pack assemblies. *Microelectronics Reliability* 114.
- Dang, T. and J.-T. Teng (2011). Comparisons of the heat transfer and pressure drop of the microchannel and minichannel heat exchangers. *Heat Mass Transfer* 47, 1311–1322.
- Della Torre, A., G. Montenegro, A. Onorati, S. Khadilkar, and R. Icarelli (2019). Multi-scale CFD modeling of plate heat exchangers including offset-strip fins and dimple-type turbulators for automotive applications. *Energies* 12(15), 2965.
- DiMarino, C. (2020). Navy integrated power electronics building block (iPEBB). ONR Program Review, November 2020.
- Engineering ToolBox (2003). Water - density, specific weight and thermal expansion coefficients. https://www.engineeringtoolbox.com/water-density-specific-weight-d_595.html. Accessed March 31, 2022.
- Engineering ToolBox (2004). Water- dynamic (absolute) and kinematic viscosity vs. temperature and pressure. https://www.engineeringtoolbox.com/water-dynamic-kinematic-viscosity-d_596.html. Accessed March 31, 2022.
- Favre-Marinet, M., S. Le Person, and A. Bejan (2004). Maximum heat transfer rate density in two-dimensional minichannels and microchannels. *Microscale Thermophysical Engineering* 8(3), 225–237.
- Gaikwad, V., S. Mohite, S. Shinde, and M. Dherange (2020). Enhancement in thermo-hydraulic sink with secondary flows of leaf venation pattern. *Journal of Thermal Engineering*, 677–696.

- Gao, P., S. Le Person, and M. Favre-Marinet (2002). Scale effects on hydrodynamics and heat transfer in two-dimensional mini and microchannels. *International Journal of Thermal Sciences* 41(11), 1017–1027.
- Giuliani, F., N. Delmonte, and P. Cova (2012). Thermal-fluid dynamic FEM simulation of advanced water cold plates for power electronics. *Proceedings of the 2012 COMSOL Conference in Milan*.
- Giurgiu, O., A. Pleşa, and L. Socaciu (2016). Plate heat exchangers – flow analysis through mini channels. *Energy Procedia* 85, 244–251.
- Gong, L., K. Kota, W. Tao, and Y. Joshi (2011). Parametric numerical study of flow and heat transfer in microchannels with wavy walls. *Journal of Heat Transfer* 2011.
- Gunnasegaran, P., H. Mohammed, N. Shuaib, and R. Saidur (2010). The effect of geometrical parameters on heat transfer characteristics of microchannels heat sink with different shapes. *International Communications in Heat and Mass Transfer* 37(8), 1078–1086.
- Huang, B., H. Li, S. Xia, and T. Xu (2020). Experimental investigation of the flow and heat transfer performance in micro-channel heat exchangers with cavities. *International Journal of Heat and Mass Transfer* 159, 120075.
- Incropera, F. P., D. P. DeWitt, T. L. Bergman, and A. S. Lavine (2007). *Fundamentals of Heat and Mass Transfer* (6 ed.). Dover.
- International Association for the Properties of Water and Steam (2007). Revised release on the IAPWS industrial formulation 1997 for the thermodynamic properties of water and steam. <http://www.iapws.org/relguide/IF97-Rev.html>. Accessed April 4, 2022.
- Khan, M. G. and A. Fartaj (2020). A review on microchannel heat exchangers and potential applications. *International Journal of Energy Research* 35(7), 553–582. eprint: <https://onlinelibrary.wiley.com/doi/pdf/10.1002/er.1720>.
- Khorasani, S. and D. Abdolrahman (2017). Effect of air bubble injection on the performance of horizontal helical shell and coil tube heat exchanger: An experimental study. *Applied Thermal Engineering* 111, 676–683.
- Kim, D.-K. and S. J. Kim (2006). Averaging approach for microchannel heat sinks subject of the uniform wall temperature condition. *International Journal of Heat and Mass Transfer* 49, 695–706.
- Kim, S. J. (2004). Methods for thermal optimization of microchannel heat sinks. *Heat Transfer Engineering* 25(1), 37–49.
- Kim, S. J. and D. Kim (1999). Forced convection in microstructures for electronic equipment cooling. *Journal of Heat Transfer* 121(3), 639–645.
- Kitagawa, A., K. Kosuge, K. Uchida, and Y. Hagiwara (2008). Heat transfer enhancement for laminar natural convection along a vertical plate due to sub-millimeter-bubble injection. *Experiments in Fluids* 45(3), 473–484.
- Knight, R. W., J. S. Goodling, and D. J. Hall (1991). Optimal thermal design of forced convection heat sinks-analytical. *Journal of Electronic Packaging* 113(3), 313–321.

- Kowsary, F., N. Noroozi, and M. Rezaei Barmi (2008). Optimization of heat transfer rate in the rectangular microchannel of different aspect ratios with constant cross sectional area. In *ASME 2008 First International Conference on Micro/Nanoscale Heat Transfer, Parts A and B*, pp. 285–292. ASME.
- Kumaraguruparan, G., R. Manikanda Kumaran, T. Sornakumar, and T. Sundararajan (2011). A numerical and experimental investigation of flow maldistribution in a micro-channel heat sink. *International Communications in Heat and Mass Transfer* 38, 1349–1353.
- Labade, M., V. Kumar, and M. Chaudhari (2019). A conjugate heat transfer CFD model of cold plate used in high end computing server. *Twelve International Conference on Thermal Engineering: Theory and Applications*, 1–5.
- Lan, X., G. Xie, S. Ji, Q. Tang, X. Li, X. Wang, and B. Wang (2021). Experimental and numerical study on the temperature uniformity of a variable density alternating obliquely truncated microchannel. *International Journal of Heat and Mass Transfer* 176.
- Lee, Y. J., P. S. Lee, and S. K. Chou (2012). Enhanced thermal transport in microchannel using oblique fins. *Journal of Heat Transfer* 134(10), 101901.
- Lienhard IV, J. H. and J. H. Lienhard V (2019). *A Heat Transfer Textbook*. Dover.
- Liu, D. and S. V. Garimella (2005). Analysis and optimization of the thermal performance of microchannel heat sinks. *International Journal for Numerical Methods in Heat Fluid Flow* 15(1), 7–26.
- Luo, L. and Y. Fan (2008). Recent applications of advances in microchannel heat exchangers and multi-scale design optimization. *Heat Transfer Engineering* 29(5), 461–474.
- Manca, O., S. Nardini, and D. Ricci (2011). Numerical analysis of water forced convection in channels with differently shaped transverse ribs. *Journal of Applied Mathematics*.
- McCandless, M., C. Cooke, J. Chalfant, C. Chrysostomidis, A. Colavitto, A. Vicenzutti, A. Contin, and G. Sulligoi (2019). Thermal analysis of MVDC power corridor. *IEEE ESTS 2019*, 106–112.
- Moharana, M. and S. Khandekar (2012). Effect of aspect ratio of rectangular microchannels on the axial back conduction in its solid substrate. *International Journal of Microscale, Nanoscale, Thermal Fluid Transport Phenomenon* 4, 211–229.
- Moria, H. (2021). Compound usage of twisted tape turbulator and air injection for heat transfer augmentation in a vertical straight tube with upward stream. *Case Studies in Thermal Engineering*.
- Pan, M., H. Wang, Y. Zhong, M. Hu, X. Zhou, G. Dong, and P. Huang (2019). Experimental investigation of the heat transfer performance of microchannel heat exchangers with fan-shaped cavities. *International Journal of Heat and Mass Transfer* 134, 1199–1208.
- Panchal, S., R. Khaso, I. Dincer, M. Agelin-Chaab, R. Fraser, and M. Folwer (2017). Thermal design and simulation of mini-channel cold plate for water cooled large sized prismatic lithium-ion battery. *Applied Thermal Engineering*.
- Perry, J. (2018). Thermal Performance of Macro and Microchannel Cold Plates in Electronics Cooling. <https://www.qats.com/cms/2018/01/08/>

- thermal-performance-of-macro-and-microchannel-cold-plates-in-electronics-cooling/. Online; accessed 22 July 2021.
- Qu, W., G. M. Mala, and D. Li (2000). Heat transfer for water flow in trapezoidal silicon microchannels. *Int. J. Heat Mass Transfer*, 12.
- Qu, W. and I. Mudawar (2003). Thermal design methodology for high-heat-flux single-phase and two-phase micro-channel heat sinks. *IEEE Transactions on Components and Packaging Technologies* 26(3), 598–609. Conference Name: IEEE Transactions on Components and Packaging Technologies.
- Qu, W., I. Mudawar, S.-Y. Lee, and S. T. Wereley (2006). Experimental and computational investigation of flow development and pressure drop in a rectangular micro-channel. *Journal of Electronic Packaging* 128(1), 1–9.
- Raghuraman, D., R. Thundil Karuppa Raj, P. Nagarajan, and B. Rao (2017). Influence of aspect ratio on the thermal performance of rectangular shaped micro channel heat sink using CFD code. *Alexandria Engineering Journal* 56(1), 43–54.
- Ramakrishnan, B., Y. Hadad, S. Alkharabsheh, P. R. Chiarot, K. Ghose, B. Sammakia, V. Gektin, and W. Chao (2018). Experimental characterization of cold plates used in multi chip server modules (MCM). <https://par.nsf.gov/servlets/purl/10058150>. Accessed July 14, 2021.
- Rosa, P., T. Karayiannis, and M. Collins (2009). Single-phase heat transfer in microchannels: The importance of scaling effects. *Applied Thermal Engineering* 29(17), 3447–3468.
- Sabin, M. and S. Piva (2014). Numerical analysis of a cold plate for FM radio power amplifiers. *Journal of Physics: Conference Series*.
- Shah, R. and M. Bhatti (1987). *Handbook of Single-Phase Convective Heat Transfer*.
- Shah, R. and A. London (1978). *Advances in Heat Transfer: Supplement 1 Laminar Flow Forced Convection in Ducts*. Academic Press.
- Siemens Digital Industries Software (2017). How can I know what the y^+ value of the wall cell will be when creating the grid? https://support.sw.siemens.com/knowledge-base/KB000033516_EN_US.
- SIEMENS Digital Industries Software (2021). Simcenter STAR-CCM+ User Guide.
- Singh, G., R. Kumar, and D. Mikielwicz (2021). Effect of flow normalization in micro-pin-finned heat sink: Numerical study. *Journal of Thermophysics and Heat Transfer* 35(1), 28–37.
- Steinke, M. E. and S. G. Kandlikar (2006). Single-phase liquid friction factors in microchannels. *International Journal of Thermal Sciences* 45(11), 1073–1083.
- Tikadar, A. (2019). Enhancing thermal-hydraulic performance of parallel and counter flow mini-channel heat sinks utilizing secondary flow: A numerical and experimental study. (Master's Thesis, University of South Carolina). Retrieved from <https://scholarcommons.sc.edu/etd/5453>.
- T'Jollyn, I., B. Ameel, S. Devos, J. Bienstman, S. Schlimpert, and M. D. Paepe (2017). Experimental

- study of design parameter influence on thermal and hydraulic performance of cold plates. *IEEE ITHERM Conference* 16.
- Tuckerman, D. and R. Pease (1981). High-performance heat sinking for VLSI. *IEEE Electron Device Letters* 2(5).
- Vaisi, A., R. Moosavi, M. Lashkari, and M. Mohsen Soltani (2020). Experimental investigation of perforated twisted tapes turbulator on thermal performance in double pipe heat exchangers. *Chemical Engineering and Processing - Process Intensification* 154, 108028.
- Wang, B. and X. Peng (1994). Experimental investigation on liquid forced-convection heat transfer through microchannels. *International Journal of Heat and Mass Transfer*, 73–82.
- Wang, Y., B. Zhou, Z. Liu, Z. Tu, and W. Liu (2014). Numerical study and performance analyses of the mini-channel with discrete double-inclined ribs. *International Journal of Heat and Mass Transfer* 78, 498–505.
- Weilin, Q., G. M. Mala, and L. Dongqing (2000). Pressure-driven water flows in trapezoidal silicon microchannels. *Int. J. Heat Mass Transfer*, 12.
- White, F. M. (1974). *Viscous Fluid Flow*. McGraw-Hill Book Company.
- Xia, G., L. Chai, H. Wang, M. Zhou, and C. Zhenzhen (2011). Optimum thermal design of microchannel heat sink with triangular reentrant cavities. *Applied Thermal Engineering* 31.
- Xu, J., Y. Song, W. Zhang, H. Zhang, and Y. Gan (2008). Numerical simulations of interrupted and conventional microchannel heat sinks. *International Journal of Heat and Mass Transfer* 51, 5906–5917.
- Yang, S., J. Chalfant, J. Ordonez, J. Khan, C. Li, I. Cvetkovic, J. Vargas, M. Chagas, Y. Xu, R. Burgos, and D. Boroyevich (2019). Shipboard PEBB cooling strategies. *IEEE ESTS 2019*, 24–31.

A Microchannel Simulation Library Tool User's Guide

A.1 Getting Started

1. Establish Software Pre-Requisites:

- Star-CCM+ installed on local and remote server
- Matlab installed on local or remote server
- Establish passwordless connection between the local computer and the remote server. If due to security reasons this is not desired or possible, the tool will still function with additional steps which will be described below.
- Set-up described in this User's Guide
 - Matlab (Version R2020.b) installed on local computer (from here on out referred to as *client* to keep congruence with Star-CCM+ User Guide)
 - X Steam for Matlab downloaded in local home directory. X Steam download can be found here.
 - Star-CCM+ 2021.1 installed on remote server (from here on out referred to as *server* to keep congruence with Star-CCM+ User Guide)
 - Star-CCM+ 2021.1 installed on *client*
- Download and Decompress the Microchannel Simulation Library Tool (MSLT)
 - Transfer MSLT_remote.tar.gz to desired directory on *server*. Take note of this location. From here on out the pathway which MSLT_remote.tar.gz was transferred to will be referred to as the *remote_directory*.
 - Decompress MSLT_remote.tar.gz by using command:tar -xvf MSLT_remote.tar.gz
 - Transfer MSLT_local.tar.gz to desired directory on *client*.
 - Decompress MSLT_local.zip to desired directory by right clicking and using your unzip software of choice.

A.2 Tool Overview

The tool is designed to allow as much user interaction with the underlying Star-CCM+ simulation models as the user desires. The MSLT allows for the user to interact with simulation development and post-processing at just the Matlab user interface level by inputting design parameters and extracting results. However, it can also be used by those wishing to edit baseline simulation files to augment the geometric definitions and include new geometries while still being able to use the Matlab user interface for post-processing of results. The tool as a whole functions as a library of base simulation files generated in Star-CCM+ which are manipulated to run with the Design Manager application within Star-CCM+ by a java script tailored by Matlab. Matlab then processes the data points gathered from the simulation to provide the user with processed useful performance metrics. The individual files included are described in more detail below:

1. *Simulation Base Files*: Each of the 4 base geometries (straight channels, pin fins, fan cavities, and zig-zags) are available for use with either water as the working fluid or another fluid dictated by user-provided material properties and in symmetric half models geometry or whole models. These combinations constitute the 16 base geometry files which are available for tailoring and manipulation dependent on the user's specific problem statement. These simulation base files were generated in Star-CCM+ and are set up with geometric relationships, meshing characteristics, model physics and boundary conditions, and flow conditions pre-defined.
2. *DEFAULT.dmprj*: This Design Manager Project file serves as the baseline canvas for future Design Manager Project file generation. The Design Manager functionality within Star-CCM+ allows for interaction with individual Star-CCM+ simulation files (.sim files) via exposed parameters and to quickly and easily generate sweeps to identify the effects of varying parameters on design outputs. *DEFAULT.dmprj* is pre-loaded with the Simulation Base Files linked. Copies are made of it with each new project generated using the MSLT with tailored sweep parameters based on the user's design space exploration needs.
3. *MSLT_INTERFACE.mlx*: This file is the main user interface for the MSLT. The user defines their problem using the editable field text boxes shown for a chosen geometry. A java file is then generated which will tailor a copy of *DEFAULT.dmprj* by using macro commands used by Star-CCM+ to manipulate Design Manager Projects. *MSLT_INTERFACE.mlx* will then copy the java file to the remote server, and output the code needed for the user to enter into a command prompt to start the Design Manager Project running. The interface tool has the ability to check if the Design Manager Project has completed all runs. Finally, post-processing and graph generation can be completed from the same user interface using data collected from the Star-CCM+ simulations output into a CSV file.
4. *DatabaseParse.m*: This file parses the data returned in the results CSV file based on how the user wants it serialized. The user can choose to sort the data returned by many of the geometric parameters available for manipulation. *DatabaseParse.m* will sort and split up the data based on the separation parameter selected from *MSLT_INTERFACE.mlx*

A number of files are generated throughout the process of running a Design Manager sweep. These are named based on the name given to the project at the onset of defining the problem. This naming convention and process allows the user to graphically display results from multiple projects and keep inputs, outputs, and project manager files accessible by generated project to ensure streamlined future data tracking for the user.

1. *project_name.java*: This file is generated by *MSLT_INTERFACE.mlx* and is what the Design Manager within Star-CCM+ reads to designate inputs and sweep parameters for the Design Manager Project.
2. *project_name.dmprj*: This file is initially a copy of *DEFAULT.dmprj*, described above, and is edited by the macro commands contained within *project_name.java*. This is the file with all the Sweep data and what runs in Star-CCM+ to generate results.
3. *project_name_key_inputs.txt* and *project_name_value_inputs.txt*: These files are text files with the inputs provided by the user which are stored on the *client* and accesible for post-processing and for the user to look back on later to see what inputs were given for a particular sweep. Most

of the inputs are also provided as outputs from Star-CCM+ in the generated CSV file for data processing.

4. *project_name.csv*: This file is generated by Star-CCM+ at the conclusion of the Design Sweep and subsequently copied back over to the *client*. It contains all the output data from the sweep and is used for post-processing by *MSLT_INTERFACE.mlx*.

A.2.1 Work Flow

The work flow for the MSLT is run completely from the single script Matlab interface file *MSLT_INTERFACE.mlx* and a single shell command prompt. The user enters parameters that pertain to their computer setup to allow the script to dictate commands between the *client* and the *server* if passwordless shell connection is enabled. Each project is named by the user and that project name is used to link all output files generated throughout the process of running the Design Manager Sweeps. Using *MSLT_INTERFACE.mlx*, the user inputs values for parameters that define the sweep they'd like to run. *MSLT_INTERFACE.mlx* generates a java macro script adapted from recorded macro commands from Star-CCM+ tailored to the base simulation files and set up to be customizable to user inputs. This java file is copied to the *server* from Matlab. User commands are generated for the user to copy and paste into a shell based on the project name and *client/server* configuration. These commands will start the Design Manager project running in Star-CCM+. Upon completion of all runs, a CSV file of the raw results will be generated by the Design Manager. When the user is ready to check on the results, they can execute a command within *MSLT_INTERFACE.mlx* to check on the status of the simulations, and if complete copy the CSV results back to the *client* directory for post-processing. Results can be viewed by the user in the CSV file that is copied back over and graphical post-processing can be completed by the user from within *MSLT_INTERFACE.mlx*.

A.3 Step by Step Guide to Using the MSLT

This section is intended for use after completing all the steps in Section A.1. For users accessing a remote server requiring a VPN, it is important to establish the VPN connection prior to step one. The VPN connection can be terminated while the simulations are running in step 8.

1. Open a command prompt on *client* to establish remote server connection with *client*. To establish the connection insert the following command inserting the username and IP address of the *server*:
 - `ssh username@xx.xx.xx.xx`
2. Open *MSLT_INTERFACE.mlx*
3. Fill in information pertaining to the computer setup and run time inputs. Details on each of these inputs is found in Section A.4.1.
4. Fill in information defining the basic model choice. Single sweep files can be used to manipulate geometric and heat condition parameters, however separate sweeps are required for variations in baseline geometry, working fluid and cold plate material properties, and model size (half symmetric or whole model). Details on these inputs are found in Section A.4.2.

5. Fill in information defining the geometric and heat condition parameters for the sweep which define the problem and the independent variables of choice. Check the box if you would like to define the details of that specific parameter, and set the minimum value, maximum value and resolution. The Resolution is how many even set points you would like to break the range between the minimum and maximum into, inclusively. For instance if you set a minimum of 0.8 mm and a maximum of 1.0 mm with a resolution of 3, the Design Manager will have 3 set points for that parameter at 0.8 mm, 0.9 mm and 1.0 mm. If the value is desired to be set as a constant, set the minimum and maximum to the same value and set the Resolution to 1. Details on these inputs are found in Section A.4.3. It is important to check each block for any setting that you would like to control directly. Each input will default to either a set value or a value which is a relationship of other parameters. It is important define each variable which is truly independent but NOT to overdefine the problem. Any set parameter will overwrite the geometric relationships defined in the base simulation files. For example, plenum width is controlled by number of channels, fin width and channel width and is calculated to equal the total width of the channel and fin region of the cold plate. If any of the 3 input variables for plenum width (channel width, fin width or number of channels) are set to have multiple values throughout the sweep, setting plenum width to a set constant value will overwrite that geometric relationship setting, and you may run into geometric build issues within the simulation where the plenum will be improperly sized to accommodate for the channel width, fin width and number of channels combination. Specific relationship constraints are detailed as necessary in A.4.3.
6. Click “Run Button”. This will compile the inputs set into the project java file.
7. Copy appropriate lines of commands into the local and/or remote shell as necessary. If passwordless setup is enabled, the java file will automatically be copied to the remote directory and Matlab will output commands to enter into a server-side connected shell. If passwordless setup is not enabled, Matlab will display 2 sets of commands. The first will be to input into a client side command prompt to copy the java file to the remote directory. The second will be to input into a server-side connected shell to start the simulations running.
8. Allow time for the simulations to run. At this point simulations can be checked on if the user goes into Star-CCM+ on the client side. If passwordless setup is enabled, to check on the status of the simulations without opening Star-CCM+, press the button ”Check if Sim is Done Running”. This command will attempt to copy the CSV of results from the server back to the client, and if able to do so, will return “SIM IS DONE RUNNING”. If unable to do so, it will return “SIM IS NOT DONE RUNNING”. If passwordless setup is not enabled, the command to check for the CSV will be printed as an output when the “Check if Sim is Done Running”. Enter this in a client side command prompt located in the client side directory that *MSLT_INTERFACE.mlx* is saved into. If a file is copied to the client side, the sweep is done running, otherwise the sweep is not done running.
9. When the CSV results are copied back to the client side, enter the current project title in the post-processing section. Choose a separation key and the x and y axis data desired to be plotted to generate desired graphs. The details for options are detailed in Section . The CSV results can also be accessed via your program of choice for more specific post-processing.

A.4 Case Setup Problem Definition

A.4.1 Computer Setup and Run Time Inputs

The following inputs are pertaining to the server and will allow seamless flow between using the Matlab interface and the server side Star-CCM+ application.

- Remote Server User Name: Enter the username on the server side where *remote_directory* is located.
- Remote Server IP Address: Enter the remote Server IP address where *remote_directory* is located.
- Remote Server Directory for Files: Enter the file pathway from the home directory to the *remote_directory*. This must end in a ‘`’` and it must be a directory (folder). If it does not end in a ‘`’` an error will generate prompting the user to end it in a slash.
- POD License Key: Enter the Power On Demand License Key used to run Star-CCM+ simulations. If you do not have a Power on Demand License set-up you will need to edit the commands used to start the batch simulation run. Refer to Star-CCM+ documentation for guidance on that.
- Star-CCM+ Run Command: Enter the Star-CCM+ command used to launch Star-CCM+ on your server. This is by default ‘`starccm+`’ but can be different if it was given an alias during installation and setup. For example, some servers have multiple versions of Star-CCM+ installed and therefore each version is given a different launch alias.
- Project Name: This user defined project name will be used throughout the files created to denote parameters, inputs, and outputs specific to the specific project about to be defined. Choose something unique as to not overwrite previous work.
- Number of Compute Processes: This should be an integer less than or equal to the number of cores available on your server. This number will dictate how many cores Star-CCM+ uses when it is running simulation files and therefore any other work or processes occurring on the server should be taken into consideration when dictating this value. Of note, this cannot be changed throughout the simulation sweep.
- Save Simulations?: This box should be checked if it is desired to save the entire simulation file for each run conducted. If further post-processing, verification of setup, data collection, or imaging is desired from each simulation file other than the data output in the CSV and detailed in Section 4.4.3.2 then the simulation files should be saved.
- Passwordless connection enabled?: This box should be checked if a passwordless setup is enabled between the client and the server. By checking this box, most commands can be run directly from the *MSLT_INTERFACE.mlx*, rather than being copied and pasted into a command prompt.

A.4.2 Baseline Model Inputs

The following are baseline model defining parameters. They will be constant for all simulations run in the current sweep and if manipulation is desired to any of the following, a new project will be required to be set-up and run.

- Geometry: The four baseline geometries are optioned here: Straight, Zig-Zag, Pin Finned and Channels With Cavities. Choose one from the drop down menu.
- Working Fluid: Choose between Water and Other Fluid. If Water is selected, the Star-CCM+ fluid model will use water material properties in accordance with IAPWS-IF97 equations which adjust water material properties based on the actual conditions (temperature, pressure etc.). If Other Fluid is selected, the working fluid material properties must be denoted by the user and these will be treated by Star-CCM+ as constant properties.
- Model Size: This will run either a half model with symmetry planes denoted at the midline of the model or a full model. The half model numbers and values will save computational power and time due to a smaller overall model needing to be solved for. However, there are some limitations with running a half model. The Zig-Zag and Pin Fin geometry models may not truly be designed symmetrically in practical usage. Additionally, the amount of horizontal offset done by the Zig-Zag model is limited in the half symmetric model to prevent the channel wall from crossing over the center line and therefore preventing the model from building. Finally, there may be inaccuracies with using a half model vice modeling the entire cold plate.
- Cold Plate Material Properties: The following properties are applicable to the cold plate or solid regime of the simulation. They are constant properties, meaning that the simulation does not take into account any environmental dependence and treats the parameters as constant throughout the domain.
 - Solid Density: Enter the density in kg/m^3 of the solid domain.
 - Solid c_p : Enter the Constant Pressure specific heat in $J/kg - K$ of the solid domain.
 - Solid k : Enter the thermal conductivity in $W/m - K$ of the solid domain.
- Working Fluid Material Properties: The following parameters are required if anything other than water is chosen. These are constant properties and will not be treated as temperature or pressure dependent. Additionally, the fluid will be treated as an incompressible fluid.
 - Working Fluid Density: Enter the density of the desired working fluid in kg/m^3 .
 - Working Fluid c_p : Enter the constant pressure specific heat of the working fluid in $J/kg - K$ of the desired working fluid.
 - Working Fluid k : Enter the thermal conductivity of the working fluid in $W/m - K$.
 - Working Fluid Turbulent Prandtl Number (dimensionless): Enter the Turbulent Prandtl Number
 - Working Fluid Dynamic Viscosity: Enter the working fluid dynamic viscosity in $Pa - s$

A.4.3 Problem Definition Inputs

The following are parameters that define the problem geometry, heating, and flow conditions for each sweep. Each parameter that is going to be changed from the default needs to be checked. The default is listed here as either a hard value or a relational equation. If a default is an equation in relation to other parameters, it will be over written by providing specific values. Therefore, care must be taken

to properly define the cases. For any parameters that you wish to set as a constant value across all simulation runs, set the maximum and minimum to the same value and set the resolution to 1. For any parameters that you wish to set as a variable, set the minimum and maximum value and resolution. The resolution will dictate how many evenly spaced set points are run by Star-CCM+ inclusive of the maximum and minimum value. For instance, if channel width is set with a maximum value of 0.8 mm, minimum value of 0.6 mm and resolution of 3 - the set points will be at 0.6 mm, 0.7 mm and 0.8 mm. Of note, Star-CCM+ will run every combination of every set point dictated. For instance, if 2 different parameters are dictated to have a resolution of 3, and all other parameters are set to a resolution of 1, there will be a total of 9 simulation runs. This is important to note for several reasons. If every simulation file is saved, memory constraints may be run into depending on how much space is available on the remote directory. Additionally, for each simulation run, additional time is required. Finally, there may not need be a desire to test every combination of every data set point. In this case, different projects should be set up to pare down which combinations are required. Default values or equations are denoted next to each parameter. The necessary units are the default units listed here and in *MSLT_INTERFACE.mlx*.

- **Inlet Velocity** [0.4m/s]: Constant inlet velocity to the inlet of the model in m/s. The inlet is a circle denoted by Inlet Radius parameter. Between these two parameters (and water and/or other fluid material properties) inlet mass flow rate is dictated.
- **Channel Width** [0.8mm]: The width across the inlet of each channel in mm.
- **Channel Height** [1.2mm]: The depth of each channel in mm.
- **Channel Length** [20mm]: The length of each channel in mm.
- **Working Fluid Inlet Temperature** [293K]: The uniform, constant temperature of the working fluid flow into the inlet of the model in K.
- **Fin Width** [$FinWidth = ChannelWidth$]: The width of the cold plate material in between channels in mm. By default it will be equal to Channel Width.
- **Heater Surface Length** [20mm]: The length of the heater patch centered length and width wise on the bottom of the cold plate in mm.
- **Heater Surface Width** [20mm]: The width of the heater patch centered length and width wise on the bottom of the cold plate in mm.
- **Number of Channels** [See Section 4.4.2]: The number of channels across the width of the full cold plate (whether the whole model or half model is chosen). Further details about how number of channels is determined if NOT explicitly set by the user are in Section 4.4.2. Number of Channels must be an integer, and if used as a variable parameter care must be taken to not set a resolution which will result in any set points NOT being an integer. For example, an acceptable input would be minimum = 3, maximum =5, resolution =3. An unacceptable input would be minimum=3, maximum=6, resolution = 3, because it will cause Star-CCM+ to fail in the geometry building phase with an inapplicable number of channels equal to 4.5.
- **Plate Length** [$PlateLength = ChannelLength + 2 * PlenumLength + 2 * Overhead$]: The overall plate length is dependent on the channel length, plenum length and overhead. If overwritten, care must be taken to not set it shorter than the total length of the channels and the plenums

to avoid an invalid geometry. Plate Length is defined in mm. The overhead length will automatically be calculated and input into the simulation based on the defined plate length, channel length and plenum length either left as default or defined by the user. The channels will always be centered longitudinally and horizontally on the plate.

- **Outlet Pressure** [$0Pa(Gauge)$]: The outlet surface is defined by a user-defined pressure. The default is 0 Pa Gauge, or 101325 Pa Absolute Pressure (equal to 1 atm of pressure). This must be defined as a gauge pressure.
- **Plate Width** [$0.041m$]: The overall plate width in mm. Care must be taken not to define the plate width as less than the plenum width or total width of the channels and fins.
- **Plate Depth** [$PlateDepth = ChannelHeight + 2.4mm$]: The overall plate depth in mm. Care must be taken to not define the plate depth as less than the Channel Height.
- **Inlet Radius** [$3mm$]: The radius of the circular inlet to the cold plate. This in concert with the inlet velocity will determine the volumetric flow rate of the working fluid through the system.
- **Inlet Plenum Length** [$8mm$]: The plenum length in mm.
- **Heat Flux** [$312500W/m^2$]: The even heat flux into the heater patch at the bottom of the cold plate.

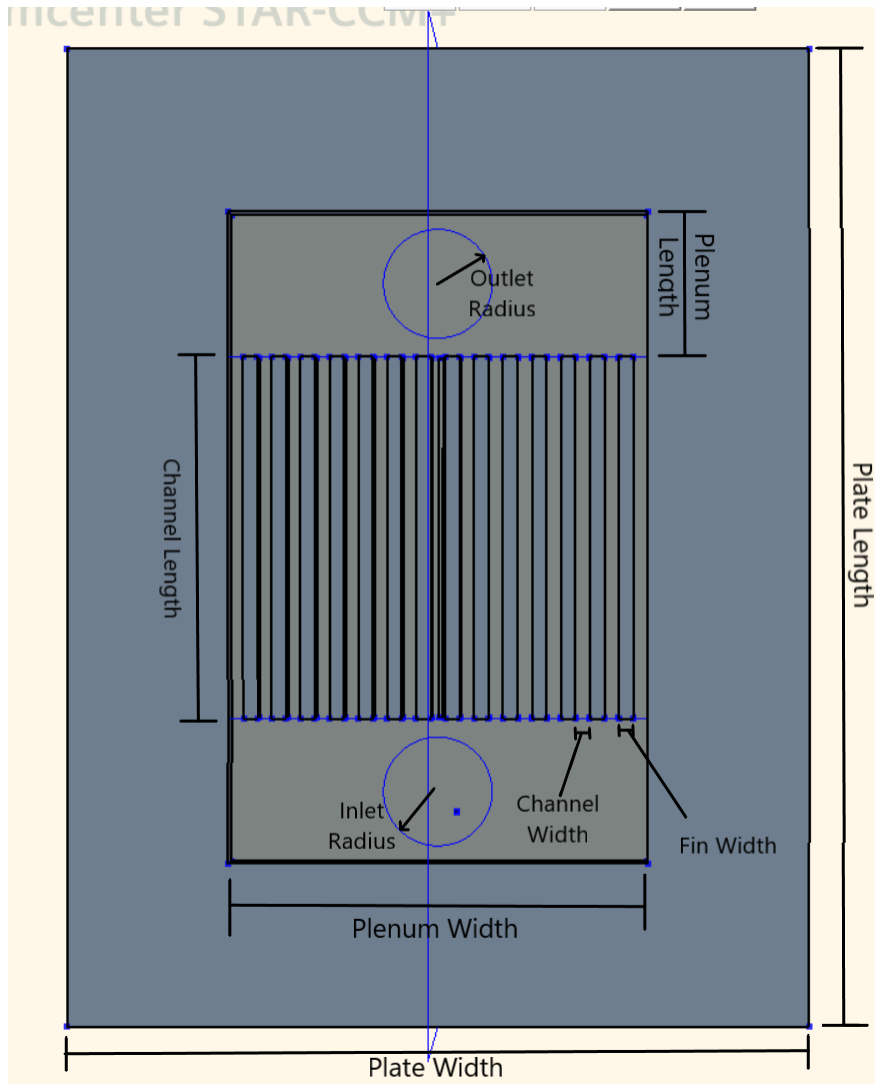


Figure A.1: Straight Microchannels Base Geometry

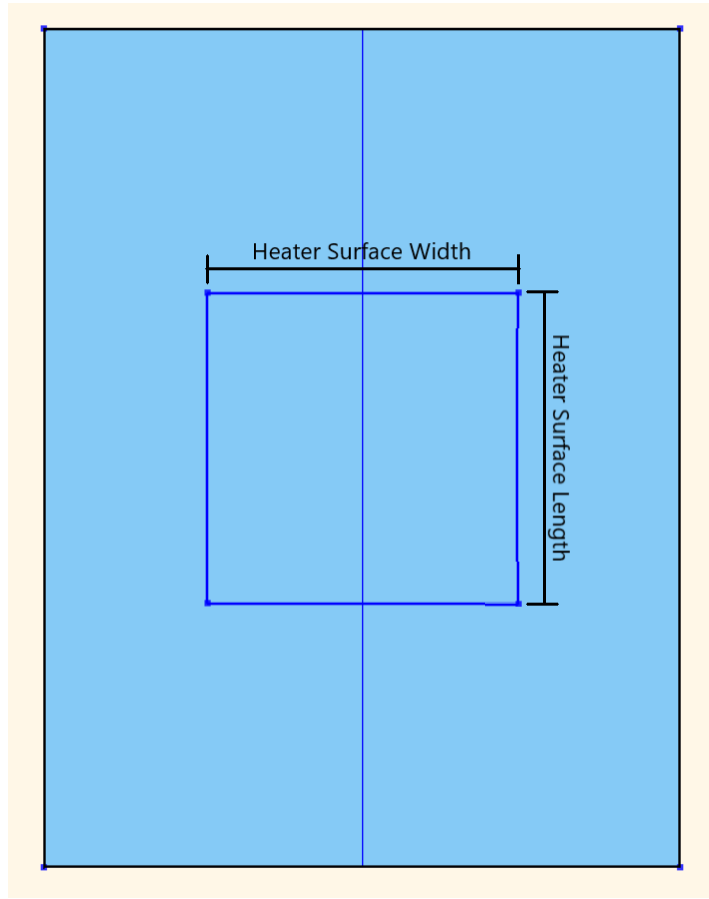


Figure A.2: Bottom View of Base Geometry

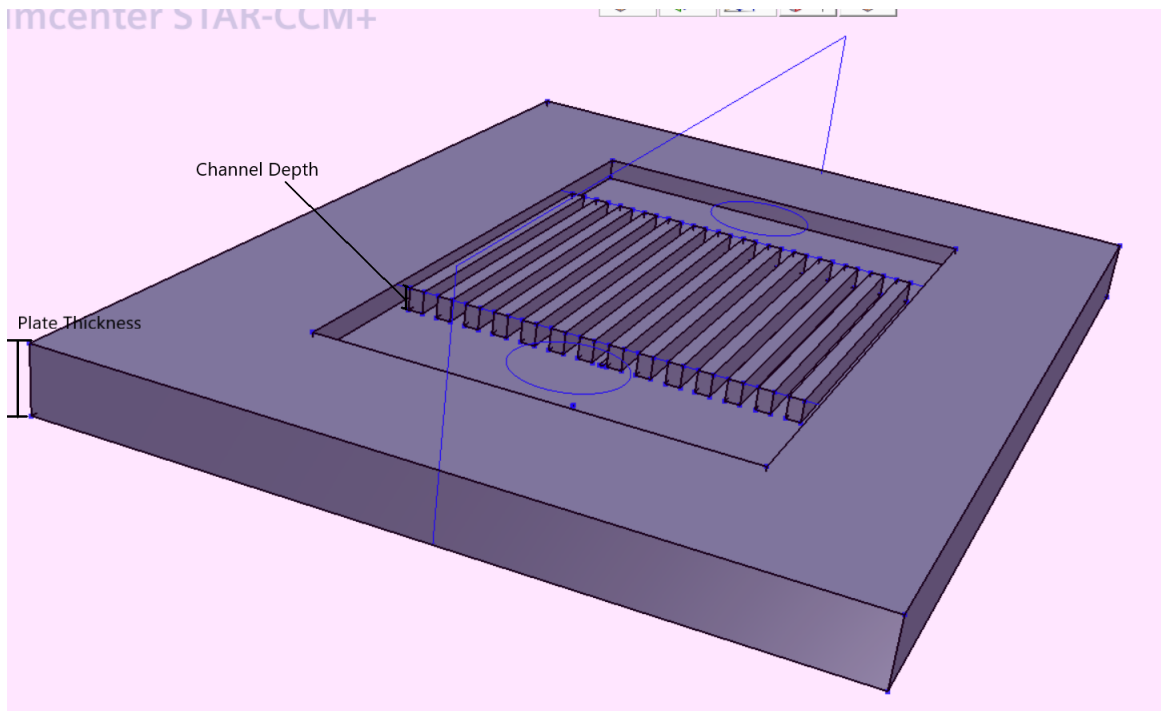


Figure A.3: Isometric view of Cold Plate

- Zig Zag Specific Parameters:

- Zig Height [5mm]: The height of the repeatable zig-zag pattern in mm. By defining the height of the zig-zag and the channel length, the number of turns per channel length is determined.
- Zig Offset [$ZigOffset = 0.4ChannelWidth$]: The horizontal total offset of the zig-zag pattern from the leading edge of the channel. For symmetric half model simulations, the Zig Offset cannot be greater than half the channel width or else the model will fail to build. If desired to make the Zig Offset greater than half the channel width, the full model must be used.

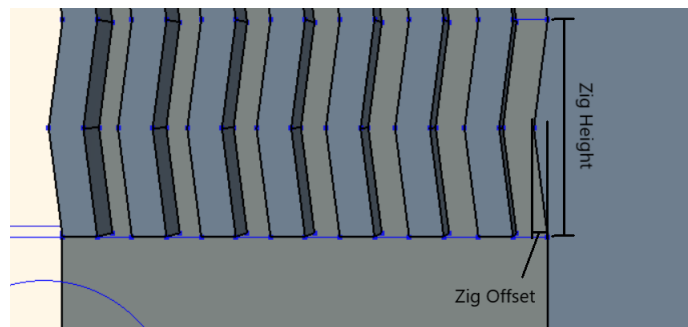


Figure A.4: Zig Features Close Up

- **Finned Geometry Specific Parameters:**

- **Fin Angle** [$45degrees$]: The interior angle of the parallelogram shape that each fin is in degrees.
- **Fin Spacing** [$FinSpacing = FinLength$]: The longitudinal spacing between the fins along the length of the channels in mm.
- **Fin Length** [$FinLength = ChannelWidth$]: The length of the fin in the channel length dimension in mm. Horizontal fin width is defined by the generic fin width parameter described above.

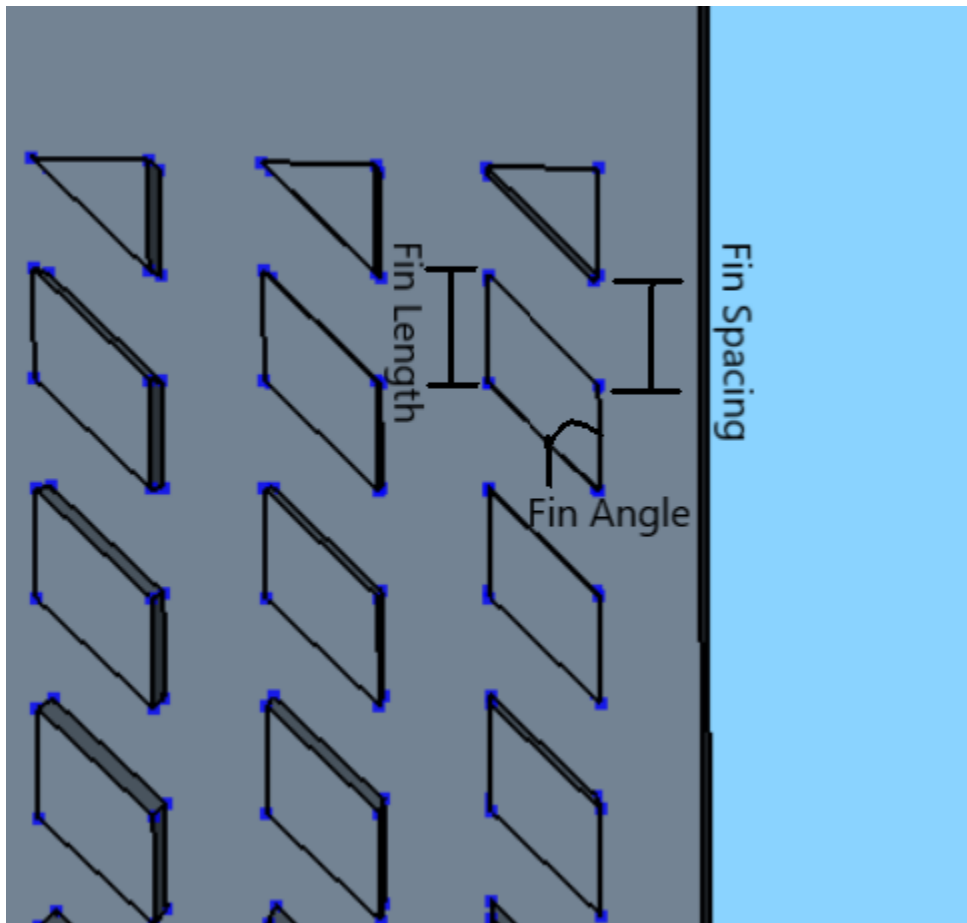


Figure A.5: Fin Parameters

- **Fan Cavity Specific Parameters**

- **Fan R** [$FanR = 0.4 * ChannelWidth$]: The radius of the semi-circular cavities in mm. Care must be taken not to exceed half the distance of the fin to avoid intersecting with the adjacent channel's cavity.
- **Fan E** [$FanE = FanR$]: The offset of the cavity from the side wall of the channel in mm,

or cavity depth. It is set to be equal to the Fan Radius so the entirety of the cavity is protruding from the channel.

- **Fan C** [0mm]: The longitudinal offset from the cavity on the opposite side of the channel in mm.
- **Fan Distance** [$FanDistance = 2 * Fan$]: The distance between cavities along the length of the channel, from trailing edge of one cavity to leading edge of the first.

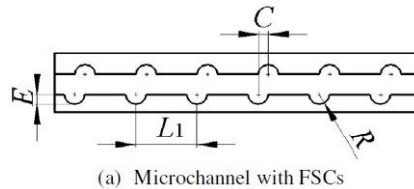


Figure A.6: Pan et al. (2019) Fan Shaped Cavity Geometric Setup

Geometric Definitions not Accessible to be changed:

1. **Inlet Plenum Depth:** Inlet Plenum Depth will be equal to the channel depth.
2. **Inlet Plenum Width** [$PlenumWidth = ChannelWidth * NumberofChannels + FinWidth * (NumberofChannels - 1)$]: The plenum width in mm. This will be set to match the total width of the number of channels, fin width and channel width.
3. **Number of Pin Fins Along Length of Channel** [$FinNumber = floor(ChannelLength / (FinLength + FinSpacing))$]: The number of fins along the length of the channel is determined by fitting the most whole number of fins along the length of the channel as defined by the Fin Length, Channel Length and Fin Spacing.
4. **Number of Cavities Along the Length of Channel** [$CavityNumber = floor(ChannelLength) / (2 * FanRadius + FanDistance)$]: The number of cavities along the length of the channel is determined by fitting the most whole number of cavities along the length of the channel as defined by the Fan Radius, Channel Length and Fan Spacing.

A.5 Relationship Between Channel Width, Fin Width, Number of Channels and Plenum Width

If the channel width, fin width and number of channels is defined by the user, then the plenum width is sized accordingly to be flush with the outside walls of the outside channels. If the channel width and fin width are defined by the user, then the number of channels are sized based on the maximum odd number of channels that can fit in the original 23.2 mm plenum width using the following process.

The number of channels is determined using an approach to garner as close to the defined plenum width defined while keeping the number of channels at an odd number. This is important because the temperatures taken to compute wall temperatures at the channel walls are taken at the centerline of the overall cold plate (the edge of the symmetry plane for half model simulations) and need to be

taken at a fluid boundary with the solid wall at the bottom of the channel in order to be an adequate comparison. If some simulations are taking measurements in the middle of solid substrate fins and some at the liquid/solid interface at the bottom of the channel wall, the results would be incomparable due to the difference in how heat conducts and convects in those scenarios. Plenum width can be calculated using Equation 1.

$$width_{plenum} = n_{chans} * width_{chan} + (n_{chans} - 1) * width_{fin} \quad (1)$$

Rearranging Equation 16 to solve for number of channels, initial determination of the maximum number of channels was calculated using Equation 2.

$$n_{chans,init} = floor(width_{plenum} + 0.1mm + width_{fin}) / (width_{chan} + width_{fin}) \quad (2)$$

The floor function rounds the answer down to the closest scalar to avoid making a larger plenum and to allow the maximum channels possible in the original 23.2 mm plenum width. $n_{chans,init}$ was then checked to for evenness by verifying the modulus of $n_{chans,init}/2$. If the modulus was 0, the number of channels was reduced by one, otherwise the final number of channels was equal to $n_{chans,init}$.

Actual plenum width for the simulation geometry is then calculated using actual n_{chans} and Equation 1.

A.6 Over-Definition Preventions

Within the Matlab user interface, there are a number of user inputs that will generate an error and exit the running of the script in order to prevent a sweep from running that will crash due to errant inputs. The following are implemented in the Matlab script:

1. Geometry specific parameter setting: If features for a geometry not in use are defined, an error will display showing that the wrong parameters are selected
2. Channel Depth vs Plate Depth: If the channel depth is equal to or greater than the plate depth an error will display prompting the user to ensure the plate depth is greater than the channel depth
3. Zig Height vs Channel Length: If Zig Height is greater than Channel Length, the user will be prompted to enter a Zig Height equal to or less than Channel Length
4. Zig Offset vs Channel Width: If the half symmetric model choice is selected and the greatest zig offset entered is greater than half the smallest channel width entered, the program will not build due to the fins intersecting the midline symmetry plane. An error will prompt the user to either switch to a whole model or to decrease the offset.
5. Fan_E vs Fin Width: If the fan cavity depth is greater than half the fin width, the cavities will intersect cavities of adjacent channels. Values which will cause this intersection will cause an error to display prompting the user to change the fan offset in relation to the fin width.
6. Plenum Length vs Inlet Size: If the inlet radius is greater than or equal to half the plenum length, the user is prompted to change the dimensions such that the plenum length is greater than the inlet diameter.

7. Over Definition of channel area: If channel width and/or fin width, number of channels and plenum width are all defined as constants (resolution of 1) and they do not resolve such that the plenum width is equal to the total width of channels and fins, an error will display prompting the user to make the values resolve. Additionally, all those parameters are defined and any of them are set to variable, an error will display prompting the user to either remove the plenum width constraint or make all the values constant.
8. Resolution Set to 1: If the resolution is set to 1 and the minimum and maximum values are not set to the same value, an error will display prompting the user to make the values match.
9. Heater Surface Length and Width: If the Heater Surface length or width are greater than or equal to the plate length or width (respectively) an error will display prompting the user that the heater surface length or width must be less than the plate width. Due to the nature of the surface assignment within the base geometry files, the heater surface cannot be equal to the length or width of the plate and must be less than the length or width of the plate.

A.7 Post Processing Functionality

The CSV copied from Star-CCM+ includes many reports, including some which may seem redundant. These are for verification to the user that the intended setup was indeed the conditions the simulation was run with.

- Channel Wall Temperatures (K): 5 Temperature probe points evenly spaced along the length of the centerline of the center channel bottom wall
- Cold Plate Temperature Spreading Points: 20 Temperature Points evenly spaced throughout the Cold Plate in 4 columns of 5 data points each evenly spaced along the length of the channels and across the width of the cold plate. These temperature points are located at half the distance between the bottom of the cold plate to the bottom of the channels
- Absolute Inlet Pressure (Pa): Surface average of pressure across the inlet surface. This report reflects the last iteration run of each simulation.
- Outlet Temp (K): Surface Average of temperature across the outlet surface. This report reflects the last iteration run of each simulation.
- Total Heat Transfer (W): The total combined heat transfer across all surfaces in the system. This is used as a metric of convergence. This report reflects the last iteration run of each simulation. Further methods of convergence verification are discussed in Section 4.4.4.5.
- Max Cold Plate Temp (K): The maximum temperature seen across the cold plate solid domain region.
- Verification Reports: The following inputs are reported as outputs for each simulation and have ‘_out’ following them in the CSV column header
 - n_chans: Number of channels
 - inlet_vel: Inlet Velocity (m/s)
 - fin_width: Fin Width (mm)

- chan_width: Channel Width (mm) plenum_width: Plenum Width (mm)
- inlet_temp: Inlet Temperature (K)
- chan_height: Channel depth (mm)
- chan_length: Channel Length (mm)
- r_inlet: Inlet Radius (mm)
- solid_k: Solid regime thermal conductivity (W/m-K)
- heat_flux: Heat flux into the heater surface (W/m²)
- heater_length: Heater surface length (mm)
- heater_width: Heater surface width (mm)
- zig_height: Zig-Zag Height (mm)
- zig_offset: Zig-Zag Offset (mm)
- n_fins: Number of Fins
- fins_length: Fin Length (mm)
- fin_spacing: Fin Spacing (mm)
- fin_angle: Fin angle (degrees)

All of the above reports, as well as the following performance metrics can be graphed on either axis:

- Average Centerline Channel Wall Temperature [K]: $temp_{wall,avg} = \Sigma(t_i)/n_{temp\ points}$
- Average Working Fluid Pressure [Pa]: $p_{wf,avg} = (p_{wf,inlet} + p_{wf,outlet})/2$
- Average Working Fluid Temperature [K]: $temp_{wf,avg} = (temp_{inlet} + temp_{outlet})/2$
- Average Working Fluid Specific Heat [$\frac{J}{kg-K}$]: $c_{p,wf,avg}$ Calculated using XSteam Matlab application based on $temp_{wf,avg}$
- Average Working Fluid Density [kg/m^3]: $\rho_{wf,avg}$ is calculated using XSteam Matlab application based on $temp_{wf,avg}$ and $p_{wf,avg}$
- Temperature Rise Factor as defined by Equation 14
- Pressure Drop Across Cold Plate [Pa]: $p_{drop} = p_{wf,inlet} - p_{wf,outlet}$
- Plate Temperature Deviation [K]: $\sigma = \sqrt{\Sigma(t_i - temp_{plate,avg})^2 / (N - 1)}$
- Theoretical Pressue Drop Across Cold Plate [Pa] as defined in Thesis Section 5.3.3

The data can be parsed by a number of variables, which are available by the drop down menu labeled ‘Separation Key’. The separation key allows the data set to be parsed by metrics such as channel width or pin angle, such that the data can be grouped in the graph according to a relevant parameter based on the sweep conducted.

A.7.1 Scene Outputs

Within the folder created on the client side for the project are subfolders for each Design. Scenes are captured from Star-CCM+ for the temperature and velocity profiles of each Design and are in the folder. These scenes are based on Derived Parts created within each base simulation. If desired to add more scenes or change the location of the Scenes, this can be done from within base simulation files. If only changing location of cutaway, no modification will need to be done to `MSLT_INTERACTIVE.mlx`. However, if adding the scene, it must be added in the macro generation section of the file as a scene to collect, and the `DEFAULT.dmprj` must be updated to have access to the new report. Refer to the Star-CCM+ User Guide for more information on updating the Design Manager files post changes to simulation base files.

A.7.2 Report and Scene Output Variations

In order to change the simulation outputs, such as where reports are taken from, editing of the simulation basefiles themselves is required. In general, if the report already exists, what data it pulls from can be changed within the simulation file can be changed and as long as no report names are changed, the data will be reflected in the results CSVs. This is especially useful for the temperature points which go into the Σ and Wall Temperature calculations. These reports are pulled from derived parts created within the simulation files. Editing the coordinates of these derived parts will edit what data is output in the results CSV. This applies to the scenes as well. The scenes are taken from a cross-section which bisects the channel depth. If a different slice is desired, the location of the derived parts that the scenes are based off of can be edited within the base simulation files.

If additional data is required, new reports can be generated within the base simulation files. In this case, the report will also need to be added to the reports gathered in multiple places:

- `DEFAULT.dmprj`: The base simulation file edited will need to be updated within `DEFAULT.dmprj`. This will allow it to be accessed by the Design Manager when running new sweeps.
- `MSLT_INTERACTIVE.mlx`: Following the same format as used to add reports to the macro file generated, text will need to be added for the new report within the Matlab script. Look for comments within the script to identify what augmentations are needed.

Refer to the Star-CCM+ User Guide for more information about each of the field reports and how to manipulate derived reports.

A.8 Considerations for Alternate Setups

1. No Power On Demand (POD) License setup - The batch command for Star-CCM+ generated in the user interface is for Power on Demand License setup. If a different license setup is used, the command will be different and the Star-CCM+ User's Guide must be consulted to get the proper command to run the `.dmprj` files.
2. Using a single computer - If a single computer is used, files will not need to be copied from the client to the server. Within the Matlab user interface, all `'scp'` and `'cp'` commands can be ignored.

A.9 Program Accessibility From Various Levels

1. Accessing the Results Mid-Simulation Run - In the event that the user checks on the simulation run and it is not complete but the user would like to check on where in the sweep the project is, this can be done by checking on the files generated on the *server*. The following commands can be used from a command prompt shell logged into the *server*.
 - (a) Navigate to the *remote_directory*.
 - (b) 'cd *project_name*' - this should bring you to a directory created with the project name given to the project.
 - (c) 'cd Design.Study.2' - this will bring you into the directory created for the Design Study in progress
 - (d) 'ls' - this will list directories for all the completed runs. For instance if 4 distinct runs were directed for your project, and using the 'ls' command only returns 'Design.1 Design.2' then the 3rd run is in progress and the 4th run remains to be started.
2. Accessing the Base Simulation Files - There are a number of reasons the user may want to access the Base Simulation Files. Some of these include manipulating the meshing characteristics, boundary conditions, stopping criteria, turbulence parameters and collecting more data from the results. In order to change parameters from Base Simulation files prior to simulations running, the base files in decompressed into the *remote_directory* can be edited by opening them in Star-CCM+. As long as no parameter names are changed, no edits are made to the 3D CAD modeling process, and the surfaces and boundary definitions are not changed, any tweaks to parameter values, boundary conditions, and stopping criteria should have no impact on the functionality of the MSLT. However, it is recommended that copies are made of the base simulation files in the event of file corruption when changes are being made. In order to access more data from the simulation runs, the selection should be made to save simulation files. Each of these will save as a .sim file that can be accessed for any post-processing the user would like to accomplish. If generating new reports for post-processing use in Matlab, the code within MSLT_INTERACTIVE.mlx can be augmented to ensure that data is included in the results file generated by Star-CCM+. As with modifications to the Base Simulation Files, it is recommended a copy of MSLT_INTERACTIVE.mlx is made prior to implementing any code changes.

A.10 Stopping Criteria

Stopping criteria for each simulation is based on getting to 15000 iterations, or meeting all three of the following criteria:

- Total Heat Transfer Asymptotic Limit: Over the most recent 100 samples, the total heat transfer can not have changed more than 10% of the current values (normalized change minimization of less than 0.1)
- Total Heat Transfer Maximum and Minimum: The absolute value of Total Heat Transfer must be less than the user defined percentage of the Heat Transfer introduced to the system via the heater surface. The default value is 2%. The Total Heat Transfer is defined as all heat leaving

and entering the system and for a perfect steady state solution would be equal to 0 W. This is controlled using two different stopping criteria settings within Star-CCM+ - a maximum total heat transfer and a minimum total heat transfer. Both of these must be satisfied for the simulation to stop running prior to 15000 iterations.

The 15000 steps are included as a fail safe to keep the program from running indefinitely if settings are chosen that may not lead to steady state convergence within the parameters above. However, each base simulation file has a solution pre-loaded to lead to quicker convergence (base geometry settings and boundary conditions described in Section 6). The further away the settings are from those in the pre-set solution, the longer it may take to converge and 15000 iterations may not be sufficient. As the program is written, the stopping criteria maximum steps is embedded within the base files and cannot be accessed from the MSLT interface so if the simulation parameters are different enough from the base case such that greater than a total of 15000 iterations is desired, stopping criteria must be adjusted within the base files.

The total heat transfer is included as an output accessible via the results CSV file generated and the Matlab interface for users to validate that metric of convergence. If the total heat transfer is high, particularly if it's outside of the maximum heat transfer percentage set by the user, the log files can be explored to check for good convergence. Additionally, the number of iterations it took for the simulation to converge will be reported in the results CSV as well as output for each run results values when graphs are generated. If the value is 15000 this means that the simulation was stopped by maximum number of steps, not by meeting convergence criteria. Exploration as to why this may be desired by the user, by looking past the data available by the MSLT.

A.11 Solver Effect

The following variables are set to only affect the solver and therefore changes in them do not generate a new mesh for each simulation run. All other variables affect geometry and therefore affect the mesh and will generate a new mesh for each design including a difference in them.

1. Inlet Velocity
2. Inlet Temperature
3. Heat Flux
4. Solid c_p
5. Solid k
6. Solid density

A.12 Troubleshooting Tips

Here are some tips to get past errors.

1. Error 'Remote Directory input is incorrect.' : Verify that your directory on the remote server is correct. Remember this must be in relation to the home directory on your remote server. If unsure, ssh into the remote server by entering :`'ssh username@xx.xx.xx.xx'` with your username and IP address. Determine the relative path from the current directory to the one where

MSLT_remote.tar.gz was decompressed. This may include using the command `../` to move up a directory. File paths must also end in `/`. Failure to include `/` will also generate an error. There is one exception to this: if the files were decompressed directly in the home directory of the remote server, the file path input box can be left completely blank. Some examples of valid remote directory paths are included below.

- `'bob/coldplates/MSLT/'`
- `'../ExtraHardDrive4/users/Mary/microchannels/'`
- `''`

2. Stopping and Restarting Design Manager: More information is available in the Star-CCM+ User Guide if choosing to interact directly with the Design Manager to start and stop the simulation sweeps. However, the following can be used to direct the simulation runs with the command prompt and Matlab interfaces:

- To Abort Design Manager Project: From the User's Guide, entering `'touch DM_ABORT'` in the directory of the command prompt will stop the Design Manager Project in run. In order to garner any results previously recorded prior to aborting the Design Manager Project, refer to the section in `MSLT_INTERACTIVE.mlx`. Refer to the Star-CCM+ User's Guide for more information if interacting directly with the `.dmprj` files. In order to get any results
- To retrieve the interim results from the aborted Design Manager project, the user can re-enter relevant parameters and click Retrieve Results. This will display a line of code that can be copied to a server connected shell (in the correct remote directory). This line of code will run a java script generated to extract the results file from the terminated Design Manager Project.
- To restart an aborted Design Manager project, the user can re-enter the relevant parameters and click Restart. This will restart the project from the last completed design thru completion and CSV results retrieval. While restarting can be done from within the Design Manager project itself, this will not lead to results extraction via CSV as the initial macro was interrupted.

3. Sweep not finished but no processes running: If a sweep is not showing as finished, but there are no processes running on the remote server, something caused the sweep to fail. In many cases, this could be a storage space issue. Star-CCM+ automatically generates log files within the folder created for each sweep, and within the run time folder (`.mdxruntime`). In general, if the error was due to lack of storage space, freeing up space on the drive and restarting the sweep with the steps described above for re-starting should allow for the sweep to continue from its last saved simulation run. If the sweep failed due to geometric builds, the logs for each simulation file will point to this by showing failed processes.